

MULTILEVEL STRUCTURAL ANALYSIS OF GFRP-STEEL HYBRID BRIDGE DECK



Image courtesy of FiberCore Europe

DESIGN OF A BRIDGE OVER THE ROTTE NEAR PRINS ALEXANDER DISTRICT, ROTTERDAM

Final report

Abstract

The current research and design thesis deals with implementation of a 30-meter-long bridge with a cross section made with an innovative hybrid material composed of GFRP composite and steel members. A preliminary design consisting of analytical calculations creates a reference line on top of which FEM modelling is added with the purpose of investigating potentially critical effects that can render the structure unusable. These effects include buckling of composite webs under wheel loads, thermal stresses due to temperature variation over the lifespan of the bridge and stresses in the resin layer binding the composite to the steel member. After producing and interpreting the results, a conclusion summarizes the content and states whether such a bridge can be implemented. Finally, several requirements suggest further research possibilities that can help to offer a complete picture regarding the structural behavior of this material in a bridge deck.

Multilevel structural analysis of GFRP-steel hybrid bridge deck

Design of a bridge over the Rotte near Prins Alexander district, Rotterdam

Final report

Name:	Teodor Gheorghe
University 1 st examiner:	A. Repko
University 2 nd examiner:	J. de Keijzer
Company supervisor:	M. Veltkamp
Date:	03/06/2016
Place:	Rotterdam, The Netherlands
Revision no.:	3

Acknowledgements

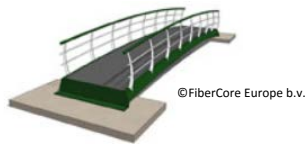
The author of the present research and design thesis would like to offer thanks to all the parties involved, without which the current project could not have been completed:

Firstly, to Mr. M. Veltkamp and Mr. A. Haffmans, my direct supervisors at FiberCore. They offered guidance and assistance along the way, ensuring smooth progress. In addition they took the time to teach

Secondly, to all my colleagues from FiberCore Europe who were more than willing to collaborate and made it easy for me to accommodate and integrate in a fully Dutch speaking environment.

Thirdly, to Mr. A. Repko, my university supervisor who ensured my thesis is on track and offered valuable guidance and feedback in order to facilitate my progress.

Last but not least, to my fiancée and family, who not only supported me morally, but also literally, through proof reading and useful suggestions.

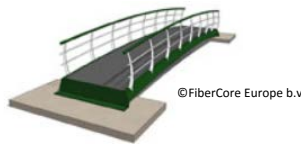


Executive summary

Glass fibre reinforced polymers is a widely known material with numerous applications. It is however not traditionally used as a building material unlike steel or concrete. FiberCore Europe is one of the few companies that have chosen to work with it in the bridge building industry, and have determined that with increasing bridge spans, its properties are slowly reaching their upper limit. In order to overcome this, improvements are necessary.

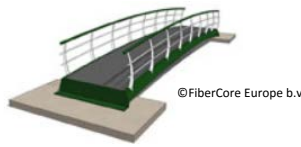
One of the recent developments suggested that combining the glass fibre reinforced polymer with steel components will improve a bridge deck's stiffness, which is the main disadvantage of GFRP. The current document aimed at designing a bridge over the Rotte river, in Rotterdam, the Netherlands.

Thus, the current project can be seen as a stepping stone for FiberCore Europe who, based on the results and conclusion hereby provided, will be able to design and build longer and larger bridges in the future.

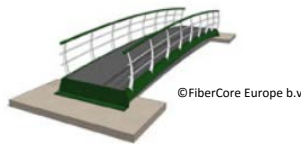


Contents

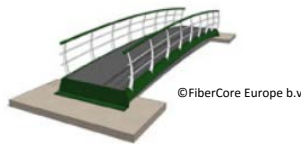
Acknowledgements	i
Executive summary	ii
List of figures	ix
List of tables	x
List of abbreviations	xi
Nomenclature.....	xii
1. Introduction.....	1
1.1. Terms of reference	1
1.2. Company background.....	1
1.3. Assignment background	1
1.4. Project location background	2
1.5. Problem statement.....	3
1.6. Research goal	3
1.7. Research question	3
1.8. Procedure	4
2. Theoretical framework.....	6
2.1. Starting points and design considerations	6
2.2. Concept designs	6
2.2.1. Concept design 1 – steel bars.....	7
2.2.2. Concept design 2 – steel sheets	7
2.2.3. Concept design 3– Rectangular hollow profiles	8
2.3. Composite properties.....	8
2.3.1. General considerations	8
2.3.2. Composite design	8
2.3.3. Sandwich panels	9
2.3.4. InfraCore® technology.....	9
2.3.5. Laminate properties	9
2.3.6. Material properties	10
2.4. Finite Element Analysis	10
2.5. Calculation algorithms.....	11
2.5.1. Transformed area method	11
2.5.2. Corrosion of steel embedded in GFRP	11
2.5.3. Adhesive bond strength between steel and GFRP	12
2.5.4. Thermal stresses.....	12
2.5.5. Dynamic behaviour.....	12



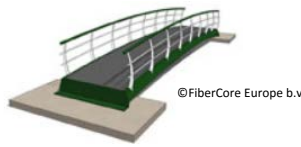
2.5.6.	Creep behaviour of GFRP members	13
2.5.7.	Buckling of composite plates.....	13
2.5.8.	Shear stresses between two different materials	14
3.	Methodology	15
3.1.	Overview of content and scope limitations	15
3.2.	Research method	15
3.3.	List of requirements	15
3.4.	Starting points and design considerations	16
3.4.1.	30 meter bridge	16
3.4.2.	Maximum span bridge.....	17
3.5.	Concept designs	17
3.5.1.	Multi criteria analysis	18
3.5.1.1.	Criteria	18
3.5.1.2.	Coefficients.....	18
3.5.1.3.	Criteria evaluation	19
3.5.1.3.1.	Design challenges	19
3.5.1.3.2.	Material costs	19
3.5.1.3.3.	Procurement challenges.....	19
3.5.1.3.4.	Fabrication costs	19
3.5.1.3.5.	Fabrication time	20
3.5.1.3.6.	Manufacturing challenges.....	20
3.5.1.3.7.	Risks.....	20
3.5.1.3.8.	Contribution of steel to bending stiffness.....	20
3.6.	Preliminary design	20
3.6.1.	Reliability and validity	21
3.6.2.	Bridge dimensions and cross section	22
3.6.3.	Material properties	22
3.6.4.	Loads.....	22
3.6.5.	Partial factors	23
3.6.6.	Load combinations	23
3.6.7.	Analytical calculations for the preliminary design	23
3.6.7.1.	SLS checks	23
3.6.7.2.	ULS checks	23
3.6.7.3.	Thermal checks.....	24
3.6.7.4.	Adhesive bond checks	24
3.6.8.	FEM analysis	24



3.6.8.1.	1D FEM model	25
3.6.8.1.1.	Geometry	25
3.6.8.1.2.	Material properties	25
3.6.8.1.3.	Boundary conditions	25
3.6.8.1.4.	Loads	25
3.6.8.1.5.	Mesh.....	25
3.6.8.1.6.	Analysis and results.....	25
3.6.8.2.	2D FEM model	26
3.6.8.2.1.	Geometry	26
3.6.8.2.2.	Material properties	26
3.6.8.2.3.	Loads and boundary conditions	27
3.6.8.2.4.	Mesh.....	27
3.6.8.2.5.	Analysis and results.....	27
3.7.	Detailed design.....	28
3.5.1.	Reliability and validity	28
3.5.3.	3D FEM model	29
3.5.3.1.	Geometry.....	29
3.5.3.2.	Material properties	29
3.5.3.3.	Loads and boundary conditions	30
3.5.3.4.	Mesh.....	30
3.5.3.5.	Analysis and results	30
3.5.3.6.	Adjustments and optimizations.....	30
3.5.3.6.1.	Natural frequency	30
3.5.3.6.2.	Inter-laminar stresses.....	31
3.5.3.6.3.	Per ply stresses.....	31
3.5.3.6.4.	Local web buckling	31
3.5.3.6.5.	Thermal stresses.....	31
3.5.3.6.6.	Shear stresses in the adhesive bond.....	31
3.6.	Drawings.....	31
4.	Results	32
4.1.	List of requirements	32
4.2.	Starting points and design considerations	32
4.5.1.	30 meter bridge.....	32
4.5.2.	Maximum span bridge.....	33
4.3.	Most feasible concept design.....	34
4.4.	Preliminary design	34



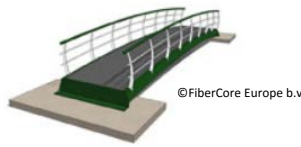
4.4.1.	SLS checks	34
4.4.1.1.	Natural frequency.....	34
4.4.1.2.	Deflection check	34
4.4.2.	ULS checks	35
4.4.2.1.	Normal stress.....	35
4.4.2.2.	Bending stress – Skin bending strength	35
4.4.2.3.	Shear stress – Web shear strength.....	35
4.4.2.4.	Compression stress – Webs compression strength	35
4.4.2.5.	Maximum shear stress	35
4.4.2.6.	Shear stress – Web buckling.....	35
4.4.3.	Thermal expansion analysis.....	36
4.4.4.	Shear stresses in the adhesive bond between steel plate and GFRP skin	36
4.4.5.	Sand addition.....	36
4.5.	Cross section optimization based on preliminary design.....	37
4.6.	Detailed design.....	38
4.7.	Results comparison	41
4.8.	Drawings.....	41
5.	Analysis and interpretation of results	43
5.1.	Causes for results difference between analytical and FEM calculations.	43
5.2.	Evaluation of results	44
5.2.1.	Evaluation of results from preliminary design	44
5.2.2.	Evaluation of results from detailed design.....	45
5.2.2.1.	Web buckling under wheel load.....	45
5.2.2.2.	Thermal stresses.....	45
5.2.2.3.	Adhesive bond stresses	46
5.2.3.	Evaluation of available optimization techniques	46
6.	Conclusion	47
7.	Recommendations	50
	Bibliography.....	51
	Appendix 1 – validation of Excel spreadsheet.....	53
	Appendix 2 – thermal expansion and thermal stresses algorithm	54
	Appendix 3 – deflection due to creep algorithm	55
	Appendix 4 – plate buckling algorithm.....	56
	Appendix 5 – Interface shear stresses algorithm	58
	Appendix 6 – Transformed area method	59
	Appendix 7 – Concept designs – advantages and disadvantages	61



A7.1. Concept design 1 – Steel bars	61
A7.2. Concept design 2 – Steel sheets.....	62
A7.3. Concept design 3 – Rectangular hollow profiles.....	63
Appendix 8 – Initial dimensions and cross section design	64
Appendix 9 – Material properties – Young moduli, strength values, densities	65
Appendix 10 – Calculated properties – moment of inertia, bending stiffness, weights.....	66
Appendix 11 – Loads	67
A11.1. Permanent loads	67
A11.2. Live loads.....	68
A11.2.1. Uniformly distributed load.....	68
A11.2.2. Concentrated load	68
A11.3.3. Maintenance vehicle load	68
A11.3.4. Unauthorized vehicle load	69
A11.3.5. Load on handrail	69
A11.3.6. Load of pedestrian traffic.....	69
Appendix 12 – Partial factors	70
Appendix 13 – Load combinations	71
Appendix 14 –Material properties	72
Appendix 15 – Patran input – Laminates layup.....	73
Appendix 16 – soil information	74
Appendix 17 – surface and water levels.....	75
Appendix 18 – list of requirements.....	76
A18.1. Standards	76
A18.2. Functional requirements imposed by the city of Rotterdam:	76
A18.3. Technical design requirements:.....	77
Appendix 20 – Detailed calculation algorithms.....	78
A20.1. Preliminary design.....	78
A20.1.1. SLS checks	78
A20.1.1.1. Natural frequency	78
A20.1.1.2. Deflection check.....	79
A20.1.2. ULS checks.....	81
A20.1.2.1. Normal stress	81
A20.1.2.2. Bending stress – Skin bending strength	82
A20.1.2.3. Shear stress – Web shear strength	83
A20.1.2.4. Compression stress – Webs compression strength	84
A20.1.2.5. Maximum shear stress	85

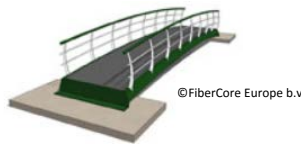


A20.1.2.6. Shear stress – Web buckling	86
A20.1.3. Thermal expansion analysis	87
A20.1.4. Shear stresses in the adhesive bond between steel plate and GFRP skin	88
A20.1.5. Foundation calculations	88
Appendix 21 – Drawings of 30 meter bridge.....	89
Appendix 22 – drawings of 60 meter bridge	90
Appendix 23 – CROW section related to cycling and pedestrian bridge design	91



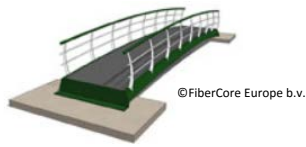
List of figures

Figure 1 - Overview of Rotterdam with the general project area circled in red	2
Figure 2 - Overview of the Rotte with existing crosses shown in red	2
Figure 3 - Location of the bridge	2
Figure 4 - General overview of the project phases	5
Figure 5 - process diagram	5
Figure 6 –GFRP deck with steel bars; drawing not on scale.....	7
Figure 7 – GFRP deck with steel strips; drawing not on scale.....	7
Figure 8 – GFRP deck with rectangular hollow steel profiles; drawing not on scale	8
Figure 9 - InfraCore® inside bridges build-up principle; (FiberCore Europe, 2016)	9
Figure 10 - General layout of an ABD matrix.....	10
Figure 11 - Cross section of bridge deck, not on scale	22
Figure 12 – Top view of plate geometry showing the strips	26
Figure 13 - Top view of the deck with the mesh and nodes present; (Marc-Patran, 2016)	27
Figure 14 - 3D model with 2D elements of bridge deck - cross section	29
Figure 15 - small model with solid elements, representing a part of the deck, used for local effects analysis	29
Figure 16 - Buckling check with different wheel position	31
Figure 17 - Most feasible cross section design.....	34
Figure 18 – buckling of the web under SLS load in eLamX.....	36
Figure 19 - ABD matrix of web	56
Figure 20 – α coefficients	56
Figure 21 - Cross section of one normal core cell with thicknesses and one converted to steel with the transformed area method with equivalent widths.....	60
Figure 22 – GFRP deck with steel bars; drawing not on scale.....	61
Figure 23 – GFRP deck with steel strips; drawing not on scale.....	62
Figure 24 – GFRP deck with rectangular hollow steel profiles; drawing not on scale	63
Figure 25 – Cross section of bridge deck; drawing not on scale	64
Figure 26 - Map showing the positions of the two CPT test in relation to the project location.....	74
Figure 27 - Soil profiles for the north (left) and south (right) bank of the Rotte	74
Figure 28 - road level for the north and south bank of the Rotte at the location of the proposed bridge	75
Figure 29 - Location of the water level information and table showing the minimum water level towards NAP.....	75
Figure 30 – N line of largest horizontal load	81
Figure 31 – M-line of Load case 3 – decisive	82
Figure 32 – V-line of Load case 3 – decisive	83
Figure 33 – buckling of the web under SLS load in eLamX.....	86



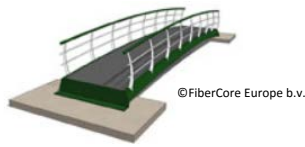
List of tables

Table 1 - most feasible concept designs as concluded by Wilken, (2015)	6
Table 2 - Unit consistency	11
Table 3 - Analysis criteria	18
Table 4 - Initial bridge dimensions	22
Table 5 - Multi Criteria Analysis table with scores	34
Table 6 – Optimized bridge dimensions in meters and millimetres	37
Table 7 - overview showing properties and calculated effects of the deck for initial and optimised dimensions; design values.....	37
Table 8 - Results comparison between analytical and FEM calculations.....	41
Table 9 – Bridge dimensions in meters and millimetres	64
Table 10 – Material stiffnesses.....	65
Table 11 – Material strengths and Poisson’s ratios	65
Table 12 – Densities and weights.....	65
Table 13 – Flexural rigidity	66
Table 14 – Moment of inertia	66
Table 15 – Masses	66
Table 16 - Load Cases according to EN.1990+A1+A1/C2:2011	70
Table 17 - Characteristic loads according to Chapter 3.4.3.....	71
Table 18 - Load combinations according to Chapter 3.4.5.....	71
Table 19 - Material properties	72
Table 20 - Nominal value for shear strength.....	72
Table 21 - Plies layup in the webs	73
Table 22 - properties of bulkhead laminate.....	73
Table 23 - properties of top skin laminate	73
Table 24 – structure of the core with and without steel members	73
Table 25 – properties of bottom skin laminate.....	73
Table 26 – properties of flange laminate	73
Table 27 – properties of side laminate.....	73



List of abbreviations

CROW	Centrum voor Regelgeving en Onderzoek in de Grond-, Water- en Wegenbouw en de Verkeerstechniek
CTE	Coefficient of thermal expansion
CUR	Civieletechnisch Centrum Uitvoering Research en Regelgeving
FEA	Finite Elements Analysis
FEM	Finite Elements Modelling
FRP	Fibre reinforced polymer
GFRP	Glass fibre reinforced polymer
SLS	Serviceability limit state
ULS	Ultimate limit state
UDL	Uniformly distributed load



Nomenclature

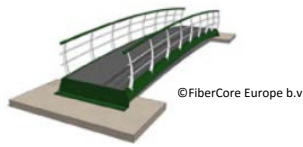
A	Surface area
L	Length of the bridge
b	Width of the bridge
h	Height of the bridge
t	Thickness
E	Stiffness
I	Second moment of area (moment of inertia)
EI	Flexural rigidity
f	Natural Frequency
K	Harmonic constant
g	Gravitational acceleration
m	Mass of the bridge
P	Applied force
p	Pressure
q	Distributed load
T	Temperature
w	Weight of the bridge

Greek letters

α	Coefficient of thermal expansion
γ	Reduction factor
Δ	Change or difference of a quantity
δ	Deflection
ν_f	Fibre-volume fraction
ρ	Density
σ	Normal stress
τ	Shear stress

Subscripts

0	design or initial value
c	composite
exp	expansion
f	fibre
m	material
max	maximum
min	minimum
n	natural or related to the mode of vibration
sls	serviceability limit state
uls	ultimate limit state
x	in longitudinal or 0° direction
y	in transverse or 90° direction
ts	top skin
bs	bottom skin
w	web
steel	steel



1. Introduction

The first chapter of the current document firstly introduces the company where the researcher performed the graduation thesis, then presents general information regarding the location where the project will be implemented. Afterwards, the problem FiberCore Europe is currently facing is developed. Subsequently, the research goal, main and sub questions are formed. Lastly, the procedure of the current research is outlined.

1.1. Terms of reference

This report is a part of the graduation portfolio of Teodor Gheorghe, graduation candidate from the HZ University of Applied Sciences. The beneficiaries of this paper are FiberCore Europe and HZ University of Applied Sciences. The deadline for completion is 06 June 2016. The research will be structured as a case study and its scope is to design a 30-meter-long bridge made from an innovative GFRP-steel hybrid material for the Municipality of Rotterdam. This supervisors for the current report are M. Veltkamp from FiberCore Europe and A. Repko and J. de Keijzer from HZ.

1.2. Company background

FiberCore Europe is a Dutch company that specialises in the design and construction of load-bearing structures in fibre reinforced polymers, (FRP), also referred to as fibre-reinforced plastic, which is a composite material made of a polymer matrix reinforced with fibres.

Currently, the company focuses on glass fibre reinforced polymer (i.e. GFRP) bridges. They have already successfully implemented a wide variety of these structures, ranging from lightweight short-span bridges in golf courses to larger cycling or road bridges. These bridges meet all design requirements as imposed by the Eurocodes, which includes 60t vehicles. One of the company's latest developments is the design construction and subsequent installation of GFRP lock gates.

As stated before, the material used by FiberCore Europe in its bridges is glass fibre reinforced polymer (GFRP). The company has developed a construction method for robust, heavy-duty, load-bearing panels, named InfraCore®, where the top-skin of the panels is integrally connected with their bottom skin through the continuity of glass fibres. This material and its technology have several decisive advantages when compared to its conventional counterparts, namely steel and concrete.

First and foremost, it will not corrode in wet environments and it is not sensitive to de-icing salts. Another competitive strength of this material is that it is considerably lighter than the conventional alternatives. Consequently, transportation and installation costs are relatively low, and foundations can be constructed simpler and less costly. Additionally, the GFRP structures are virtually maintenance free. Finally, even though initial production costs may be higher than those of a conventional bridge, due to the long technical lifespan, light and shallow foundations (e.g. no piling necessary), easy transportation, fast installation and low maintenance costs, the total life-cycle costs are considerably less.

1.3. Assignment background

It has been determined by FiberCore Europe that with bridge spans increasing beyond 30 m, the buildability and competitiveness determined by cost effectiveness and lightness become problematic. Consequently, in order to be able to implement longer bridges, the GFRP composite must be combined with other materials to increase its stiffness.

Generally speaking, the main contributor to costs for a bridge is the height of the cross section, however, with the material currently used by FiberCore Europe (i.e. GFRP) in its bridges, the height provides the necessary stiffness. The arising challenge was to determine that if by replacing certain components of the cross section with stiffer materials, the design height and consequently the overall mass and costs could be reduced.

Two hybrid composite materials had been analysed in a previous research done by Wilken (2015) at FiberCore Europe. These alternatives, namely a combination of glass fibres and carbon fibres in a polyester matrix and a combination of glass fibres and steel components were proposed and examined in order to determine whether these hybrids were able to overcome the limits of the material being currently used.

Several cross section designs were proposed for each hybrid material and they were analysed with regards to costs, weight and slenderness. Subsequently, the dimensions of the cross sections were optimised using an Excel algorithm developed by the researcher, wherein the bridge was modelled as a beam. Additionally, several small scale tests were performed in order to ensure the effectiveness and feasibility of such hybrid materials. These tests were aimed at checking whether steel fully embedded in GFRP corrodes or not and whether the resin used to bind the steel to the skin is strong enough to deal with occurring stresses. Further detailing of the experiments and relevant conclusions for the present research can be found in Chapter 2. It is important to mention however that no structural analysis was performed on any of the cross sections when applied in a bridge design during the aforementioned research, thus the purpose of the current project.

1.4. Project location background

In the north-eastern part of Rotterdam, in the outskirts, there is a tranquil area, popular among cyclists, especially during the summer, as there are several parks, a golf course as well as some water bodies, making it an attractive location for sports and recreation. The area in question is located at the border between Prins Alexander district, belonging to the city of Rotterdam, and the city of Bergschenhoek, belonging to the municipality of Lansingerland. The two aforementioned municipalities are separated by the river Rotte (see Figure 1).



Figure 1 - Overview of Rotterdam with the general project area circled in red

The site is presently served by several roads and many cycling tracks, however, there are only two crossings of the Rotte river over a distance of more than one kilometre (see Figure 2). Therefore, due to the popularity of the area, the City of Rotterdam desires a third bridge to ease the crossing of the river and consequently improve access to the recreational area.



Figure 2 - Overview of the Rotte with existing crosses shown in red

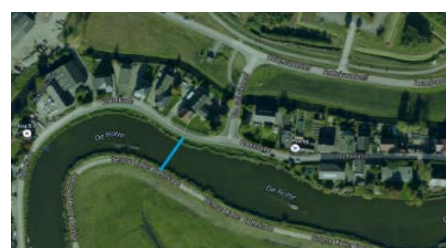
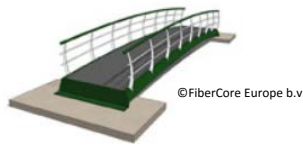


Figure 3 - Location of the bridge



The future bridge will connect the Bergse Linker Rottekade with the Rottekade, the two roads on either side of the Rotte. It will be located in the upside down V shaped meander of the river (see Figure 2). The reason for choosing this crossing point is that at this location the Bergse Linker Rottekade is connected to the larger Rottebandreef via the Van Schaikdreef, therefore access to the recreational facilities is provided. At this location the crossing distance is 30 meters (see Figure 3).

1.5. Problem statement

With bridge spans increasing beyond 30 m, the buildability and competitiveness of FRP bridges become problematic. In order to be able to overcome this limitation, it has been concluded in a previous research done by FiberCore Europe that the GFRP composite should be combined with steel components in order to increase its stiffness.

1.6. Research goal

The current research will address the structural analysis on both a global and a detailed level of scale, in particular on the aspects related to the hybrid material. The global aspect will deal with overall behaviour of the deck under the influence of external actions while the local aspect will deal with specific behaviour of cross sectional elements, either on their own, or in relation with others, when subjected to the same external actions.

Therefore, the goal of the hereby proposed research is to determine the optimum cross section of a 30 meter bridge deck, made of a GFRP-steel hybrid material which will be implemented in a cycling and pedestrian bridge over the Rotte near Prins Alexander district, Rotterdam.

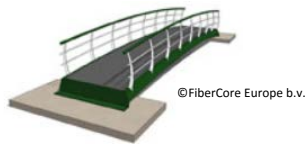
1.7. Research question

The main research question that has been derived from the goal is formulated as follows:

How can an optimal, structurally justified GFRP-steel hybrid bridge deck be designed so that it is suitable to be implemented in a 30-meter-long cycling and pedestrian bridge over the Rotte near Prins Alexander district, Rotterdam?

In order to answer the main question, several more specific sub questions can be devised that will ease the process by dividing the project into smaller areas focused on particular objectives:

- What are the requirements necessary for a successful implementation of a 30 meter span cycling and pedestrian bridge with a GFRP-steel composite deck over the Rotte near Prins Alexander district, Rotterdam?
- What are the boundary conditions and assumptions required for designing such a structure?
- How can the most feasible solution be implemented?
- How can the chosen concept design be structurally analysed and proven feasible for implementation over the Rotte, in Rotterdam?
- How can the design be made efficient, with regards to cross section elements' dimensions, using the FEM software Marc-Patran?
- What mandatory structural checks must be performed in order to ensure the deck's compliance with regulations and requirements?
- How is thermal expansion influencing the solicitation if the bonding between GFRP and steel?
- How are the external forces acting on the deck influencing the bond between steel and GFRP?
- What happens when the adhesive bond fails?
- Having designed an optimum cross section for a 30 meter bridge, what is the maximum span that can be achieved with it if fully fixed supports were used?



1.8. Procedure

In February 2016, the city of Rotterdam expressed their need for a new 30-meter-long bridge over the Rotte in Rotterdam. FiberCore Europe initiated a research and design project, aimed at determining the optimum bridge cross section made from a steel-GFRP hybrid composite material and implementing it into the design of the bridge as per the client's specifications.

The first step was to devise the theoretical framework, presenting information about the composite material and its properties, as well as important considerations when designing a bridge with such materials. Therefore, algorithms and design values for calculating adhesive bond stresses, thermal stresses, natural frequency and composite plate buckling were researched and presented.

The next step was to define three concept designs and determine the most suitable one via a multi criteria analysis. The aforementioned concept designs were based on the findings of a previous research while the multi criteria analysis was designed specifically for this research. The latter compared the proposed concept designs in matters of design, procurement and production challenges, material and production costs, fabrication time, risks, as well as steel contribution to overall stiffness.

Subsequently, using the previously determined concept design and information provided by FiberCore Europe, a cross section with initial dimensions was developed

The algorithms described in the theoretical framework were compiled into a spreadsheet, used to analytically determine the values for natural frequency and deflection, normal, bending and shear stresses, together with the compression stresses and critical buckling factor of the webs, thermal and adhesive bond stresses. The aforementioned dimensions were inputted and the results, together with the design values, served at optimizing the cross section.

At the same time, 1D and 2D FEM models were created. Their purpose was to enable the researcher to learn the software while at the same time getting closer to the detailed design phase which involved 3D FEM models. The results of these models were checked against the ones obtained analytically, as a validation of the former.

Afterwards, the optimised cross section was modelled in 3D and thus, more detailed effects (i.e. adhesive bond stresses, thermal stresses, natural frequency and web buckling) could be observed and checked against the design values.

The results obtained using FEM modelling were used to determine the optimum dimensions for a bridge's cross section that satisfied the initial project requirements.

In order to provide a more complete picture of the research, using the same cross section, but renouncing the simply supported foundation, the maximum span for which the natural frequency requirement could be met was determined and a possible design of such a bridge (i.e. comprising of design considerations and drawings) was briefly outlined.

Finally, the conclusion of the report was that such a bridge can indeed be constructed with the specified hybrid composite material which fulfilled the design requirements. Additionally, the results can be used for designing and building longer spans in the future. Moreover, the limit of this cross section can be tested by determining the longest span a bridge can have with fully fixed supports.

Figure 4 presents a brief overview of the general sections of the project, while Figure 5 presents the process diagram which illustrates all the steps that were taken in order to successfully complete the current project. Additionally, the preliminary and detailed design phases are highlighted in order to facilitate the understanding of the dependencies between them.

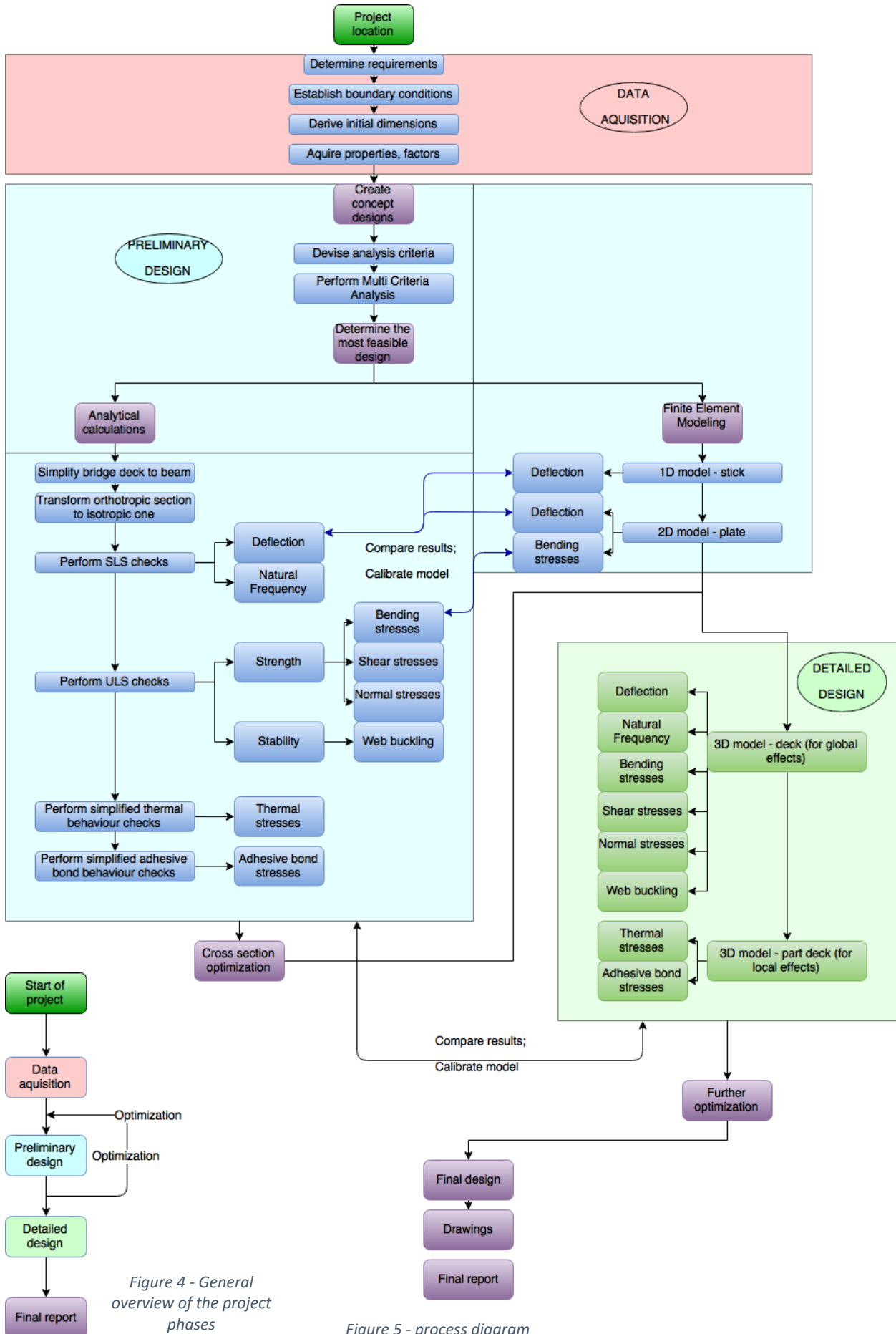
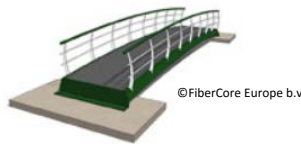


Figure 4 - General overview of the project phases

Figure 5 - process diagram



2. Theoretical framework

The purpose of this chapter is to present the theoretical knowledge related to the topic researched in the present report. The information is to be classified into sub-chapters in order to give a clear overview about the topics the thesis dealt with. The first subchapters present the starting points of the project. Furthermore, the origin together with the advantages and disadvantages of the concept designs are presented. Furthermore, the composite material, properties and design considerations are introduced. Afterwards, the concept of FEM is explained together with its purpose in this project. Lastly, the calculation algorithms and principles relevant for the preliminary and detailed design phases are explained with their full descriptions and formulae being presented in the relevant appendices.

2.1. Starting points and design considerations

The current subchapter briefly outlines major aspects that had a considerable impact on the design. These were subsequently detailed in chapter 3.3

- The overall length of the bridge had to be 30 meters, due to the location imposed by the client;
- The width of the bridge had to be 4,5 meters due to the necessity to accommodate a 2-lane cycling path and facilitate 2-way pedestrian traffic flow;
- The clearance, both related to the width and height, was specified by the City of Rotterdam, as required for the respective location
- The required clearance and local bank levels imposed higher abutments and soil addition
- The soil conditions indicate that the usual pad foundation is sufficient for such a bridge.

2.2. Concept designs

The current subchapter presents the concept designs that were selected for the alternative study, explains their source and reasons for choosing and formulates the theoretical knowledge required for creating the analysis criteria to evaluate them.

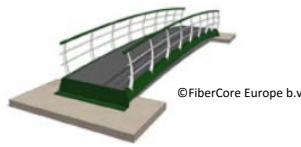
As stated in the introduction, a previous research had already been conducted at FiberCore Europe by Wilken, (2015) on the topic of determining the most economically advantageous combination of steel and GFRP in a bridge deck longer than 26 meters. The researcher proposed methods for increasing the stiffness of a GFRP bridge in the shape of adding either steel or carbon fibre elements. Subsequently, concept designs containing different sizes and placement of these members were developed. The purpose was to decide at a concept level, which material and which placement would be advantageous in relation to costs deck thickness and mass.

Therefore, for the current project, the top three solutions determined to be the most advantageous in the research conducted by Wilken (2015) were considered for implanting in a 30 meter bridge to be placed over the Rotte. These solutions are briefly presented in Table 1 and further detailed below.

Table 1 - most feasible concept designs as concluded by Wilken, (2015)



Following an interview with FiberCore Europe, the criteria on which the analysis of the three cross sections was based were defined. It was established that, considering FiberCore Europe also deals with the production of bridges, not only design but also procurement and manufacturing challenges should be considered. Subsequently, the advantages and disadvantages posed by each of the three designs in relation to the abovementioned criteria were determined.



2.2.1. Concept design 1 – steel bars

The first concept proposed the introduction of steel components as steel bars, fully enclosed in the GFRP deck, attached to the bottom of the top skin and the top of the bottom skin in every core cell, as shown in Figure 6. Below, the advantages and disadvantages posed by this design are listed. For a comprehensive explanation, see Appendix 7

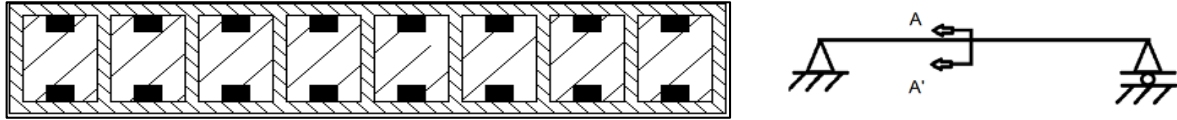


Figure 6 –GFRP deck with steel bars; drawing not on scale

Advantages:	Disadvantages
Flexibility of steel bars;	Design challenges
Shape of steel bars;	Connection between steel members and GFRP skins along the entire length.
Contribution of steel members to bending stiffness;	Procurement challenges
Low stress concentrations.	Procurement of steel members;
	Procurement of different foam blocks;
	Increase in procurement costs;
	Increase in lead time.
	Manufacturing challenges
	Number of cranes required for the placement of the steel members;
	Increase in production time;
	Placement of steel in the optimal position;
	Different web fabrication design;
	Risks posed by new manufacturing processes.

2.2.2. Concept design 2 – steel sheets

The second concept design was similar to the first one. The difference was that the steel bars were wider so that they filled the entire width of the core cell. As before, the steel sheets will be present both at the top and bottom of the cross section (see Figure 7). Below, the advantages and disadvantages posed by this design are listed. For a comprehensive explanation, see Appendix 7

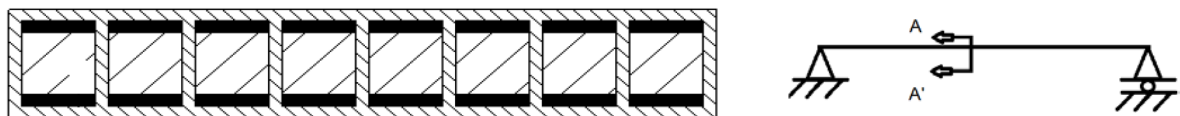
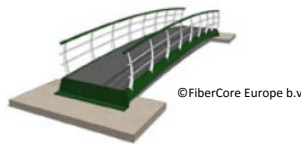


Figure 7 – GFRP deck with steel strips; drawing not on scale

Advantages:	Disadvantages
Flexibility of steel bars;	Design challenges
Shape of steel bars;	Connection between steel members and GFRP skins along the entire length.
Contribution of steel members to bending stiffness;	Procurement challenges
Low stress concentrations.	Procurement of steel members;
	Customization of steel members;
	Procurement of different foam blocks;
	Increase in procurement costs;
	Increase in lead time.
	Manufacturing challenges
	Number of cranes required for the placement of the steel members;
	Increase in production time;
	Different web fabrication design;
	Risks posed by new manufacturing processes.



2.2.3. Concept design 3– Rectangular hollow profiles

The last concept proposes the introduction of steel rectangular hollow sections only in the outermost core cells (see Figure 8), thus acting like the beams supporting the concrete slab on a traditional bridge. Below, its advantages and disadvantages are listed. For a detailed explanation, see Appendix 7.

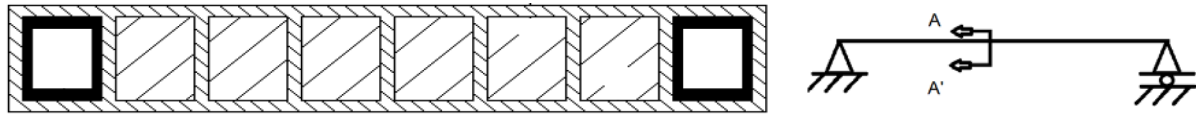


Figure 8 – GFRP deck with rectangular hollow steel profiles; drawing not on scale

Advantages:	Disadvantages
Number of required steel profiles;	Design challenges
Placement of steel profiles;	Stress concentrations around the steel members (i.e. near the sides of the deck).
No changes to the deck apart from the edges;	Procurement challenges
Adhesive bond is no longer a concern;	Procurement of steel members;
Less foam is required;	Customization of steel members;
Increase in torsional rigidity.	Pre cambering of beams;
	Welding of steel;
	Increase in procurement costs;
	Increase in lead time.
	Manufacturing challenges
	Number of cranes required for the placement of the steel members;
	Increase in production time;
	Necessity to make the steel profiles airtight during the infusion process;
	Risks posed by new manufacturing processes.

2.3. Composite properties

The present sub-chapter provides insight into the material that was used over the course of the current project, starting from basic elements, and ending with the composite material that will subsequently be combined with steel.

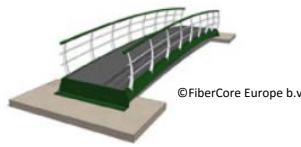
2.3.1. General considerations

According to Gurit (2016), a composite material is composed of at least two elements that, when put together, produce different material properties than each of them on their own. He then explains that usually, most composites consist of a bulk material or a matrix and reinforcement, that is usually in fibre form, and whose purpose is to increase the strength and stiffness of the matrix. Furthermore, Gurit (2016) states that the most common type of composites are the polymer matrix composites, also known as Fibre Reinforced Polymers (FRP).

Afterwards, Gurit (2016) outlines the properties that determine the characteristics of a composite laminate, namely: the properties of the fibres and resin, the ratio of fibres to resin (i.e. the Fibre Volume Fraction) together with the geometry and orientation of the fibres.

2.3.2. Composite design

When designing a structure with any materials, composites included, a structure has to withstand the following direct loads: tension, compression, shear and flexure. Characteristic of composite materials is that the tensile and bending strength is given by the fibres and the compressive and shear strength is dictated by the properties of the resin binding the glass fibre plies.



Furthermore, another important aspect in composite design is the Rule of Mixtures which states that simple properties of composite materials can be estimated based on the contribution of each part to the composite with the following equation summarizing this concept for a 2 component composite:

$$V_f + V_m = 1 \text{ (Where } V_f = \text{ volume fraction fibre and } V_m = \text{ volume fraction matrix)}$$

Another important aspect when designing with composites is the build-up of a laminate. Specifically, the stacking sequence and the two properties, namely symmetry and balance. The former refers to having the same number and orientation of plies above and below the mid-plane of the laminate and the latter denotes a laminate having an equal number of +/-45° plies. Having a symmetric laminate prevents warping and having a symmetric one prevents shear coupling (i.e. twisting of the laminate under certain loading).

2.3.3. Sandwich panels

Gurit (2016) states that single skin laminates are strong, but they can lack stiffness due to their relatively low thickness. The stiffness of these panels can be increased by the addition of frames and stiffeners, which add weight and complexity to the structure.

A sandwich normally consists of two skins separated by a core material whose purpose is to increase the panel's stiffness without adding much weight as results from the engineering theory that describes the bending stiffness of a panel as being directly proportional with the cube of its thickness. Thus, a sandwich acts as an I beam with the skins corresponding to the flanges and the core to the web.

Ordinary panels possess inherent weaknesses, such as cracking, delamination or de-bonding. These failure mechanisms occur due to the way the components are connected to one another, thereby making them unsuitable for use in bridges with high intensity traffic.

2.3.4. InfraCore® technology

FiberCore Europe developed an innovative way to manufacture composite bridges so that the abovementioned weaknesses of the traditional sandwiches are overcome. Due to the application of a proprietary technique, named InfraCore® Inside, structures become very robust and keep performing their function under continuous loading and even after impact damage.

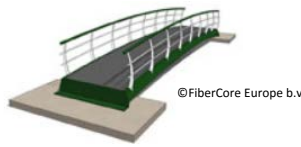
According to FiberCore Europe (2016), an InfraCore® Inside bridge is built from lightweight foam core cells, wrapped in dry fabric of glass reinforcement fibres. Between, over and under these cells, one or more so-called Z-layers are draped (see Figure 9). The number and orientation of the plies is determined by the loadings that act on the deck. Thus, each of the four fibre orientations is the best in dealing with a certain kind of loading type (i.e. bending, shear, normal).



Figure 9 - InfraCore® inside bridges build-up principle; (FiberCore Europe, 2016)

2.3.5. Laminate properties

The properties of a laminate can be shown in an ABD matrix. Autodesk (2014) explains that in Classical Laminate Theory, the [A], [B] and [D] matrices jointly form the laminate compliance matrix that is used



to express laminate resultant forces per unit width $\{N\}$ and laminate resultant moments per unit width $\{M\}$ in terms of laminate mid-plane strains $\{\epsilon^0\}$ and laminate mid-plane curvatures $\{k\}$ (see Figure 10).

$$\begin{Bmatrix} N_x \\ N_y \\ N_{xy} \\ \dots \\ M_x \\ M_y \\ M_{xy} \end{Bmatrix} = \begin{bmatrix} A_{11} & A_{12} & A_{16} & | & B_{11} & B_{12} & B_{16} \\ A_{12} & A_{22} & A_{26} & | & B_{12} & B_{22} & B_{26} \\ A_{16} & A_{26} & A_{66} & | & B_{16} & B_{26} & B_{66} \\ \dots & \dots & \dots & \dots & \dots & \dots & \dots \\ B_{11} & B_{12} & B_{16} & | & D_{11} & D_{12} & D_{16} \\ B_{12} & B_{22} & B_{26} & | & D_{12} & D_{22} & D_{26} \\ B_{16} & B_{26} & B_{66} & | & D_{16} & D_{26} & D_{66} \end{bmatrix} \begin{Bmatrix} \epsilon_x^0 \\ \epsilon_y^0 \\ \gamma_{xy}^0 \\ \dots \\ \kappa_x \\ \kappa_y \\ \kappa_{xy} \end{Bmatrix}$$

The individual [A], [B] and [D] matrices are termed:

- [A] – extensional stiffness matrix;
- [B] – extension – bending coupling matrix;
- [D] – bending stiffness matrix.

Figure 10 - General layout of an ABD matrix

According to Warnet & Akkerman (2009), the components of the ABD matrix have distinct units. Due to the fact that loading is usually expressed per unit width, the A components are expressed in [N/m], the B-components in [N] and the D-components in [Nm]. For the purpose of calculating certain laminate properties during the current project, only the D values of the matrix were required.

In order to obtain the ABD matrices for the laminates used in the current bridge design, the eLamX software was used. It calculates the ABD matrix of a laminate from the properties of a ply together with the number and orientation of plies in a certain laminate. (Hauffe, 2016)

2.3.6. Material properties

In order to perform both analytical calculations and FEM modelling of a bridge deck, the properties of the materials are required. For undertaking the current project, several specific properties are required for GFRP laminates, steel, PU foam cores and polyester resin. These properties were provided by FiberCore Europe, (2016) and an overview has been provided in Appendices 9 and 14. The former presents the properties required for the analytical part and the second contains the properties required for the FEM software, transformed for unit consistency purposes.

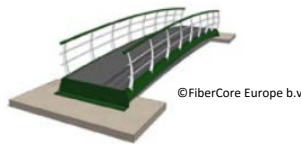
2.4. Finite Element Analysis

The current subchapter defines what Finite Element Modelling is and what its purpose in the current project was. Furthermore, it outlines several points of attention, important to consider when using such a software.

Autodesk (2015) describes finite element analysis (FEA) as a computerized method for predicting how an object reacts to real-world forces, vibration, heat, fluid flow, and other physical effects. Specifically, it shows whether a product will deform, or simply work the way it was designed. It is called analysis, but in the product development process, it is used to predict what is going to happen when the product is used, this way allowing fast design iterations.

Furthermore, Autodesk (2015) states that FEA works by breaking down a real object into a large number (thousands to hundreds of thousands) of finite elements, such as little sticks, plates and cubes, together forming a Finite Element Model (FEM). Mathematical equations for each individual element predict the behaviour of each element. A computer then adds up all the individual behaviours to show the overall behaviour of the actual object.

For the current research and design thesis, the software combination Marc-Patran was used for modelling. Patran is the pre- and post- processing tool used for creating the geometry, inputting and assigning materials, creating loads and boundary conditions and meshing the model in order to create final elements. Afterwards, the solver, Marc, analyses the model. The outcome can be viewed in Patran and can be customized in order to ensure the desired results are visible.



It is important for the current project to take into account an important pitfall of modelling in such a program, specifically the mesh size. It defines the accuracy of the results of the analysis, while at the same time having an impact on the analysis time. The generic rule is to use a coarse mesh at first. Subsequently, it can be refined by creating smaller elements. If the results vary only slightly, the original mesh size should be used since thus, the analysis takes less time. Additionally, the mesh can be fine-tuned in such a way that it is finer in an area of interest and coarser elsewhere in order to reach a compromise between analysis time and results accuracy.

Table 2 - Unit consistency

Another aspect to consider is that Patran does not show units for the values inputted. Therefore, consistency had to be ensured by establishing the correct units for all parameters, as described by Gokhale et al, (2008) and presented in Table 2. Comparison between analytical and FEM results served as demonstration of the consistency of these units. (Gokhale, Deshpande, Bedekar, & Thite, 2008)

Property or load	Unit
Mass	tonne
Length	mm
Temperature	K
Force	N
Moment	N*mm
Density	tonne/mm ³
E-modulus	MPa = N/mm ²

2.5. Calculation algorithms

The current chapter presents the algorithms that were used for the proposed design. Each of the following subchapters defines an individual calculation method, explains its principle and states its source.

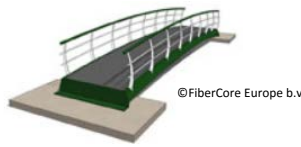
2.5.1. Transformed area method

This method is used when the structural member that needs to be analysed is not homogenous (i.e. it is comprised of more than one material). According to Philpot (2011), using this method, the original cross section (comprised of two materials) can be transformed into an equivalent cross section consisting of only one material. The method takes into account the difference between elasticity moduli and converts the transformed material into the original one with a different width.

The advantage provided by this algorithm was that the cross section used in the current project could be analytically analysed. Specifically, by converting the orthotropic section to a homogenous one, the bending stresses could be determined with the Euler-Bernoulli beam equation, due to the fact that it now fulfils all the simple bending theory conditions. Furthermore, shear stresses could be determined with the beam shear or Zhuravskii shear stress formula. The detailed description of this algorithm and its application to the current project is presented in Appendix 6.

2.5.2. Corrosion of steel embedded in GFRP

Steel is a material well known for its degradation over time under the influence of oxygen and moisture. This process is known as corrosion and it affects the lifespan of a structure when it manifests. It is important for FiberCore Europe to know whether incorporating steel in a GFRP cross bridge deck will affect the lifespan of 100 years that can currently be achieved. For this purpose, Wilken (2015) performed corrosion tests on steel embedded in GFRP in order to ascertain the behaviour. The experiment concluded that by fully encapsulating the steel inside the GFRP, and covering the latter with a layer of gelcoat and one of topcoat the steel will be prevented from corroding, as long as the protective outer surface remains intact. Therefore, for the current project, due to the fact that only fully encapsulated steel is considered in the design, the assumption that it will not corrode is valid.



2.5.3. Adhesive bond strength between steel and GFRP

An important aspect to consider when analysing hybrid materials is the strength of the connection between the individual components. In order to determine the stresses that occur in the bonding layer between a steel plate and GFRP skin, Wilken (2015) tested the adhesive bond strength between SR235JR structural steel and glass fibre reinforced Synolite 1967 polyester with respect to two different pre-treatments. The experiment concluded that the shear strength of the adhesive bond was 5,9 MPa. He then states that this is considered to be a conservative value due to the nature of the test which consisted of small sized samples. Therefore, the 5,9 MPa was considered the design strength value of the adhesive bond between steel and GFRP.

2.5.4. Thermal stresses

Most materials exhibit changes in dimension in reaction to changes in temperature, specifically expand when warmed up and contract when cooled down. The degree to which a material changes its dimensional properties as a result of changes in temperature is indicated by its coefficient of thermal expansion (CTE), often indicated by the Greek letter α . When materials with different CTE's are interconnected and movement is constrained, thermal stresses occur as a result of changes in temperature. Through Classical Laminate Theory the CTE of laminates can be determined, since the individual components vary depending on the fibre volume content and the fibre orientation. During the current project, the CTE of the laminate was used, not the ones of the component materials. The laminate's CTEs in the longitudinal (i.e. x) and transverse (i.e. y) direction as used in typical bridge designs by FiberCore Europe, (2016) are: $\alpha_x = 8.22 * 10^{-6} \frac{m}{m*K}$; and $\alpha_y = 3.71 * 10^{-5} \frac{m}{m*K}$

For composite bridges, there are no regulatory guidelines for thermal loads. In practice, the temperatures used for calculations of thermal expansions and stresses were derived from the NEN-EN-1991-1-5 standard with national annexes NEN 1 and NEN 2. This standard prescribes temperature ranges for bridges made from concrete and steel. The reaction of composite bridges to temperature is more similar to concrete bridges than to steel bridges, mainly due to its relatively low conductivity and therefore the temperatures prescribed for the former structures are used. The temperatures used in the current design are defined as follows:

- Maximum temperature range contraction: $\Delta T_{N.con} = T_0 - T_{e.min} = 27 \text{ }^\circ\text{C}$
- Maximum temperature range expansion: $\Delta T_{N.exp} = T_{e.max} - T_0 = 22 \text{ }^\circ\text{C}$

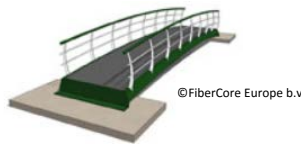
Wilken (2015) performed an experiment on thermal stresses whose conclusion was that the compressive and tensile stresses in the individual materials are considerably low compared to allowable stresses in the materials. This result was considered as an initial assumption in the current report's calculations.

Appendix 2 provides a more detailed description of the algorithm used to calculate the thermal, expansion and corresponding stresses generated in the two materials, as derived from the information provided above.

2.5.5. Dynamic behaviour

According to Feldmann & Heinemeyer (2008), lightweight footbridges have small mass, which reduces the mass inertia and which lowers natural frequencies, resulting in a greater risk of resonance.

Feldmann & Heinemeyer (2008) then explain that resonance occurs if the frequency of the bridge coincides with the frequency of the excitation. Pedestrian induced excitation is an important source of vibration of footbridges and the loading caused by it is unsteady, transient and oscillating in a small



range of excitation frequency. It is therefore clear that dynamic responses play a fundamental role in the design of vibration susceptible structures. Vibrations of footbridges can lead to serviceability problems, as effects on the comfort of pedestrians might occur.

Since the bridge designed in the current project is modelled as a simply supported beam, the first natural frequency can be calculated with the following formula:

$$f_{K,dTC} = \frac{K_n}{2\pi} * \sqrt{\frac{\frac{EI}{\gamma_{m,SLS} * \gamma_{cl,v}} * g}{(q_M + d_{TC} * b_{eff}) * L^4}}$$

For a uniform beam with the aforementioned support and loading conditions, K_n has a value of 9.87. This value is based on perfectly hinged supports without any restraining moment. The actual frequency is higher. For this reason, FiberCore Europe studied the influence of abutment supports and the added stiffness of the railings on 20 bridges after installation and determined that the natural frequency can be increased by 18%, incorporating a so called Panos-factor yield for the harmonic constant. Therefore,

$$K_n = 9.87 * 1.18 = 11.65$$

It can be observed that the flexural rigidity, weight and the dimensions of the deck have considerable influence on the natural frequency, with the length having the largest impact. Additionally, it can be noted that with increasing the dimensions and weight, the natural frequency decreases.

A critical range is determined by the dominant contribution of the first harmonic which characterises pedestrian effects. For longitudinal vibrations, this range is calculated as: $1,25 \text{ Hz} \leq f_i \leq 2,3 \text{ Hz}$. (Feldmann & Heinemeyer, 2008)

The Eurocodes do not specify a limit for the frequency, only for maximum vertical accelerations. However, a relation between deflection and natural frequency is provided in EN 1991-2:2003 6.4.4 [Note 8] in the shape of:

$$n_0 = \frac{17,75}{\sqrt{\delta_0}}$$

Where n_0 represents the natural frequency and δ_0 the deflection at mid-span due to permanent loads.

2.5.6. Creep behaviour of GFRP members

GFRP members creep over time. The creep is translated into design parameters as long term creep. In order to realistically determine the deflection of a bridge deck, not only deflection due to self-weight and live load are required, but also the deflection at the end of the lifespan, defined to be 100 years.

In order to determine the additional deflection caused by creep, the CUR-aanbevelingen 96. (Civieltechnisch Centrum Uitvoering Research en Regelgeving, 2003) provides an algorithm whose purpose is to determine an adjusted lower value of the laminate's elasticity modulus. The explicit algorithm that was used for determining this value is shown in Appendix 3.

2.5.7. Buckling of composite plates

In case of large magnitude concentrated loads, such as wheel loads of maintenance or accidental vehicles being applied on a bridge deck, the webs can buckle. In order to check the stability of the webs, an algorithm also provided in the CUR was used.



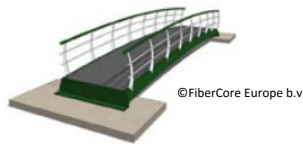
The algorithm only assumes uniformly distributed loads being applied on edges of composite plates, therefore it was only used to determine a critical buckling factor under the ULS uniformly distributed load which was afterwards used to check the FEM results. Having established that the FE model was accurate, the buckling factor under wheel load was determined.

The critical buckling factor represents the bearing capacity of the plate before it buckles. In order to determine the critical buckling load (i.e. the load under which the plate buckles), the critical buckling factor has to be multiplied with the applied load. Therefore, in order to prevent a plate from buckling, a critical buckling factor larger than 1 is required.

The formula for calculating the abovementioned factor together with the required parameters are presented in Appendix 4.

2.5.8. Shear stresses between two different materials

Another important check that had to be made was shear stresses in the adhesive bond between the steel plates and the GFRP skins. In order to determine these stresses analytically, the Zhuravskii shear stress formula can be used, with a modification that accounts for the difference in elastic moduli between the two materials and the location of the adhesive bond with regards to the neutral line of the cross section. The detailed algorithm can be seen in Appendix 5.



3. Methodology

The aim of the current chapter is to use the knowledge provided above in order to form the procedure that was used to answer the sub questions and, in turn, the main question stated in the first chapter of the present document.

3.1. Overview of content and scope limitations

The current subchapter outlines the aspects the current thesis is dealing with and those that have been left outside its scope due to time limitations.

Therefore, the current thesis dealt with:

- Determining the most suitable cross section design made from GFRP-steel hybrid;
- Structurally analysing it analytically in order to optimise its dimensions;
- Structurally analysing it with FEM in order to further optimise it;
- Proving that the combination of steel and GFRP technically feasible to build;
- Providing a design for a 30 meter bridge having the aforementioned optimised cross section;
- Testing the limits of the respective cross section by proposing the longest fully fixed bridge that can meet the most critical requirement

Furthermore, due to time constraints, the scope of the thesis was limited by not considering or detailing the following:

- No new cross section designs were considered, due to the fact that the chosen ones were already favoured due to their advantages outlined by Wilken, (2015).
- The impact of the GFRP-steel material combination on the existing production process was only briefly considered.
- Accessories, such as pipes, cables, sidewalks were not considered on the deck for the structural analysis.
- Detailed complex effects such as thermal fatigue, thermal cycles, impact of production temperature were not analysed.
- The structural effect of the railings on the deck was not analysed.

3.2. Research method

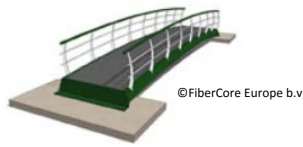
The research method employed for the current project was desk research. This can further be divided into analytical part and FEM modelling. Furthermore, it was a mixed method research, combining qualitative and quantitative methods.

3.3. List of requirements

In order to design a bridge, the necessary requirements had to be determined first. They originated from different sources, based on the aspects they are related to.

The most important requirements when designing a structure come from the Eurocodes together with the national annex for the country the structure is intended for. Additionally, each country has strict regulations for buildings and civil engineering structures that must be met before it is approved.

Therefore, for the current project, the general construction regulations could be found in the Bouwbesluit. Furthermore, the elements related limit states, design limits, combinations and load factors have been taken from Eurocode 0, EN 1990.2002 (European Committee for standardization, 2002) and the actions on bridges, namely permanent and live loads have been obtained from Eurocode



1, EN 1991.2.2003. (European Committee for standardization, 2003) Subsequently, the material factors and properties for GFRP such as density, design strength values, stiffness, Poisson's ratio together with those for the polyester resin were taken from the CUR aanbevelingen 96, since there are no for designing structures with this material. (Civieltechnisch Centrum Uitvoering Research en Regelgeving, 2003) All these sources are formally accepted, thereby proving them reliable for the aforementioned purpose.

Furthermore, additional or specific requirements related to location, dimensions, function, lifespan, materials, clearance, accessibility, comfort, maintenance and traffic disruptions were provided by the client, namely the Municipality of Rotterdam. These prerequisites are important since the product has to satisfy the client's necessities.

The requirements obtained as described above are presented in the corresponding chapter of the results section of the current document.

3.4. Starting points and design considerations

By analyzing the current situation, several starting points could be formulated. Therefore, the current sub chapter presents the method through which the design decisions were taken together with their sources. Furthermore, these decisions are presented in the results chapter.

3.4.1. 30 meter bridge

Several design aspects had to be established in order to successfully implement the proposed bridge over the Rotte in Prince Alexander district.

The first step was to research soil information. Therefore, soil profiles for the area have been obtained from Dinolocket, (2016), for both the left and right bank. The website provides a map with CPT tests at various locations in the Netherlands. The reliability of the information provided is backed by the fact that they are an advisory body to the Dutch Central Government regarding the use of the underground. The organization collecting and organising the data on the aforementioned website is "TNO Geologische Dienst" Nederland. (DINOloket, 2016)

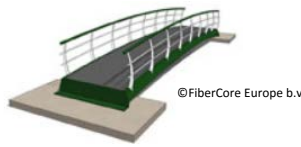
The second step involved obtaining the levels of the north and south side roads and banks. These were obtained from the "Actueel Hoogbestand Nederland" website. The information provided on this website has been realised in cooperation with Rijkswaterstaat, therefore it is valid for infrastructure purposes. (Actueel Hoogbestand Nederland, 2016)

Furthermore, the level of the surface of the water had to be determined. This information can be obtained from the Rijkswaterstaat website that has different monitoring locations where the water level is recorded and plotted in a graph in real time. (Rijkswaterstaat, 2016)

In addition to the information related to the location, several other parameters need to be defined.

The required configuration of lanes, kerbs, sidewalks applicable for a cycling and pedestrian bridge in the Netherlands is regulated by the CROW. (CROW, 2016). Due to the fact that information is available on a membership basis, the source document cannot be viewed without credentials. The information relevant to the current project as prescribed in the CROW can be found in Appendix 23.

Moreover, related to the foundation design for a simply supported bridge, the current design used by FiberCore Europe, (2016) was used. Additionally, the information related to the curvature of the deck and finishing layers was also imposed by FiberCore Europe, (2016).



3.4.2. Maximum span bridge

An important point to FiberCore Europe is the versatility of the current design. Specifically, the range of spans the current cross section design can be applied to. To determine the range, the key aspect that had to be determined was the maximum span that can be achieved using the optimized cross section hereby proposed and designed while satisfying the most critical requirement, the natural frequency. For this purpose, the 3D model with 2D elements was adapted to a longer span and the natural frequency was checked. Since the 30 meter bridge was optimised for the lowest natural frequency, designing a longer simply supported deck with the same cross section was not possible. Therefore, to add the required stiffness, a piled foundation was proposed.

To determine the rotation stiffness of the pile foundation the following procedure was used:

Firstly, the elasticity constant of the pile was determined: $k_{pile} = \frac{E \cdot A}{1,5 \cdot L}$

Next, the reaction forces generated by each row of piles were determined:

$$F_i = \text{no. of piles} * \text{dist. from pile's centre to foundation's centre} * F_{foundation}$$

Afterwards, the moment generated by the foundation was calculated:

$$M = \sum_{i=1}^2 (2 * \text{no. of piles} * \text{dist. from pile's centre to foundation's centre} * F_i)$$

Subsequently, the maximum displacement was determined: $u_{max} = \frac{F_i}{\text{no of piles} * k_{pile}} * F_{foundation}$

Then, the angle of rotation was calculated: $\varphi = \frac{u_{max}}{\text{distance to the centre}} * F_{foundation}$

Finally, the rotation stiffness was determined: $C = \frac{M}{\varphi}$

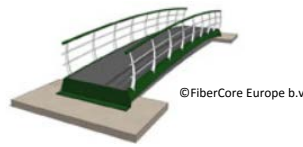
3.5. Concept designs

In order to ensure the most suitable bridge design was going to be implemented, the three concept designs introduced in chapter 2.2 were considered and then, based on the aforementioned design requirements, the most feasible was chosen with the aid of a multi-criteria analysis.

The characteristics on which the analysis criteria were based had to be determined.

The location could not be changed because the general area was imposed by the client and the exact position was restricted by the 30 meter span which was sufficient for crossing the river only at the chosen site. Additionally, the material was restricted to GFRP composite or hybrids because the city of Rotterdam only requires GFRP and high strength concrete bridges and the focus of FiberCore Europe is the former. Furthermore, the economic advantage of all three was proved by Wilken, (2015).

Therefore, considering the abovementioned limitations, the advantages and disadvantages uncovered during the data acquisition phase were used to devise analysis criteria. The disadvantages have been divided into design, procurement and manufacturing challenges. Design challenges describe additional problems that can be caused by the positioning of the steel, necessary connections or internal stresses. Procurement challenges refer to issues that will arise from the need to purchase additional materials (i.e. steel) or different types of currently used materials (i.e. foam with different groove pattern). Manufacturing challenges refer to changes in the current production process that are necessary in



order to successfully build the bridge with the desired cross section (i.e. vacuum infusion changes, steel placement, increases in production time).

3.5.1. Multi criteria analysis

The current subchapter starts by converting the information provided in chapter 2.2 into quantifiable criteria that can be used to differentiate between the chosen concept designs. Furthermore, based on their importance to the overall design, each criterion was assigned a coefficient and the reasoning behind it is explained. Afterwards, the scoring system is explained.

The complete table together with the most feasible option is presented in chapter 4.3.

3.5.1.1. Criteria

The criteria were derived from the challenges posed by every design and are listed in Table 3.

As stated in chapter 2.2, due to the fact that FiberCore Europe not only designs, but also manufactures bridges, the production process is of paramount importance for them. Thus, most of the criteria are related, to some extent, to fabrication, such as fabrication time, costs and challenges. Another driver important to FiberCore Europe, is related to the procurement of materials. Since they produce bridges, they have to purchase the raw materials. When changing or adding new materials in the production process, these also need to be acquired.

Table 3 - - Analysis criteria

Design challenges
Material costs
Procurement challenges
Fabrication costs
Fabrication time
Manufacturing challenges
Risks
Contribution of steel to bending stiffness

Depending on the complexity, new or different materials can have an impact on the overall cost or lead time. Also of interest are the design challenges which refer to calculation and, if necessary, FEM modelling for a bridge with the respective cross section.

3.5.1.2. Coefficients

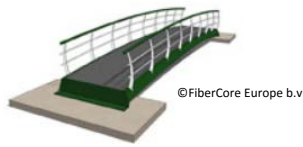
In order to perform an efficient Multi Criteria Analysis, each criterion was assigned a coefficient based on its importance in the decision making process. It has been decided together with FiberCore Europe to assign coefficients in the range from 1 to 4.

Firstly, 1 has been given to the contribution of steel to the bending stiffness due to the fact that it was not decisive. It only serves as general guideline for determining the relation between the amount of steel and its contribution to the stiffness of the deck for a particular design. It becomes apparent that the values will be adjusted during the optimization phase of the most feasible concept.

Secondly, 2 has been attributed to the material costs due to the fact that they might not vary considerably between the designs. Nevertheless, for optimisation purposes it is of interest to see which concept is the least expensive to begin with.

Thirdly, 3 has been attributed to the criteria representing design challenges and procurement challenges. The design challenges are critical for the current research since they will influence greatly the chosen cross section. Moreover, an increase in design time means an increase in overall costs and production time. Additionally, procurement challenges do not have a significant impact since they affect lead time and overall costs by a certain extent and therefore their impact has to be considered.

Lastly, 4 has been assigned to fabrication time, manufacturing challenges and risks since these are the most important aspects that decide whether FiberCore Europe starts designing and building a bridge. The reason is that because production is done in-house, major increases in total costs are not associated with material or transportation costs, but with the production process itself. Therefore, activities that cause an increase in production time have a significant impact. The same applies for new



and complex (i.e. labour- or equipment-intensive) production techniques. Moreover, the implementation of new or different fabrication techniques requires additional research, followed by testing, adjustments and finally implementation on a large scale bridge. Additionally, the addition of new materials or the need to change the specifications of others also requires planning and collaboration with additional material providers.

Furthermore, having established the coefficients, the scores were assigned for each concept. The reasoning for assigning the values is explained below.

3.5.1.3. *Criteria evaluation*

Each of the concepts had to receive a score for each criterion. Determining the correct scores for each criterion is detailed below.

For each criterion, the scores will be assigned based on information provided by FiberCore Europe, (2016) related to the importance and impact of the aforementioned advantages and disadvantages.

3.5.1.3.1. *Design challenges*

Related to design challenges, the first two concepts presented the same challenge, namely the necessity to bond the steel to the skins along the full length of the bridge. The third concept posed the problem of stress concentrations occurring around the steel beams at the sides of the deck. The former problem was related to using appropriate calculation and modelling techniques while the latter involved designing a different laminate for the skins and webs around the edges. Thus, the first two concepts received a high score and the third one a lower one.

3.5.1.3.2. *Material costs*

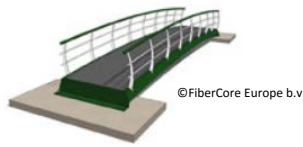
Material costs refer to additional expenses that were arising from the necessity of extra materials specified in the design. All three designs required steel in addition to currently used materials, however, design concepts one and two required less than the third one, therefore, they were assigned higher scores.

3.5.1.3.3. *Procurement challenges*

As explained above, procurement challenges are related to whether the extra required materials (i.e. steel members) are standard elements or need to be custom made. The elements needed for design Concept 1 are standard since they are thin sheets of steel that can be cut to size by any manufacturer. Due to the bridge production process, the steel required for Concept 2 needed to have grooves and holes in it in order to allow the resin to flow normally. This created an increase in costs. Furthermore, for Concept 3, the beams needed to be fully customised and welded, since no standard rectangular hollow section with the desired dimensions exists. Therefore, the highest score was assigned to Concept 1, a lower score to Concept 2 and an even lower one to Concept 3.

3.5.1.3.4. *Fabrication costs*

Fabrication costs indicate additional expenses that arise from the necessity to implement new techniques for handling and installing new components (i.e. steel members). These included costs for new equipment, training, rearrangement of the production area and more. Hence Concepts 1 and 2 were requiring the lowest number of changes, since the relatively small steel members could be installed with the available equipment and a short period of time would be required to teach the staff the installation procedure. Concept 3 on the other hand would require an additional crane or guiding equipment to ensure safe handling. Hence, the latter was assigned a lower score than the former two.



3.5.1.3.5. Fabrication time

This criterion refers to the increase in time taken to build the bridge caused by additional lead time due to complex raw materials and extra time during the production phase due to more elements that needed to be placed. Therefore, considering that placing one steel plate takes approximately 30 minutes, Concept 1 and 2 will have an additional production time of 20 hours. Conversely, Concept 3 would only cause a 1 hour increase in the production time. Related to lead time, Concepts 2 and 3 would require a considerably longer lead time due to the complexity of the steel components which require a certain shape, grooves or welding. Therefore, Concept 1 was assigned the highest score while Concepts 2 and 3 were assigned lower ones.

3.5.1.3.6. Manufacturing challenges

The current criterion refers to the complications that arise from the addition of an extra material. Such complexities can be the necessity to modify the infusion process in order to go around or through the steel members or the necessity to change the way the fibre layup is constructed (i.e. fibres will need to be wrapped around foam cores in a different way in order to allow the steel members to be connected to the skin). Therefore, Concept 2 would pose the most challenges since the process would need to be changed for each core. Subsequently, Concept 3 would require less alterations since only the sides will need to be redesigned. Finally, Concept 1 would require the least modifications since the steel members are small and the infusion process can be adapted to suit this design.

3.5.1.3.7. Risks

Risks refer to the amount of things that can go wrong in the procurement or production process and the impact these risks may have. These include the failure of the adhesive bond between steel and GFRP in Concept 1 and 2, the delamination of GFRP in all concepts due to inadequate reach of the resin during infusion and so on. Thus Concept 1 has the lowest risks associated with it due to the relatively small differences from the current production process. Concept two poses higher risks due to the changes to the infusion process, and custom made steel members and Concept 3 presents risks due to the steel members being placed on the outside and the necessity of a strong connection in order not to break glass layers

3.5.1.3.8. Contribution of steel to bending stiffness

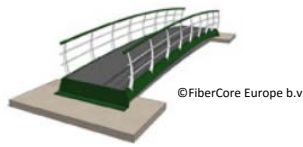
The current criteria describes the contribution of steel to bending stiffness is calculated as a percentage from the total value. Therefore, Concepts 1 and 2 have similar values while in Concept 3, the steel beams contribute less to the overall stiffness. Thus, the scores will be assigned consequently.

3.6. Preliminary design

The purpose of the preliminary design was to do the calculations presented below in order to optimise the dimensions of the cross section also presented below. With the optimised values, were used as input values for the detailed design.

The current chapter starts by ensuring the reliability of the results that were obtained at this stage, then continues by defining the initial dimensions of the cross section's components based on the client's specifications (i.e. length and width) and FiberCore Europe's experience from current production process (i.e. width of foam cores, thickness of skins and web). Furthermore, the loads and further requirements defined in chapter 3.2 are quantified.

The next part describes the analytical calculation algorithms that are based on the aforementioned information. Firstly, the method for transforming the cross section into a homogenous material is explained. Then, the SLS checks related to deflection and natural frequency are done. Furthermore, the ULS checks related to normal, bending and shear stresses are explained as well. Additionally, the



stability of the webs is checked against buckling from a wheel load. Afterwards, the thermal expansion calculation procedure for the different materials together with the thermal stresses determination procedure is described. Lastly, the methodology behind the 1D and 2D FEM models is explained.

3.6.1. Reliability and validity

An Excel spreadsheet was developed in order to organise and facilitate easy access to all the calculations. It was divided into sheets based on the information present therein (i.e. Dimensions, Loads and Factors, ULS, SLS, Thermal stresses and Adhesive bond stresses). The formulae were designed to be parametric, in order to enable the user to check the effects of modifying one of the dimensions and determine whether the updated structure is still viable. Due to the fact that the purpose of the current project was to design a bridge with an optimised cross section, the reliability of the spreadsheet becomes critical since the optimization was done by changing the input values until the unity check for the most critical parameter is close to 1.

In order to validate the Excel spreadsheet, one of the calculations was also done by hand and the results were compared. It can be seen in Appendix 1 that the results of the deflection calculations obtained through the two different means are equal. Therefore the spreadsheet was reliable and the subsequent results were accurate.

Related to input parameters, factors and design values, they were obtained from the Eurocodes (i.e. EN 1990.2002 and EN 1991.2.2003), CUR-aanbevelingen 96 and FiberCore Europe.

For the calculation of bending, shear, normal and adhesive bond stresses, the corresponding algorithms are taken from the Hibbeler, (2011) and from FiberCore Europe, (2016).

3.6.2. Bridge dimensions and cross section

For the preliminary design, a bridge with the dimensions given in Table 4 was considered. The detailed dimensioning of the bridge cross section can be found in Appendix 8. The values were adjusted after performing the calculations described in Chapter 3.4.6 in order to obtain an optimum cross section. The results of these calculations, the optimised cross section and the results of the calculations performed with the optimized dimensions are presented in tables in Chapter 4.2.

Table 4 - Initial bridge dimensions

bridge length (L)	m	30	mm	30000
bridge width (b)	m	4,5	mm	4500
bridge height (h)	m	1	mm	1000

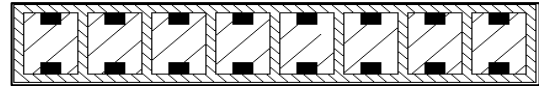


Figure 11 - Cross section of bridge deck, not on scale

The cross section to which these dimensions apply is presented in Figure 11. It features GFRP skins and webs, steel members connected both to the top and bottom skins along the full length of the deck and PU foam core that connects the top and bottom layers.

3.6.3. Material properties

The bridge deck is made of a steel-GFRP hybrid composite material. In order to be able to perform structural calculations, several properties of the basic materials were required. From these, several additional properties were determined. All material properties were provided by FiberCore Europe, (2016): the material stiffnesses (i.e. E moduli), strengths (i.e. σ_{design}) and densities. These values can be found in Appendix 9. Subsequently, the moments of inertia, bending stiffnesses masses and weights were determined. These values can be found in Appendix 10.

3.6.4. Loads

The loads described in the current chapter are characteristic to a cycling and pedestrian bridge and are taken from the NEN-EN.1990+A1+A1/C2/NB:2011 (European Committee for standardization, 2003):

- Permanent loads
 - uniformly distributed load due to self-weight of the structure – calculated from the combined weight of all components of the cross section (see Appendix 5) as being:

$$q_{total} = 315,97 \text{ kN uniformly distributed as } q_M = \frac{315,97 \text{ kN}}{30 \text{ m}} = \frac{10,53 \frac{\text{kN}}{\text{m}}}{4,5 \text{ m}} = 2,34 \frac{\text{kN}}{\text{m}^2}$$

- Live loads
 - Uniformly distributed load – calculated in Appendix 5 as:

$$q_{fk} = 4 \frac{\text{kN}}{\text{m}^2} * 4,5 \text{ m} = 18 \frac{\text{kN}}{\text{m}} \text{ with horizontal load of } Q_{h,q} = 54 \text{ kN}$$

- Concentrated load – calculated in Appendix 5 as:

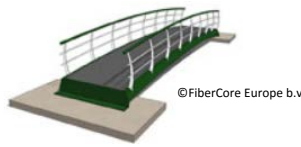
$$Q_{fvd} = 7 \text{ kN acting on } B_{fvd} = 0,1 \text{ m} * 0,1 \text{ m}$$

- Maintenance vehicle load – calculated in Appendix 11 as:

$$Q_{serv} = 12,5 \text{ kN acting on } B_{w,serv} = 0,25 \text{ m} * 0,25 \text{ m with horizontal load } Q_{h,serv} = 15 \text{ kN}$$

- Unauthorized vehicle load – calculated in Appendix 11 as:

$$Q_{acc} = 40 \text{ kN acting on } B_{w,acc} = 0,2 \text{ m} * 0,2 \text{ m with horizontal load } Q_{h,acc} = 48 \text{ kN}$$



- Load on handrail – calculated in Appendix 11 as:

$$q_{lk} = 3 \text{ kN/m}$$

- Load of pedestrian traffic – calculated in Appendix 11 as:

The weight of 1 pedestrian is taken as $P_1 = 800 \text{ N}$ and the flow has a density of $d_{TC3} = 0.5 \frac{P}{m^2}$.

3.6.5. Partial factors

The current bridge is classified as consequence class 1 (CC1). Therefore, the partial factors required for load combinations according to the Eurocode (EN1991-2+C1) for the ultimate limit state and the serviceability limit state are listed in Appendix 12.

3.6.6. Load combinations

For determining the design value for the loads acting on the bridge, the characteristic values determined above must be combined with the partial factors in order to form Load Cases. All load cases and loads relevant for the current project, according to EN.1990+A1+A1/C2:2011 can be seen in Appendix 13.

3.6.7. Analytical calculations for the preliminary design

The first stage of the present research was the preliminary design which consisted of analytical calculations. The results of these calculations have then been used for verifying and validating the outcome of the FEM. The calculations performed in this chapter are based on the cross section design presented in Chapter 3.4, together with the initial dimensions and material properties presented in the same chapter and Appendix 8.

The purpose of these checks was to adjust the dimensions of the cross section in order to be sufficiently strong while also being cost-effective. Firstly, the SLS checks were performed. These included natural frequency and deflection. Subsequently, the ULS checks were done, namely: normal stresses; skin bending strength against bending stresses, web shear strength against shear stresses, web compressive strength against compression stresses and web buckling. Finally, two additional checks were done. These were related to thermal stresses between the steel plates and GFRP skins and the bond strength of the adhesive against shear stresses at the interface.

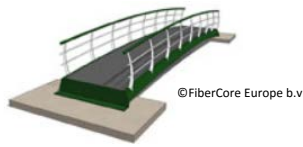
3.6.7.1. SLS checks

In order to ensure comfortable use of the bridge, Serviceability Limit State (SLS) computational checks were performed. The aim is to demonstrate that under the action of characteristic design loads, the structural behaviour complies with the SLS design criteria values, specified in EN.1990.2002. These criteria include deformation limits and dynamic behaviour limits during everyday use that when achieved provide comfortable of the structure.

To satisfy the serviceability limit state criterion, a structure must remain functional for its intended purpose subject to routine loading, and must not cause user discomfort under the abovementioned loading condition. This calculation check is performed at a point located at the lower half of the elastic zone, where characteristic actions are applied and the structural behaviour is purely elastic.

3.6.7.2. ULS checks

The Ultimate Limit State is a computational condition that has to be fulfilled in order to comply with the engineering demands for strength and stability under factored design loads. Furthermore, a structure is considered to satisfy the ultimate limit state criterion if all factored bending, shear and



tensile or compressive stresses are below the factored resistances calculated for the section under consideration.

Generally, there are three types of stresses that occur in a structural member when subjected to loading, namely normal, bending and shear. Therefore, the checks done at this stage were related to the normal stresses generated by horizontal forces, skins' strength in bending and the web's shear and compressive strength. Additionally, the maximum shear stress in the cross section and the buckling stability of the webs were verified.

3.6.7.3. Thermal checks

Another aspect that was of interest was the thermal behaviour. Specifically, the thermal expansion of the two materials that are in contact (i.e. steel and GFRP), and the shear and axial stresses generated by the difference in elongation or contraction were determined. Since these stresses are generated at the interface between the two materials in contact, the resin connecting had to withstand them.

3.6.7.4. Adhesive bond checks

Although partially included in the previous sub chapter, the stresses occurring in the resin binding the steel to the GFRP skins were also checked under the ULS udl.

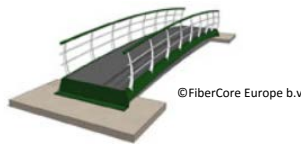
3.6.8. FEM analysis

In order to accurately determining values for deflection, strength and other properties, and, subsequently, be able to optimize the cross section accordingly, the FEM pre and post processor Patran together with the solver Marc were used.

Patran was used to create the geometry, to which materials, properties, loads and boundary conditions are added. Afterwards, the geometry was meshed into finite elements. Furthermore, the solver, Marc, analysed the elements and published the results in a file which was then imported in Patran. At this point, the results could be seen and compared with the design values of the materials. The properties and geometry could then be changed, the mesh re fitted and the analysis re run in order to check the effects of the modifications.

In order to understand the working mechanism of the program and to ensure the more complex models will be accurate, the analysis has been divided into three stages. In order to prove the accuracy of the program, the values that result from each of the stages were compared to the ones obtained through analytical calculations. When the results matched, the model was deemed reliable.

The first model contained a 1 dimensional beam, also known as a stick, the second one consisted of a 2 dimensional plate and the third one comprised of the bridge deck modelled in 3D. The former two were used in the preliminary design stage while the latter was only used for the detailed design stage.



3.6.8.1. 1D FEM model

The first phase of the calculation was done on a 1 dimensional simplified deck equivalent, namely a stick. The following sub chapters describe the actions that had to be taken and the parameters that had to be inputted in order to analyse this model.

3.6.8.1.1. Geometry

The geometry consisted of one 1D stick with the only inputted dimension corresponding to the length of the deck, 30.000 millimetres.

3.6.8.1.2. Material properties

The material was inputted as a homogenous laminate equivalent. The value of the E modulus was calculated in the spreadsheet by dividing the total composite bending stiffness to the total moment of inertia. The corresponding value was:

$$E_{equiv} = \frac{EI_{deck}}{I_{deck}} = \frac{3,81 * 10^{15} N * mm^2}{3,09 * 10^{11} mm^4} = 8125,63 \frac{N}{mm^2}$$

Similarly, an average value of 0.3 was used for the Poisson's ratio.

Subsequently, a 1D beam was created with this material. A cross section was then chosen from Patran's database. Due to the actual shape of the deck's section being relatively complex, a simplified one was chosen, namely a rectangular section with a width of 4500 mm and a height of 1000 mm which closely resembles the actual one. The important aspect to match was the cross sectional area.

3.6.8.1.3. Boundary conditions

The 1D stick was simply supported in the XY plane, with a hinge at one end, constraining the X and Y, and a roller at the other, constraining the Y. Moreover, in order to be property restrained, an additional constraint had to be introduced that restricted movement in the out of plane direction (i.e. Z direction).

3.6.8.1.4. Loads

Regarding the loading, the stick was loaded with a uniformly distributed load for the Serviceability Limit State. The decisive value of the load according to EN.1990.2002 as stated in Appendix 11.

$$LC_4 = 26,33 \frac{kN}{m} = \frac{26,33 \frac{N}{mm}}{4500 mm} = 0,00585 \frac{N}{mm^2}$$

Regarding point loads, they would not have been interesting to implement due to the way results are presented, specifically, the stresses or deflection would have been plotted on the stick, virtually a line, which would have been difficult to read and interpret.

3.6.8.1.5. Mesh

Following the input of all the properties, the element had to be meshed into finite elements. The mesh was be of the curve type, characteristic for the existing geometry. The result of this process was a number of nodes and elements on which the calculation is executed.

3.6.8.1.6. Analysis and results

After meshing, the analysis was done and the results could be checked. As stated before, the only result that was deemed of interest in this phase was the maximum mid-span deflection value which was compared with the one obtained analytically.

3.6.8.2. 2D FEM model

The second stage of the analysis introduced more complexity and more accuracy to the model. The advantage was that by moving to a 2D analysis, the results will be more informative and easier to observe.

3.6.8.2.1. Geometry

A 2-dimensional plate was created in Patran, its dimensions corresponding to the length and width of the bridge deck, namely 30 and 4.5 meters respectively. It was subsequently divided into more surfaces (see Figure 12):

- 2 * 250 mm wide surfaces at the sides representing the flanges of the bridge;
- 2 * 50 mm wide surfaces next to the flanges representing the flanges without steel;
- $(4500-500-100)/100 = 39 * 100$ mm wide surfaces representing strips with and without steel

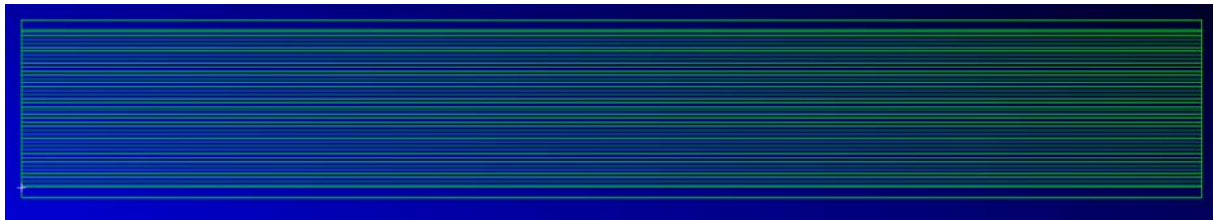


Figure 12 – Top view of plate geometry showing the strips

3.6.8.2.2. Material properties

At this stage a more accurate section was created. In order to achieve this, firstly three basic materials had to be created, two isotropic and one 3D orthotropic (i.e. steel, PU foam and GFRP ply). The properties of all three materials can be found in Appendix 14. Subsequently, the laminates were created. The first one contains the plies of the top skin, top steel plate, foam core, bottom steel plate and plies of the bottom skin. The second one only contains the top skin, foam core and bottom skin.

In order to build laminates, apart from the previously created ply, the number, orientation and thickness for each one was required.

The number and orientation of plies in the top and bottom skin was based on the three block overlap technique used by FiberCore Europe, (2016). Thus, the cross section at any given location was composed of one PU foam core wrapped in two plies with +/-45 degree orientation. Above and below, an overlap of plies from three blocks was used. Each of the three groups consisted of two plies in the 0 direction, followed by two plies with 0 and 90 degrees direction. Therefore, the layup starting from the top was defined as $[0_2/90/0/90/0_3/90/0/90/0_3/90/0/90/0/45/-45/45/-45]_s$

As can be observed (denoted by the subscript S), the layup of the bottom skin was the same as the top skin's, only mirrored. This way, the cross section is symmetrical with respect to the mid-plane which is desired in order to prevent the coupling effect from occurring which can introduce torsion in the deck.

In order to determine the thickness of each ply, the following formula was used. The parameters (i.e. fibre volume fraction, density area and glass density) were provided by FiberCore Europe, (2016).

$$t_{ply} = \frac{\rho_{area}}{\rho_{glass} * V_f} = \frac{1200 \text{ g/m}^2}{2550000 \text{ g/m}^3 * 0.52} = 9.049 * 10^{-4} \text{ m} = 0.905 \text{ mm} \approx 0.9 \text{ mm}$$

The detailed layup with the respective orientation and thickness is presented in Appendix 15. As stated above, the core part of the profiles was different since the steel bars were only present in one of the laminates.

Having built the laminates, they were assigned to the geometry thick shells. This way the stresses were shown in each cross sectional layer and also in between the plies.

Since the 2D model has a one-plane structure, it was not possible to introduce the webs which in the actual cross section divide every two cores. This is one of the causes why the results obtained from this model were slightly different than those obtained from the analytical calculation.

3.6.8.2.3. Loads and boundary conditions

The plate was supported along the short edges. Specifically, one end was constrained as a hinge (i.e. along the X and Z axes) and the other one as a roller (i.e. along the Z axis). Additionally, two corners were constrained in the third direction, corresponding to the out of plane one from the previous stage in order to fully define the deck.

Similar to the previous stage, the SLS condition regarding deflection had to be fulfilled. In addition, the ULS condition regarding stresses also needed to be analysed.

In order to perform two different analyses in the same run (i.e. ULS and SLS), for which different results are of interest (i.e. stresses and deflection), two load cases had to be created:

- ULS LC: contains all boundary conditions and the ULS load

$$\text{Max UDL according to } LC_3 = 32,39 \frac{kN}{m} = \frac{32,34 \frac{N}{mm}}{4500 \text{ mm}} = 0,0072 \frac{N}{mm^2}$$

- SLS LC contains all boundary conditions and the SLS load

$$\text{Max UDL according to } LC_4 = 26,21 \frac{kN}{m} = \frac{28,07 \frac{N}{mm}}{4500 \text{ mm}} = 0,0058 \frac{N}{mm^2}$$

3.6.8.2.4. Mesh

The plate was meshed into finite elements with a surface type mesh characteristic for a 2D element. The result of this process were a number of nodes and elements on which the calculation will be executed. A mesh seed of 60 elements (i.e. 500 mm apart) was specified for the long edge of the deck. For the short edge, every strip formed one element (see Figure 13).

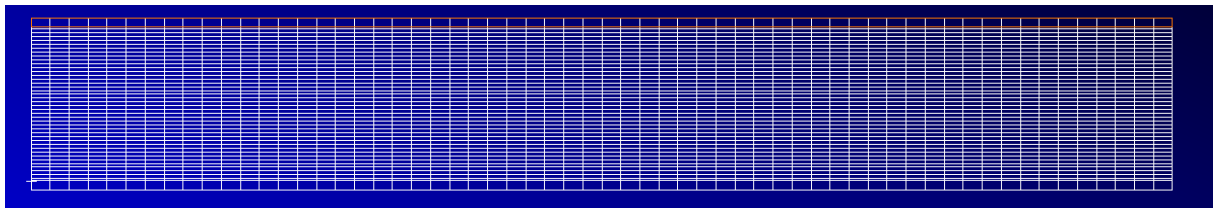
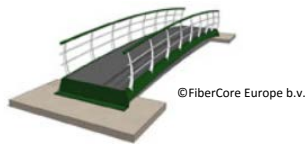


Figure 13 - Top view of the deck with the mesh and nodes present; (Marc-Patran, 2016)

3.6.8.2.5. Analysis and results

In order to perform the analysis of the two separate load cases in the same run, two calculation steps had to be made, each based on a different load case and with different output requests. This way, for the ULS load, only the stresses were calculated and for the SLS load, only the deflection.

The value of the deflection had to be similar to the one determined analytically. The stresses in the plate in the x and y direction together with the shear ones could be seen at this stage and compared with the results of the analytical calculation.



3.7. Detailed design

The purpose of the detailed design was to further optimise and improve the cross section obtained during the previous stage. Therefore, a more detailed analysis was envisaged for this stage whereby both global and local effects were considered.

The current chapter starts by ensuring the reliability of the results that were obtained at this stage, then continues by explaining the approach behind creating the 3D model including the geometry, materials, loads, boundary conditions and mesh.

The initial approach was to create a 3D model with 3D solid components. The advantage of these elements is that they have four integration points along their thickness which means that stresses through the thickness of a homogenous material are calculated and presented in more detail.

However, for the current project, there were two drawbacks associated with creating such a large 3D model. Firstly, a large and complex 3D model such as the bridge deck takes a very long time to analyse when properly meshed (i.e. creating near perfect cube elements). Secondly, the ability to see stresses through the thickness is not necessary in case of analysing laminates since the stresses in each ply and the inter-laminar ones can be determined and plotted if 2D thick shell elements are used. Additionally, the calculation time for such a model is similar with that for a thin shell elements model.

Therefore, a compromise solution was found, specifically, to create a 3D model with 2D thick shells of the entire deck for analysing global effects and a 3D model with solid elements of a portion of the deck for analysing the local ones.

3.5.1. Reliability and validity

Two software-based tools were used during the detailed phase and their reliability has to be ensured in order to obtain accurate, replicable results. The tools in question are the FEA pre-and post-processor Patran together with the solver Marc. Both programs are created by MSC software and are finite element analysis tools. They are used for validation and optimization of designs using virtual prototypes thus replacing the need of building and testing of a physical prototypes.

The models created in Patran and analysed with Marc produced certain results which were compared with the ones obtained from the analytical calculation. If the two results match or vary by a maximum of 5-10%, the model is considered accurate. The reasons why this variation occurs are related to the calculation method of the program, the size of the mesh together with inclusion or exclusion of local effects, the absence of certain elements in some of the models for simplification reasons and simplification of certain calculations, such as the transformed area method which converts two different materials into a single homogenous one. These causes for different results are explained in the relevant chapters.

Due to the complexity of some of the checks Marc Patran can do (i.e. thermal stresses, local web buckling and adhesive bond stresses), corresponding simplified checks are done analytically in order to ensure validation of these results as well.

3.5.3. 3D FEM model

As stated above, this stage involved the 3D design of the deck with 2D thick shell elements together with a smaller model with solid elements which allowed the evaluation of local effects.

The large model was used to determine the natural frequency, the stresses per ply, the inter-laminar shear stresses and the buckling of the web under wheel load while the smaller one was used for calculating thermal stresses and adhesive bond stresses.

3.5.3.1. Geometry

The large model was created with 30-meter-long surfaces with different widths, as dictated by the laminate that was applied to them (i.e. with or without steel). The top and bottom skin, webs, flanges, sides and bulkheads were created as shown in Figure 14.

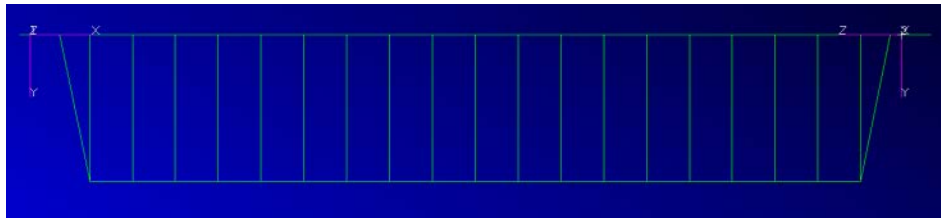


Figure 14 - 3D model with 2D elements of bridge deck - cross section

Furthermore, the smaller model, representing a part of the whole deck, comprised of 5 1-meter-long cores modelled as solid elements. As can be seen in Figure 15, the top and bottom skins, webs and steel members were modelled as individual elements. The thicknesses of the top and bottom skin and webs are dictated by those of the laminate's. The steel plates are 100mm wide x 10 mm thick.

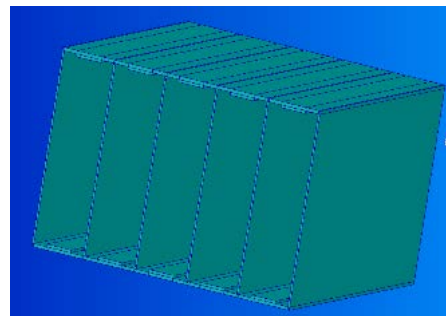


Figure 15 - small model with solid elements, representing a part of the deck, used for local effects analysis

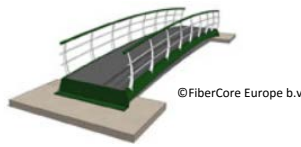
5 cores were modelled in order to obtain accurate results in the middle core, thus ignoring the edge effects. The actual edges of the deck are much stronger than the webs, therefore, the actual stresses in those area would be much smaller.

3.5.3.2. Material properties

Furthermore, the steel, PU foam and ply materials created at the previous stage were imported.

The former two were assigned to the respective elements as properties for thick shell elements in the first model and as solid elements in the second one. The ply material was used to create laminates for the top and bottom skin with and without steel, webs, flanges, sides and bulkheads. Subsequently, these materials were assigned to the geometry as thick shell elements. The thickness, layer orientation and number of layers for each laminate is listed in Appendix 15.

The laminates for the top and bottom skin without steel and for the webs together with the steel were also used in the smaller model and were assigned to the respective elements as solids. Furthermore, another homogenous material was created and the resin's properties from Appendix 14 were attributed to it.



3.5.3.3. Loads and boundary conditions

Regarding the boundary conditions, the hinge, roller and out of plane supports were defined in the same way as before. They were applied to the bottom edge of the cross section in order to accurately represent the method by which a simply supported deck is installed.

Regarding loading, the SLS and ULS load cases were imported together loads' values. Additional load cases (i.e. LC) were created for both models as follows:

For the large model:

- Buckling LC: contained wheel loads and boundary conditions;
- Buckling under SLS UDL: contained SLS UDL and boundary conditions
- Natural frequency LC: for analysis of natural frequency, three load cases were required
 - Modal Step 1: contained only the boundary conditions;
 - Tension Preload: contained the SLS UDL and the boundary conditions;
 - Modal Step 2: contained the boundary conditions.

For the small model:

- Thermal Expansion LC: contained, initial temperature (i.e. 10°C), maximum temperature (i.e. 32°C) and boundary conditions;
- Thermal Contraction LC: contained, initial temperature (i.e. 10°C), minimum temperature (i.e. -17°C) and boundary conditions;
- Adhesive bond stresses LC: contained ULS UDL and boundary conditions

3.5.3.4. Mesh

The large model was initially meshed with a 150 mm element mesh seed in the longitudinal direction (i.e. 60 elements were created length wise). In transverse direction, the size of the mesh elements was decided by the geometry, being around 50 mm. Special attention had to be paid to the orientation of the shell elements. This parameter indicates the local X, Y and Z directions for each element and is related to the laminate's thickness direction.

The small model was meshed with 10x10x10mm hex elements characteristic for solid components. This was the ideal mesh size since it is both fine and the elements are perfect cubes. Additionally, the thickness direction for the elements had to be specified.

3.5.3.5. Analysis and results

Based on the Load Cases previously created, Calculation Steps were made which were then analysed with Marc for both models.

3.5.3.6. Adjustments and optimizations

Upon calibrating the models by comparing the deflection and stresses values with the ones obtained before, the detailed checking and optimization could be started. For the large model, the effects analysed included natural frequency, inter-laminar shear stresses per ply stresses, both in shear and bending and local buckling effects due to the action of a wheel load on the deck. For the small mode, these tests included thermal stresses and stresses in the bond between steel and GFRP under ULS load.

Below, a more detailed description of the method related to these tests is given.

3.5.3.6.1. Natural frequency

Due to the fact that the current bridge is a slender structure and the natural frequency is the critical requirement that needs to be met by such constructions, it was necessary to check its value since the

deck can no longer be made thinner in case the frequency is smaller than the design value. As in the analytical part, the live load was used for this calculation step.

3.5.3.6.2. Inter-laminar stresses

The inter-laminar shear stresses of the top and bottom skins and webs were checked under the ULS udl in order to optimise the layup. The objective was to analyse whether these stresses were larger than the ones the polyester resin is able to withstand. The design values for shear strength of the resin, as specified in the CUR-aanbevelingen 96, can be found in Appendix 14.

3.5.3.6.3. Per ply stresses

Since the model contains thick shell elements, the stresses in each ply could be determined. Alternatively, the maximum or the average stress across the laminate could be plotted. As the strength of the glass fibre plies is not critical in bending, the stresses are expected to be low compared with the design values. The objective was to determine which ply orientation was subjected to the largest stresses. Thus, the amount of those plies could be increased if the stress values are too high.

3.5.3.6.4. Local web buckling

Web buckling was checked in two situations, as shown in Figure 16. The variants have been considered while accounting for the position of the load acting on the web. The two scenarios were implemented in Patran with the objective being to determine whether the webs buckled in the most critical of the two scenarios. The load considered was that of the rear axle of an unauthorised vehicle as shown in Appendix 11.

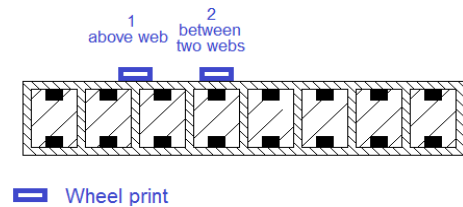


Figure 16 - Buckling check with different wheel position

3.5.3.6.5. Thermal stresses

As stated before, the thermal stresses were analysed on the small model. The objective was to determine the axial and shear stresses in the resin layer between the skins and steel. The shear stresses are critical since they are carried by the resin. Therefore, the maximum shear stress therein had to be lower than the design values specified in the CUR 96 and shown Appendix 14. Since the ΔT is larger in contraction, the stresses generated with this load case were expected to be larger than those from expansion.

3.5.3.6.6. Shear stresses in the adhesive bond

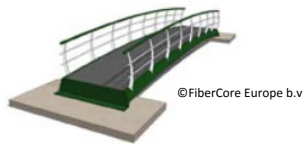
The adhesive bond stresses were also analysed on the small model due to the fact that they can pose a considerable risk on the connection between the two materials. The objective was to determine the shear stresses caused by the ULS udl in order to ensure that they are lower than the design values provided in the CUR aanbevelingen 96 which can be seen in Appendix 14. The maximum value for the shear stresses was expected to occur next to the supports.

3.6. Drawings

Considering the results of the analytical and FEM calculations, an optimised cross section was determined.

Furthermore, the using the design considerations determined as described in chapter 3.6.1., the drawings for the proposed 30 meter bridge over the Rotte were made.

In addition, several drawings were provided for the 60 meter bridge that was determined to be the maximum limit of the analysed cross section. For these drawings, the design considerations determined as described in chapter 3.6.2. were used. A list of these drawings is provided in the Results chapter.



4. Results

The current chapter presents the results obtained through the steps described in the methodology chapter. The results are explained and analysed in chapter 5.

4.1. List of requirements

The first sub chapter of the results section presents the project requirements that had to be determined in order to ensure designing a bridge that fulfils the required function.

These requirements have been classified into required standards and prerequisites from the client. Subsequently, technical requirements have been derived in order to obtain a list of clear to follow design guidelines. A complete overview of the requirements is shown in Appendix 18.

4.2. Starting points and design considerations

Furthermore, the current sub chapter presents the starting points together with the design considerations, as described in chapter 3.3.

4.5.1. 30 meter bridge

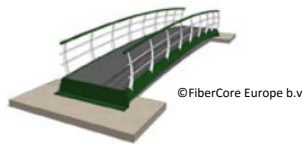
As explained in chapter 3.3.1., the soil profiles for the area have been obtained from the Dinolocket website, for both the left and right bank. (DINOloket, 2016) The map with the locations of the CPT tests in relation to the project area together with the soil layers are presented in Appendix 16. It can be noticed that the profile from the south side of the river is farther from the project location than the other. Due to lack of additional information, the same soil structure was considered at the south side of the bridge. Moreover, the soil structure under the river is an interpolation of the available information from the north and south bank.

The second step involved obtaining the levels of the north and south side roads and banks. These were obtained from the AHN website and are -0.1 m NAP on the south bank and -0.25 m NAP on the north bank. (Actueel Hoogbestand Nederland, 2016)

Furthermore, the level of the surface of the water had to be determined. Due to the fact that the Rotte is separated from the Rhine, it does not have tidal difference. Therefore, the tidal graph closest to the project location was obtained from the Rijkswaterstaat' website and the minimum value for the water level was assumed for the current project. Details about the levels and maps with the locations of the measurements are presented in Appendix 17. (Rijkswaterstaat, 2016)

Due to the small difference between the surface water level and the ground level of the banks, in order to provide the required clearance, the deck had to be raised. This meant designing tall abutments and sloped approaches that enabled connection with existing roads. The maximum slope specified in the CROW for the approach of a cycling and pedestrian bridge is 4%. Due to the topography of the area and the limited distance between the bridge and the adjoining roads, the approach roads had to be designed perpendicular to the bridge and parallel to the neighbouring roads. Furthermore, the connection with the latter is done via 90° turns.

In order to build the approach roads, the ground level on the banks has to be raised. In order to account for sand settlement, an additional 30% of the required quantity needs to be supplied. Subsequently, in order to prevent the added soil from sliding, campshedding will be provided, on the river side. The top of the piles have to be at the same level as the top of the added sand mass. Moreover, the bottom of the piles has to be situated at a depth that is equal to $2 \cdot L_{\text{above ground}}$. Moreover, in order to ensure their stability, the piles will be driven at an angle of 10° towards the river side in order to counter the



horizontal force generated by the sand. The piles are placed at a c.t.c. distance of 1 meter, over a length of 7,5 meters on either side of the Rotte.

Furthermore, according to FiberCore Europe (2016), a volume of soil with a trapezoidal cross section, having a top side of 1000 mm and a height of 600 mm has to be improved through compaction grouting. On top of the improved soil, a concrete slab of 1000*4500*100 mm is placed. It has to have a minimum of 600 mm of soil on top of it in every direction.

On top of the concrete slab, a 5 mm High Density Polyethylene layer together with 5 mm glass fibre filler are added. Afterwards, the deck is connected to the foundation slab with 2 M12x80 bolts on each side.

Furthermore, the deck itself is built as an arch with a minimum slope of 1% that ensures adequate rainwater drainage and a maximum slope of 4% that ensures facile access of bikes and wheelchairs over the bridge. The decisive slope was 4% due to the fact that it provided the shortest bridge which was advantageous given the short distance between the river and existing roads.

Regarding finishing, the deck is covered with 2 mm epoxy slurry and 3 mm of wearing surface in order to make it usable and non-slip.

A railing is provided on either side of the bridge and on the approach roads with a height of 1 m from the road level. Furthermore, according to the CROW, 250 mm wide kerbs have to be provided on either side of the cycling path. Moreover, the cycling path has to allow two cyclists passing one another, thereby requiring a width of 750 mm * 2 plus 250 mm in between. Lastly, the pedestrian sidewalk has to be at least 1600 mm wide in order to allow for two wheelchairs or prams to pass one another.

4.5.2. Maximum span bridge

Following the FEM model, the maximum span for a clamped (i.e. fully fixed) deck with the same cross section as the 30 meter bridge was 60 meters which is double than the initial design. The analysis was run on the aforementioned model in Marc Patran, and the resulting deflection was 385 mm. Due to the longer span of 60 meters, the maximum allowable deflection is 600 mm (i.e. 60.000 mm/100). Therefore, it meets this requirement for deflection. Related to natural frequency, the result obtained from Marc Patran was 2,5 Hz.

As stated in chapter 3.6.2., in order to provide fixed supports at both ends a pile foundation is required. The connection between the pile foundation and adjacent road is done via transition slabs whose purpose is to account for the difference in settlement between soil under the pile foundation and adjacent soil. Furthermore, the deck is connected to the foundation via anchors attached to the deck.

The respective connection is made by removing the foam and steel plates from four core profiles for a distance of approximately four meters and installing a casing made of steel plates, to which the M30 anchors are attached. The choice was made to use 4 anchors in the transverse direction in order to have symmetry and 3 in the longitudinal direction, giving a total of 12 anchors per abutment. In order to allow the deck to freely expand and contract due to temperature variations, the anchor's connection with the foundation has a 10 mm gap on either side.

Furthermore, the foundation is designed with 6 \varnothing 200 mm concrete piles per abutment. The length of each pile is 5 meters. This length has been decided together with FiberCore Europe as being suitable since the bridge is light and the piles are only used to provide bending resistance and increase the deck's stiffness.

The full calculation for the foundation's rotational stiffness is provided in Appendix 20. The result of the calculation is:

$$C = 843.088,74 \frac{kNm}{rad}$$

4.3. Most feasible concept design

Having assigned the coefficients and scores as explained in chapter 3.3.4, Table 5 concludes that Design Concept 1 (see Figure 17) is the most feasible option, considering the criteria analysed.

Table 5 - Multi Criteria Analysis table with scores

Criteria	Coefficient	Design Concept 1	Design Concept 2	Design Concept 3
		Score	Score	Score
Design challenges	3	5	5	2
Material costs	2	4	3	2
Procurement challenges	3	4	3	2
Fabrication costs	3	4	3	1
Fabrication time	4	4	2	2
Manufacturing challenges	4	4	2	3
Risks	4	2	1	1
Contribution of steel to bending stiffness	1	4	4	3
Total	points	91	63	46

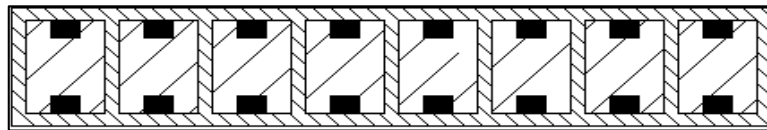


Figure 17 - Most feasible cross section design

4.4. Preliminary design

This subchapter presents the results of the analytical calculations in the shape of unity checks, in the same order as they were introduced in chapter 3.4.6. For the detailed calculations including the algorithms and formulae, see Appendix 20.

4.4.1. SLS checks

In this subchapter, the results from the SLS checks described in chapter 3.5.7.1. are presented.

4.4.1.1. Natural frequency

The unity check for the natural frequency of the bridge is: $f_{n,check} = \frac{f_{n,min}}{f_n} = \frac{2,3}{3,29} = 0,7$

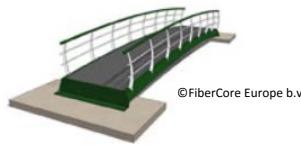
4.4.1.2. Deflection check

The deflection due to the self-weight is: $\delta_{sw} = 33,4 \text{ mm}$

The additional deflection caused by creep over the life span of the bridge, as calculated with the algorithm provided in the CUR-aanbevelingen 96 is: $\delta_{ck} = 15,56 \text{ mm}$

Therefore, the total deflection due to the self-weight and creep is: $\delta = 49 \text{ mm}$

The deflection caused by the live load is: $\delta_{fk} = 67,64 \text{ mm}$



The largest value between the two was compared with the maximum allowed deflection which has been set by FiberCore Europe, (2016) at $1/100 \cdot L = 300 \text{ mm}$: $\delta_{check} = \frac{\delta_{fk}}{\delta_{max}} = \frac{67,64}{300} = 0.225 \leq 1; ok$

4.4.2. ULS checks

In this subchapter, the results from the ULS checks described in chapter 3.5.7.2. are presented.

4.4.2.1. Normal stress

Considering the cross sectional area, the one obtained from the transformed area method and the largest horizontal load caused by the rear axle of the accidental vehicle while braking, and the design values, the unity check for the normal stresses is:

$$uc_{\sigma,ts} = \frac{\sigma_N}{\sigma_{N,x,c,all}} = \frac{2,4}{120} = 0.02 \leq 1; ok$$

4.4.2.2. Bending stress – Skin bending strength

Considering the cross sectional area, the one obtained from the transformed area method and the largest bending moment between LC3 and LC4, the skin's and steel's strength were checked. The unity checks for the bending stresses in the skin and steel members are:

$$uc_{\sigma,tsteel} = uc_{\sigma,bsteel} = \frac{\sigma_{tsteel,max,c}}{\sigma_{tsteel,x,c,all}} = \frac{\sigma_{bsteel,max,c}}{\sigma_{bsteel,x,c,all}} = \frac{6,38}{119,88} = 0.053 \leq 1; ok$$

$$uc_{\sigma,ts} = uc_{\sigma,bs} = \frac{\sigma_{ts,max,c}}{\sigma_{ts,x,c,all}} = \frac{\sigma_{bs,max,c}}{\sigma_{bs,x,c,all}} = \frac{19,07}{186,21} = 0.102 \leq 1; ok$$

4.4.2.3. Shear stress – Web shear strength

The shear webs are checked for load combinations 3 and 4. The unity check for shear stresses is:

$$uc_{\tau,web} = \frac{\tau_{web,max}}{\tau_{web,xz,all}} = \frac{9,16}{36,73} = 0,25 \leq 1; ok$$

4.4.2.4. Compression stress – Webs compression strength

The strength of the webs in compression is checked for load case 5. For this check it is assumed that the concentrated load is located directly above a web. Therefore, the unity check is:

$$uc_{\sigma,web} = \frac{\sigma_{web,c}}{\sigma_{web,z,c,all}} = \frac{35,8}{67,34} = 0,53 \leq 1; ok$$

4.4.2.5. Maximum shear stress

Shear stress results when a load is applied parallel to an area and varies across the cross sectional area. The maximum shear stress occurring in the cross section is:

$$\tau_{max} = \frac{4,85 * 10^5 \text{ N} * 38,12 * 10^6 \text{ mm}^3}{4.500 \text{ mm} * 3,094 * 10^{11} \text{ mm}^4} = 0,013 \frac{\text{N}}{\text{mm}^2}$$

4.4.2.6. Shear stress – Web buckling

Using all the parameters from Appendix 3, the formula can be filled in and the critical buckling parameter can be determined: $\lambda_{cr,ij} = 4,69$

This factor was also obtained from the eLamX software for the web laminate. It can be observed from Figure 18 that by creating the web laminate with the same dimensions, clamped along all four edges to mimic its connections with the skins and ends and with the same load acting on it, the program calculates the critical buckling factor (i.e. called eigenvalue here) to be 4,78.

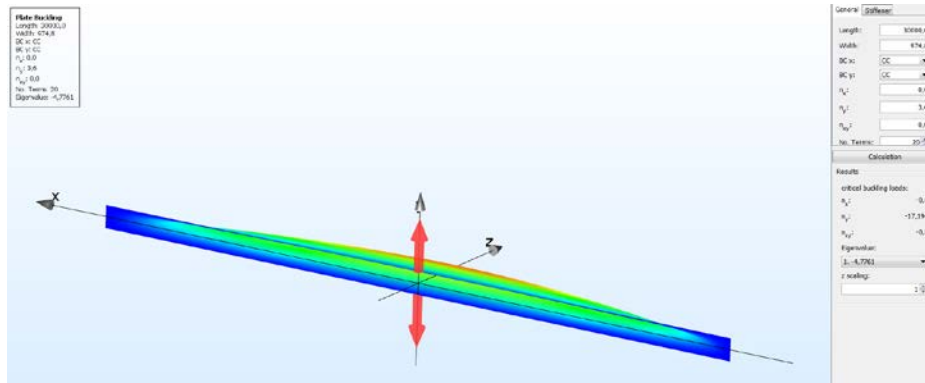


Figure 18 – buckling of the web under SLS load in eLamX

4.4.3. Thermal expansion analysis

According to the formula for linear expansion, the elongation of the two materials is:

$$\Delta l_{steel,contraction} = 8,1 \text{ mm}; \quad \Delta l_{steel,expansion} = 6,6 \text{ mm}$$

$$\Delta l_{steel,range} = \Delta l_{steel,contraction} + \Delta l_{steel,expansion} = 8,1 + 6,6 = 14,7 \text{ mm}$$

$$\Delta l_{GFRP,x,contraction} = 6,658 \text{ mm}; \quad \Delta l_{GFRP,x,expansion} = 5,425 \text{ mm}$$

$$\Delta l_{GFRP,x,range} = \Delta l_{GFRP,x,contraction} + \Delta l_{GFRP,x,expansion} = 6,658 + 5,425 = 12,08 \text{ mm}$$

Furthermore, axial force in the two materials is: $F = 2,2 \text{ N}$

Subsequently, axial stresses in each material could be determined: $\sigma_{steel} = 2,2 \frac{\text{N}}{\text{mm}^2}$ and $\sigma_{skin} = 1,75 \frac{\text{N}}{\text{mm}^2}$

4.4.4. Shear stresses in the adhesive bond between steel plate and GFRP skin

The shear stresses at the interface of the two materials is: $\tau_{adhesive,bond} = 0,056 \frac{\text{N}}{\text{mm}^2}$

4.4.5. Sand addition

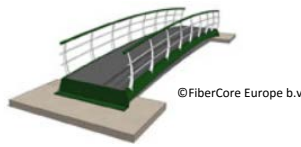
In order to provide the necessary clearance and be able to connect the bridge to the adjacent roads, the deck had to be raised and the approach roads had to be long in order to meet the required slope. Therefore, sand had to be added on either side of the bridge. Below, the amount of sand required has been determined.

$$V_{sand;1 \text{ abutment}} = \frac{0,77 \text{ m} * 7 \text{ m}}{2} * 36 \text{ m} = 194,04 \text{ m}^3 \rightarrow$$

$$V_{sand;2 \text{ abutments}} = 194,04 * 2 = 388,08 \text{ m}^3$$

In order to account for settlement, and extra 30% is required, bringing the total amount to:

$$V_{sand;total} = 388,08 + 30\% * 388,08 = 388,08 + 116,626 = 504,504 \text{ m}^3 \cong 510 \text{ m}^3$$



4.5. Cross section optimization based on preliminary design

Having determined the aforementioned values, the dimensions of the cross section could be optimized in order to achieve a more cost effective solution. The optimization was performed within the Excel spreadsheet by altering the variable dimensions of the bridge (i.e. depth of the deck, number of cores, flanges) in order for the value of the unity check for the most critical requirement, natural frequency to become 1. Therefore, the dimensions from the last column of Table 6 are the optimal ones, considering the natural frequency. The table also shows the initial dimensions for comparison:

Table 6 – Optimized bridge dimensions in meters and millimetres

Dimension	Unit	Initial value	Optimized value
bridge length (L)	mm	30000,00	30000,00
bridge width (b)	mm	4500,00	4500,00
Bridge effective width (b_eff)	mm	4448,64	4100,00
bridge height (h)	mm	1000,00	745,20
thickness top skin (tu)	mm	12,60	12,60
thickness bottom skin (t1)	mm	12,60	12,60
thickness webs (t1p)	mm	6,72	6,72
height webs (hc)	mm	974,80	720,00
number of core profiles	mm	21,00	20,00
height core (hc)	mm	974,80	720,00
width per core profile (wc)	mm	204,80	204,80
width of flange	mm	25,68	200,00
number of steel bar pairs	mm	21,00	20,00
width of steel bars (ws)	mm	100,00	100,00
Height of steel bars (hs)	mm	10,00	10,00

It can be observed that the most significant change occurred at the height of the bridge which was lowered from 1000 millimetres to 745,2 millimetres. Thus, the height of the webs and core profiles dropped as well. Other changes include wider flanges (in order to accommodate railings), and consequently, less core profiles and steel members.

Consequently, the moment of inertia, bending stiffness, weight and permanent load change. Subsequently, the results of all the checks change. Using the same algorithms and formulae described above, the values from Table 7 are obtained for the optimized cross section:

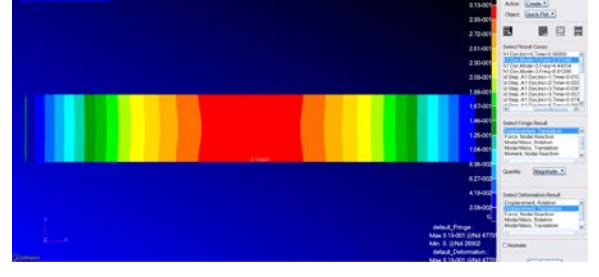
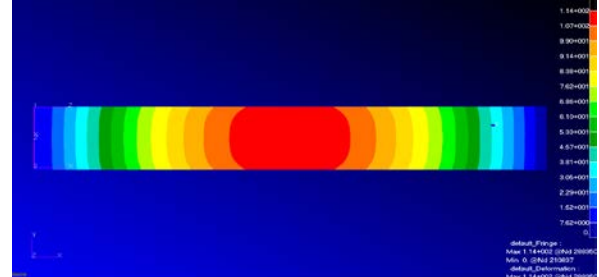
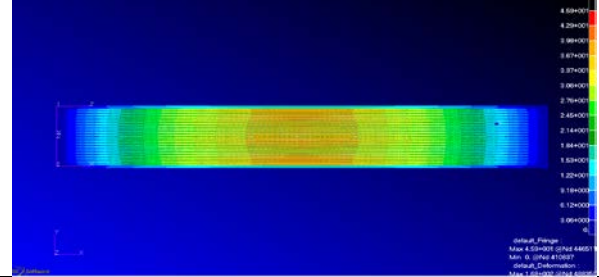
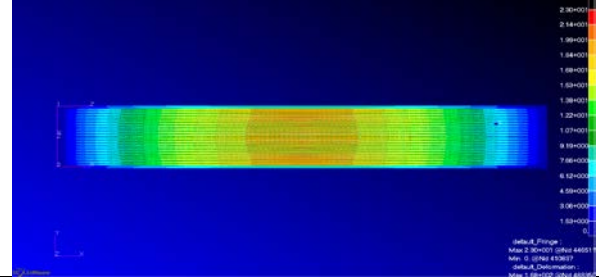
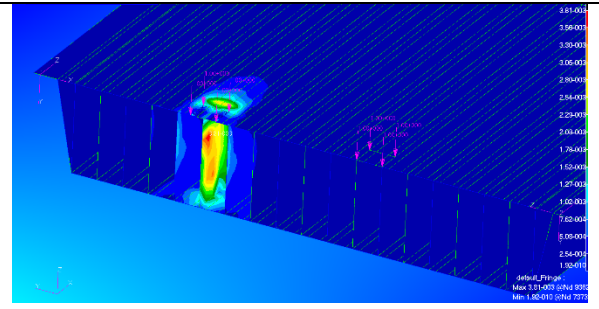
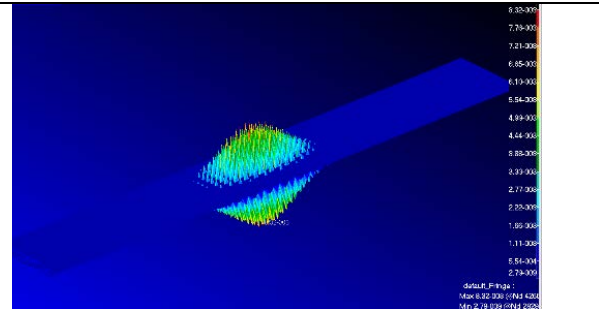
Table 7 - overview showing properties and calculated effects of the deck for initial and optimised dimensions; design values

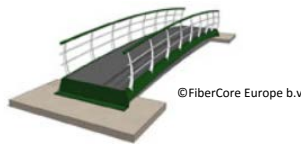
Parameter	Unit	Initial value	Optimized value	Design value
Moment of inertia	mm ⁴	3,81*10 ¹¹	1,48*10 ¹¹	-
Bending stiffness	N* mm ²	3,9*10 ¹⁵	1,59*10 ¹⁵	-
Weight	N	294.330	255.060	-
Permanent load	N/mm	9,81	7,74	-
Natural frequency	Hz	3,29	2,307	2,3
Deflection due to live load	mm	67,64	109,8	300
Normal stresses	N/mm ²	2,4	2,4	119,88
Bending stresses in skin	N/mm ²	19,07	30,43	186,2
Bending stresses in steel member		6,38	10,69	119,88
Shear stresses in web	N/mm ²	9,16	22,31	36,73
Compression stresses in web	N/mm ²	35,82	35,79	67,34
Maximum shear stress	N/mm ²⁰	0.013	1,84	
Web buckling factor	-	4,7	8,6	1
Thermal axial stresses skin	N/mm ²	1,75	1,75	10
Thermal axial stresses steel member	N/mm ²	2,21	2,21	
Adhesive bond shear stresses	N/mm ²	0.056	0.092	5.9

4.6. Detailed design

Based on the results of the preliminary design, the optimized deck is modelled in 3D and the following FEM results are obtained:

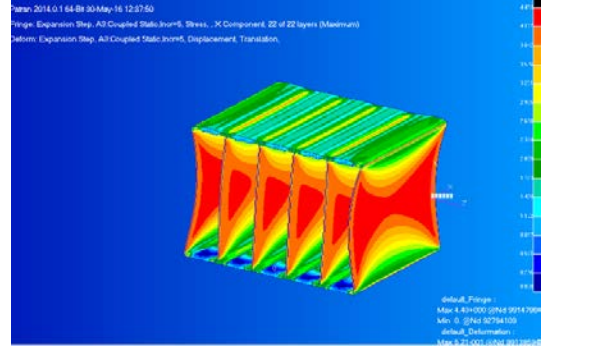
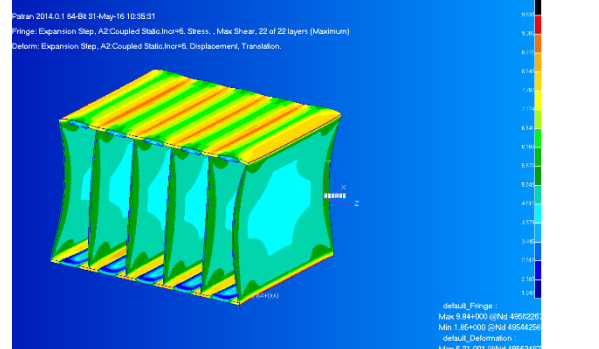
The table below presents the results of the global effects on the 3D model with 3D elements. For each result, the following information is provided: the view, desired parameter, its maximum value, where the maximum value occurs and for which load case was it analysed

	
<p>Top view; natural frequency – 2,31 Hz LC: Natural frequency (see chapter 3.1.5.3)</p>	<p>Top view; deflection due to live load – 114 mm LC: SLS (see chapter 3.1.5.3)</p>
	
<p>Top view; bending stresses – 45,9 N/mm² LC: ULS (see chapter 3.1.5.3)</p>	<p>Top view; shear stresses – 23 N/mm² LC: ULS (see chapter 3.1.5.3)</p>
	
<p>Isometric view, detail of the end of the deck where the rear wheel prints are applied; shear stresses due to wheel action; Critical buckling factor 4,78 LC: Buckling (see chapter 3.1.5.3)</p>	<p>Isometric view; shear stresses due to SLS UDL; Critical buckling factor 17,14 LC: Buckling under SLS UDL (see chapter 3.1.5.3)</p>

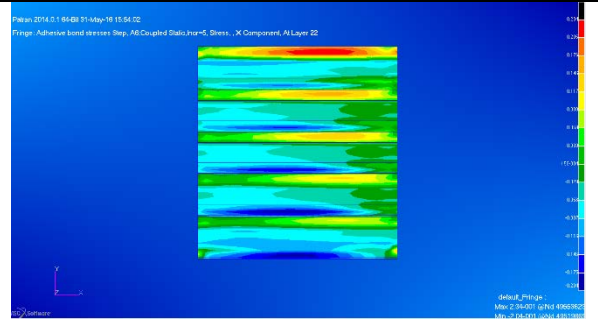
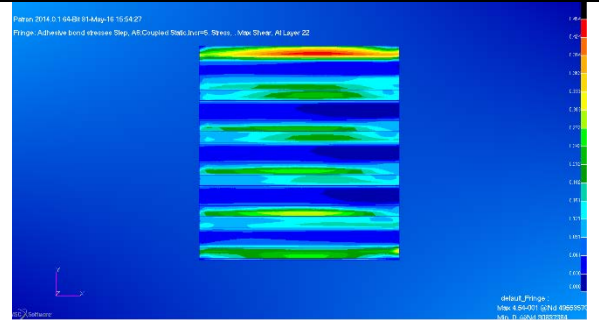
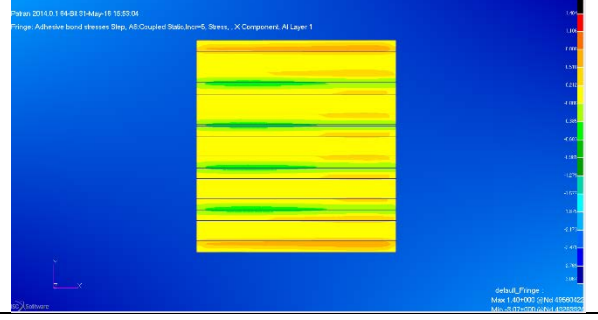


The following table shows the both bending and shear stresses, both in the innermost GFRP ply and steel member for the contraction load case. Afterwards, the maximum shear and bending stress is shown both for the contraction and expansion load cases. As explained in chapter 3.5.3.1, the results plotted on the central core are relevant for the bridge, therefore the values indicated as the maximum ones are not relevant. An explanation is provided for each result.

<p>Top skin, bottom view; Thermal axial stresses in skin; LC: Contraction (see chapter 3.1.5.3); max value: 1,72 MPa; min value: -1,89 MPa; value at the interface: -0,5 → 0,5 MPa</p>	<p>Top skin, bottom view; Thermal axial stresses in steel; LC: Contraction (see chapter 3.1.5.3); max value: 2,25 MPa; min value: -4,98MPa; value at the interface: -1,5MPa;</p>
<p>Top skin, bottom view; Thermal shear stresses in skin; LC: Contraction (see chapter 3.1.5.3); max value: 8,01 MPa; min value: 0 MPa; value at the interface: 3,2 → 5,8 MPa</p>	<p>Top skin, bottom view; Thermal shear stresses in steel; LC: Contraction (see chapter 3.1.5.3); max value: 9,05 MPa; min value: 1,96 MPa; value at the interface: 3,8 → 5,2 MPa</p>
<p>Isometric view; thermal contraction – bending stresses – 6,7 MPa LC: Contraction (see chapter 3.1.5.3)</p>	<p>Isometric view; thermal contraction –shear stresses – 12,07 MPa LC: Contraction (see chapter 3.1.5.3)</p>

	
<p>Isometric view; thermal expansion – bending stresses – 4,33 MPa LC: Expansion (see chapter 3.1.5.3)</p>	<p>Isometric view; thermal expansion – shear stresses – 9,84 MPa LC: Expansion (see chapter 3.1.5.3)</p>

The next table presents the stresses under the ULS load case both in the innermost GFRP ply and steel member. Afterwards, the maximum shear and bending stress is shown for the same load case.

	
<p>Top view; adhesive bond bending stresses in skin – 0,23 MPa LC: Adhesive bond stresses (see chapter 3.1.5.3)</p>	<p>Top view; adhesive bond shear stresses in skin – 0,45 MPa LC: Adhesive bond stresses (see chapter 3.1.5.3)</p>
	
<p>Top view; adhesive bond bending stresses in steel member – 1,4 MPa LC: Adhesive bond stresses (see chapter 3.1.5.3)</p>	<p>Top view; adhesive bond shear stresses in steel member – 3,85 MPa is indicated, however these stresses are actually located where the boundary condition is applied; can be seen from the picture that the maximum stress in the steel is around 1,2 MPa LC: Adhesive bond stresses (see chapter 3.1.5.3)</p>

4.7. Results comparison

Validation of the FEM model is done through comparison of results with analytical ones. The results can be seen in Table 8.

Table 8 - Results comparison between analytical and FEM calculations

Check	Analytical value	FEM value	Difference (%) 100%-(FEM/Analytical)	Difference (unit) FEM - Analytical
			max 10%; preferred 5%	max 10; preferred 5
SLS LC				
Deflection live load (mm)	109,80	114,00	-3,82%	4,20
Nat Frequency (Hz)	2,30	2,31	-0,30%	0,01
ULS LC				
Max Bending stress (MPa)	42,26	45,90	-8,60%	3,64
Max Shear stress (MPa)	22,30	23,00	-3,15%	0,70
Buckling under SLS UDL LC				
Buckling factor (UDL)	8,59	8,93	-3,91%	0,34
Adhesive bond stresses LC				
Shear stresses between steel and skin (MPa)	0,176	0,093	47,30%	0,08
Thermal stresses LC				
Axial thermal stresses in steel	2,206	2,25	-56,68%	0,04
Axial thermal stresses in skin	1,750	1,724	-41,36%	0,03

The table was designed to generate the difference by dividing the FEM value to the analytical one and multiplying with 100.

The issue is that in the case of large values (i.e. such as deflection), the difference between the two values is 4 units and this means approximately 4%. However, in the case of smaller values (i.e. such as thermal stresses), the difference is very small, but the difference percentage wise is very large.

A better approach is to also look at the difference in values while considering the same difference as maximum and preferred. This time, it can be seen that all values are very close to one another, most of them being less than 1 unit.

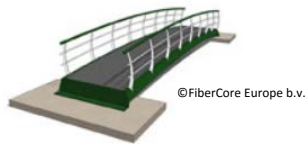
Looking at the correspondence between the two sources, it can be affirmed that the results of the model can be relied upon.

The causes for difference in results between the two sources are explained in the following chapter.

4.8. Drawings

The drawings for the 30 meter-long bridge, attached in Appendix 21 are:

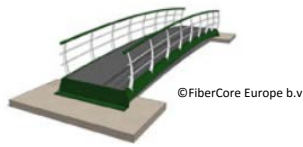
- Drawing 1
 - Overview of the situation, scale 1:500 – drawing shows the proposed bridge on the location together with its connection with existing roads;
 - Top view, scale 1:100 – drawing presents the top view of the deck and abutments with dimensions;
 - Longitudinal cross section A-A', scale 1:100 – drawing displays the longitudinal cross section through the centre of the deck, the abutments, ground and water levels and soil layers;
 - Detail 1, scale 1:10 – top view of the campshedding with dimensions;



- Detail 2, scale 1:20 – The campshedding’s cross section with dimensions;
- Detail 3, scale 1:50 – the left abutment with soil improvement, pad foundation and deck connection to it.
- Drawing 2
 - Cross section BB’, scale 1:20 – drawing shows the cross section of the bridge deck and railings with dimensions;
 - Cross section BB’, scale 1:20 – drawing shows the cross section of the bridge deck and railings with dimensions related to lanes, kerbs, sidewalks according to CROW
 - Detail 4, scale 1:5 – railing connection with deck;
 - Detail 5, scale 1:5 – connection between steel and GFRP skin.

Subsequently, a second set of drawings for the 60 meter-long bridge are provided in Appendix 22.

- Drawing 3
 - Top view, scale 1:200 – drawing presents the top view of the deck and abutments with the dimensions;
 - Side view, scale 1:200 – drawing displays a side view of the deck, the abutments, ground and water levels and soil layers;
 - Anchor plan, scale 1:200 – drawing showing the locations and position of the anchors in both abutments;
 - Pile plan, scale 1:200 – drawing showing the locations and positions of piles in the foundation for both abutments.
- Drawing 4
 - Top view of the left abutment, scale 1:25 - dimensions drawing;
 - Longitudinal cross section of the left abutment, scale 1:25 - dimensions drawing;
 - Cross section of the left abutment, scale 1:25 - dimensions drawing;
 - Top view of the left transition slab and ridge, scale 1:10 - dimensions drawing;
 - Longitudinal cross section of the left transition slab and ridge, scale 1:10 - dimensions drawing;
 - Cross section of the left transition slab and ridge, scale 1:10 - dimensions drawing;
- Drawing 5
 - Top view of the left abutment, scale 1:25 - reinforcement drawing;
 - Longitudinal cross section of the left abutment, scale 1:25 - reinforcement drawing;
 - Cross section of the left abutment, scale 1:25 - reinforcement drawing;
 - Top view of the left transition slab and ridge, scale 1:10 - reinforcement drawing;
 - Longitudinal cross section of the left transition slab and ridge, scale 1:10 - reinforcement drawing;
 - Cross section of the left transition slab and ridge, scale 1:25 - reinforcement drawing;
 - Pile foundation, scale 1:25 – reinforcement drawing;
 - Pile cross section, scale 1:5 – reinforcement drawing



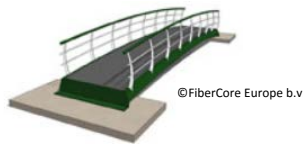
5. Analysis and interpretation of results

The current chapter aims at explaining the results presented in the previous chapter. Furthermore, the connection between the analytical and FEM results is made and the reasons results vary are explained.

5.1. Causes for results difference between analytical and FEM calculations.

As can be seen from Table 8, the results obtained from analytical calculations vary from the ones Marc Patran calculated. The current sub chapter aims at explaining the sources for these differences.

- General differences
 - For simplification purposes, during the analytical calculations, the cross section was considered perfectly rectangular thereby having the neutral line positioned exactly across the centre.
 - In the FEM model, the cross section was designed as it will be built, including flanges, bulkheads and stronger angled side webs., thereby shifting the neutral line upwards.
 - While viewing results in Marc Patran, there is no option to show a certain effect on one object at a time. This becomes increasingly problematic when a homogenous and a laminated body are in contact with each other (i.e. steel member and top skin). When viewing stresses in the first layer there is no problem since both bodies have a first layer. However, when attempting to check stresses in the other layers, the homogenous body (i.e. steel) shows a value of 0 and the laminated material shows the value for the respective layer. The problem rises from the fact that Patran attempts to bridge the difference between the values in the two bodies and show an average which for other than the first layer is wrong. The solution is to see the maximum value of all the layers which will show the stresses in the first layer for the homogenous material and the highest stresses in the respective layer of the laminate.
 - The mesh size is crucial for obtaining accurate results, however, the finer the mesh, the longer the calculation time. Therefore, in order to achieve reasonable calculation times for one model and to avoid errors and crashes of the program, the size of the elements was kept above 200 mm in the large scale model. This is also the reason why for the thermal stresses and adhesive bond stresses, a smaller model was created. On this smaller model, a much finer mesh (i.e. element size of 10 mm) could be applied and therefore, the results obtained from this model are much closer to the ones obtained analytically.
- Deflection
 - In the analytical calculation, the deflection was calculated using the deck's bending stiffness and the live load;
 - In the 3D with 2D elements FEM model, the deflection value was larger than the one obtained analytically due to the coarse mesh elements.
- Stresses
 - In the analytical calculation the bending stresses were calculated after transforming the heterogeneous cross section into a homogenous one using the transformed area method. Furthermore, the webs were not taken into account when calculating the section's bending stiffness because it was not possible to transform them to equivalent steel members as well.
 - In the FEM model, the webs are taken into account with the corresponding strength as resulted from the input properties.



- Shear stress at the interface
 - The analytical calculation was done considering only the contact area between the steel and the skin.
 - In the small scale FEM model which only comprised of a steel member and the top skin, the result was very similar to the analytical one. Upon enlarging the model and forming 5 cores with webs, bottom skin and bottom steel member, the influence of the other members reduced the final stress value. However, the last value is considered since in reality the surrounding components contribute to the stress distribution.
- Thermal stresses
 - The analytical calculation only considered the contact area between the steel and skin.
 - The FEM model contains 5 core profiles which means that there is a larger cross sectional area of the skin that is constrained by the steel; therefore the stresses in the FEM model are higher than those obtained analytically.

5.2. Evaluation of results

The current chapter aims at analysing the results and making connections between the preliminary and detailed phases of the project. Firstly, the results obtained analytically are evaluated, followed by those acquired from the FEM model.

5.2.1. Evaluation of results from preliminary design

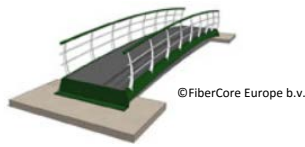
Having performed the analytical calculations using the preliminary cross section design and dimensions, the results presented in chapter 4.4 were obtained. As can be seen from the unity checks, the initial cross sectional dimensions were conservative. Designing a bridge that strong essentially means over designing it which is not desirable.

Therefore, in order to propose an optimal design, the input dimensions had to be adjusted and the calculations had to be reiterated as shown in chapter 4.5, in order for the deck to meet the most critical requirement. In case of the current bridge, the natural frequency requirement is decisive.

Thus, the optimised section has a natural frequency equal to the minimum value, consequently ensuring compliance with the regulations. Furthermore, it can be observed that the optimised thinner deck deflects 40% more however, it is not critical since the value is more than twice as low as the maximum value.

Related to bending and shear strength of the deck, even though in the optimised design, the stresses are almost twice as large, they are still far below the design strength of the material. This is to be expected since the strength of the GFRP is not an issue in the case of such structures. Additionally, normal stresses in the structure have very low values as well which is to be expected since there is no significant horizontal, apart from the one caused by braking of an unauthorised vehicle.

The stability of the webs was one of the requirements that had the potential of becoming critical. However, due to the fact that the optimisation reduced the deck's thickness, the critical buckling factor increased, which is to be expected since a smaller plate with edges closer together is stiffer. The buckling of the web is also prevented due to the spacing between the webs. It has been determined by FiberCore Europe, (2016) that by designing between 5 and 6 webs per meter, the stresses caused by concentrated loads can successfully disperse and be carried by more webs, thus reducing the number of heavily loaded webs that have the potential to buckle.



Related to the strength of the adhesive bond between GFRP and steel, the conservative design value determined by Wilken, (2015) was used as a design value. The stresses induced by the ULS udl in the GFRP skin and steel member were very low, reaching about 1% of the material's capacity. These stresses however, being obtained analytically represent an average value across the material. The exact value has been obtained during the detailed design and is analysed in the following part.

Furthermore, the thermal shear stresses in the GFRP skin and steel member have to be carried by the resin as well. The analytical calculations proved that thermal stresses in the steel and composite, caused by the temperature gradient prescribed of the Eurocodes, were low compared to the resin's design strength, which was to be expected to a certain extent, due to the similarity between the CTEs of the GFRP and steel. As before, the analytical algorithm only allowed the determination of average stresses in the members. The specific stresses in the layers adjacent to the resin were determined with the aid of the FEM model.

5.2.2. Evaluation of results from detailed design

Having implemented the optimized cross section in Marc Patran, the results presented in chapter 4.6 were obtained. The first table presents the global effects determined with the full scale model, the second page illustrates the thermal stresses obtained with the partial model and the third page shows the adhesive bond stresses also obtained in with the partial model.

The natural frequency and the deflection only served as proving the accuracy and reliability of the deck, since it was already optimised for the lowest value of the former. Related to the deflection, it can be noted that the maximum value occurs in the middle as expected, however, it is not a straight line cross wise. In the vicinity of the edges, the deformation is reduced. This is also to be expected due to the increased stiffness provided by the flanges and side laminates. Nevertheless, such a variation could not be determined analytically.

Furthermore, bending and shear stress values are considerably low compared with the design strengths of the laminates, as were the expectations. Thus those values are not detailed further. The most important effects to be discussed in the following sub chapters are: buckling of the webs under wheel load, thermal and adhesive bond stresses.

5.2.2.1. Web buckling under wheel load

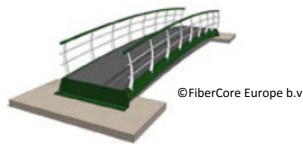
The buckling effect that can be caused by the concentrated loads of the unauthorised vehicle's wheels was checked and the results from chapter 4.6 confirm that the webs do not buckle under the 40 kN load per $0,2 \times 0,2 \text{ m}^2$, since the critical buckling factor is 4,8.

The picture also shows that both wheel positions described in chapter 3.5.3.6.4. were analysed at the same time. The situation in which the wheel is located directly above one web has been proven to be the critical one. (i.e. the buckling effect is plotted one that web, which means that it will fail before the other). The outcome is to be expected since in this situation, only one web takes most of the load, whereas in the second one, two webs carry equal amounts of the load.

5.2.2.2. Thermal stresses

Two load cases were considered for thermal stress analysis, as described in chapter 3.5.3.3. The temperature difference in contraction was larger than that of the expansion, therefore, the former was the critical load case.

As shown in the results chapter, shear and bending stresses were calculated. Furthermore, due to the possibility of evaluating stresses per ply, the maximum values in the layers of interest were selected.



Thus, it can be observed that the maximum shear stress occurring in the GFRP ply in contact with the steel ranges between 3,2 and 5,8 MPa. Additionally, the maximum shear stress occurring in the steel member ranges between 3,8 and 5,2 MPa. It can also be observed that the maximum shear stresses are around 8-9 MPa. These peak values occur at the ends of the model, where they have no importance because they are increased due to the boundary conditions.

Wilken, (2015) experimentally determined the resin's shear strength between GFRP and steel to be 5,9 MPa. However, as stated in the theoretical framework, it has been concluded that this was a conservative value due to the limitations of the experiment and "should not be used as a design allowable because of the nature of the single-lap joint tests". (Wilken, 2015)

Nevertheless, if considering the abovementioned result, the resin still has sufficient shear capacity to deal with the stresses occurring in the deck, though near the end supports the stresses approach the critical value. Consequently, two solutions can be proposed. Firstly, further testing of the resin is recommended in order to establish its actual shear strength. Secondly, use of mechanical connections in addition to the adhesive joint, specifically, shape joints in the form of bending the steel members at the ends of the deck.

Furthermore, the calculated axial stresses are relatively low compared with the shear ones. Unfortunately, there is no design value for the axial capacity of the resin between the steel and GFRP.

However, an assumption can be made based on the resin's shear and tensile inter-laminar strength, as indicated by the CUR and presented in Appendix 14 together with the shear strength determined by Wilken, (2015).

Specifically, the CUR states that the inter-laminar shear strength of polyester resin is 20 MPa and the tensile strength 10 MPa. Consequently, based on the 5,9 MPa shear strength, the tensile strength can be estimated at 3,95 MPa. Considering this value, it can be stated that the axial stresses in the GFRP and steel are considerably lower.

5.2.2.3. Adhesive bond stresses

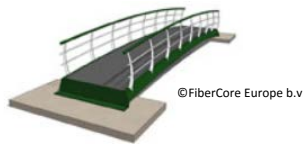
The stresses generated by the ULS udl in the adhesive bond were also computed. The results show that in this load case the shear stresses occurring in the GFRP ply and steel, (i.e. 1,2 and 1,4 MPa respectively). These values represent 20-25% of the shear strength determined by Wilken, (2015) which can only be considered as a conservative value.

5.2.3. Evaluation of available optimization techniques

The optimisation proposed with the current report is mainly related to cross sectional dimensions and does not deal with altering the deck in its entirety.

Therefore, radical changes have not been proposed due to the fact that major design principles have been decided upon by FiberCore Europe following research and testing and no advantage would come from changing either of them.

- Web spacing – It has been tested against wheel loads and proved that 4 or more webs carrying one wheel is a safe consideration
- Arched longitudinal profile of the deck – this is desired in order to limit the effect of GFRP creep which in turn causes long term deformation, in addition to the one caused by loads. Moreover, an arched deck is better able to transfer the bending towards the supports than a plane one



6. Conclusion

Over the course of realising the current research and design thesis, several considerations were formulated with regards to designing lightweight, slender composite structures.

As stated before, the critical aspect when designing a long, slender structure is the natural frequency. Although it has nothing to do with the strength of the deck, preventing vibrations from occurring during use increases the comfort of its users and in turn the likelihood the structure is going to be used.

In relation to thermal properties, considering that each material has its own coefficient for thermal expansion, and behaves differently when subjected to the same temperature gradient, the variation in expansion and contraction between the different materials has to be checked and the stresses resulting from the difference have to be within the allowable limits of the connection method.

Related to designing structures made with or incorporating composite materials, an important aspect is to check the compatibility of the materials involved. Special consideration has to be given to the interface between the two materials and the connection methods. These depend on the stresses that act on the different materials. One of the most problematic influences is temperature difference.

Furthermore, when designing a structure made with a composite material it is useful to know that not only the former, but also the latter can be adjusted to suit the needs and fulfil the function. Specifically, as has been discovered during the current project, the structure of a laminate composed of different plies can be changed by adding or removing plies of a certain orientation in order to better deal with the main direction of the stresses (e.g. in case of dominant longitudinal bending stresses, the amount of 0 degrees' plies can be increased while in the case of dominant shear stresses, the amount +/-45 degrees' plies can be increased).

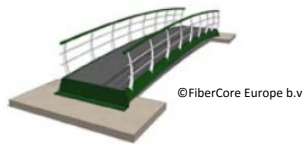
Additionally, over the course of the current project symmetrical and balanced laminates were used. This means that the plies are symmetrical with regards to the mid plane and all the +45 degrees' plies have a corresponding -45 degrees' plies. It is important to use laminates with these properties in order to have less internal stresses acting on the structure.

This composites property becomes interesting because of the range of possibilities that arise. These include the ability to change the layup in order to obtain a desired coefficient of thermal expansion in one direction or a better stress distribution at a location where stress concentrations are present.

Having outlined the general outcomes of the research, the next paragraphs describe the project specific conclusions the researcher formulated.

Hence, the purpose of the project was to design a 30 meter GFRP-steel hybrid bridge that is going to be built over the Rotte, near Rotterdam. It was divided into several phases that enabled progress, optimization and finally completion.

The first phase was to decide which of three possible cross section designs was most suitable for implementing at the aforementioned location. The concepts were analysed in a Multi Criteria analysis in relation to design, procurement and manufacturing challenges, together with costs and steel's contribution to stiffness and concept design 1 was concluded to be the most feasible due to a number of reasons. Firstly, it requires minimal alterations to the current manufacturing process due to the relatively small size of the steel members. Secondly, although it requires steel components, they can be standardized, therefore, additional lead time and costs can be reduced. Thirdly, even though the production time will increase, out of the three concepts, this one will cause the smallest growth.



The second phase was represented by the preliminary design whose purpose was to optimise the cross section based on analytical calculations. The analytical calculations comprised of the checks characteristic for a cycling and pedestrian bridge, as prescribed in the Eurocodes, in relation to the ULS and SLS. Moreover, additional checks related to buckling resistance and deflection due to creep of composite materials, only available in the CUR aanbevelingen 96, were performed. The analytical part concluded with the following optimisations. Firstly, the overall thickness of the deck was reduced by 25%, specifically from 1000 to 745,20 mm so that the unity check for the natural frequency reached 1, thus ensuring the deck is not overdesigned and secondly, the number of cores was changed in order to accommodate wider flanges, thus lowering the amount of cores and steel plates.

The third phase involved developing the detailed design which consisted of creating two 3D FEM models (i.e. the full sized one and the small one representing a part of the deck), validating them with the help of analytical calculations and then using them to check global and local effects.

A considerable advantage offered by the finite element modelling was that unlike analytical calculations where assumptions and simplifications have to be made in order to determine the value or location of maximum stresses, through FEM not only the exact location of stresses, but also their distribution into adjacent structures or members are calculated by the program. Furthermore, in case of analysing point loads on slabs (i.e. such as the wheel load on a bridge deck), the load spreading, actual stress distribution and the number of load carrying webs could be determined. These results simply could not be obtained through analytical calculations alone where through assumptions, only an indication of the area of effect could be determined.

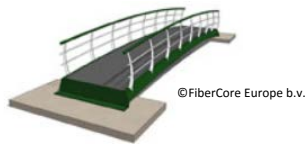
Therefore, the large model was used to determine the natural frequency and deflection together with bending and shear stresses. Using the design values for the aforementioned effects of the different laminates present in the cross section as reference, it was possible to conclude that the design fulfils the SLS and ULS criteria and the applied loads are lower than the design values. Moreover, the buckling of the webs under the wheel loads of an unauthorised vehicle was checked and the conclusion was that buckling does not occur.

Furthermore, the results provided by the small model led to the following conclusions. Firstly, the stresses in the adhesive bond between the steel and innermost GFRP layer are very low when considering the ULS udl, therefore the connection will not fail. Secondly, the thermal stresses in the steel and innermost GFRP layers can pose an issue to the adhesive bond when subjected to the temperature gradient described in the Eurocodes. Therefore, in order to eliminate the risk of failure of the adhesive bond, mechanical connections, such as extending and bending of the steel members at the ends of the deck can be investigated and implemented in the design, as stated in chapter 7.

Having produced an optimum cross section, the drawings required for implementing this bridge at its location were created, including details such as soil improvement at the abutments, railing connections, approach roads and soil retaining measures for the supplemented soil.

Therefore, due to the fact that the designed deck fulfils the criteria of the ultimate and the serviceability limit states and, in addition, the thermal stresses acting on the resin layer binding the steel to the GFRP are lower than the design strength of the material, it can be concluded that the proposed design is safe and comfortable to use and can be implemented at the desired location as it will fulfil its function as per the design requirements.

Additionally, in order to meet one of the university requirements, a separate, yet not unrelated task was undertaken. Specifically, determine the maximum span that could be achieved with the previously designed optimized cross section if a fully fixed (i.e. clamped) foundation was used. After modelling a



few options in Marc Patran, the decisive span for which the natural frequency requirement is met, was concluded to be 60 meters. Thus, several drawings were made for this bridge with emphasis on the foundation and connection between it and the deck.

Related to the method used during the current research project, it can be observed that a complex and extensive procedure was used for the design of one bridge. A combination of analytical calculations, and FEM models at three different levels of detail were employed to determine whether such a combination of materials can be implemented as a bridge. Moreover, the most critical failure modes had to be determined.

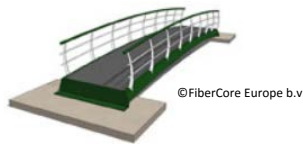
The approach used is characteristic of researching the implications and effects of a new concept, material composition or technique. Once a detailed research has been conducted and the main failure modes have been understood and prevented or, if possible, eliminated, subsequent implementations of the concept will no longer require the same detailed design procedure.

In my opinion, analytical calculations would be sufficient if making use of the same cross section for different situations. In case modifications arise, be it in relation to the size or shape, position or number of steel elements or the span of the bridge, then, in addition to meeting the natural frequency requirement, an evaluation of stresses at the interface, both due to structural and thermal loading has to be performed.

Moreover, a desirable approach would be to create, evaluate and approve standard cross sections for a certain range of spans, thus simplifying the design process for future projects.

Based on the aforementioned conclusion, it can be stated that all sub-questions posed in chapter 1.7 have been answered, therefore, the main research question, *“How can an optimal, structurally justified GFRP-steel hybrid bridge deck be designed so that it is suitable to be implemented in a 30-meter-long cycling and pedestrian bridge over the Rotte near Prins Alexander district, Rotterdam?”* has been answered.

Besides successfully completing the graduation research and acquiring the theoretical and vocational competences together with job specific knowledge, the researcher has been awarded a full time job with the host organisation for at least one year.



7. Recommendations

Having answered the main question with a suitable design that satisfies both the requirements of the client and those of FiberCore Europe of designing a 30-meter-long bridge made with a GFRP-steel hybrid material, several aspects that need further attention were discovered over the course of the current project.

Firstly, due to the time constraint, simplified FEM models were created in order to evaluate the required effects. With sufficient time and mesh optimization, one full scale 3D model can be created which can further be used for evaluating all the effects that have been obtained from separate models. Thus, the most suitable solution is to create a $\frac{1}{4}$ model of the bridge deck with solid elements, apply symmetry boundary conditions to it and then use it for all the necessary analyses. There is one point of attention related to this model, namely the fact that this method can be used in this situation since the deck has two axis of symmetry (i.e. longitudinal and transverse one).

Secondly, more local effects can be checked, including the effect of the railing on the flange, the stress distribution at the location of the connection with the deck, the effect of a wheel load being applied on the flange and the extent to which it can withstand this load.

Thirdly, the influence of thermal cycles and non-uniform heating of the deck can be investigated. The former refers to day-night or summer winter cycles while the latter refers to different portions of the deck being heated differently to mimic shade and sun exposure.

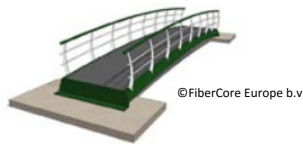
Fourthly, more research can be performed on stresses that occur during and after the curing process. Specifically, due to the fact that much higher temperatures are achieved during the fabrication process than during normal use, it is recommended to check the stresses caused by a larger temperature difference than the one prescribed in the Eurocodes and establish whether the bridge can be produced with the existing fabrication process.

More research is advisable related to integrating steel into the production process. Apart from the temperature gradient during the curing process, there are several challenges associated with adding a new material to the production process, as outlined and briefly analysed during the multi criteria analysis in Chapter 3.2.4. of the current document.

Related to the inclusion of the steel in the cross section, the calculation has provided an answer regarding to the amount that is required to achieve the desired stiffness. However, as the criteria of the Design Concepts show, the particular arrangement is not advantageous when analysing the production process. Therefore, different shapes and sizes of steel members can be analysed in order to identify the least intrusive one. The important aspect to consider is to keep the value of the moment of inertia the same and change the width, height, distance from the deck's centre of gravity.

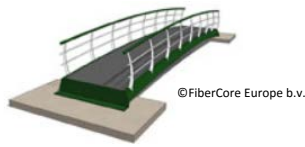
Furthermore, related to the connection between the steel and GFRP in addition to relying on resin's strength, more reliable mechanical connections can be employed. These can include:

- bolted joint covered in GFRP layers and infused with resin in order to protect against corrosion;
- shape joint achieved with grooves on the steel member which would fit into grooves in the foam and contribute to shear strength;
- steel members can be bent at the ends of the deck similar to steel reinforcement in concrete; thus, in case of joint or bond failure, the risk of the steel penetrating the GFRP and becoming exposed is greatly reduced;

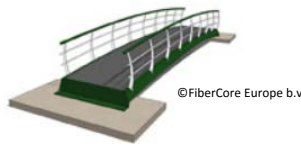


Bibliography

- European Committee for standardization. (2003). *Eurocode 1: Actions on structures - Part 2: Traffic loads on bridges*. Brussels: European Union.
- ABDmatrix. (2015). *Laminate Analysis*. Retrieved February 24, 2016, from ABDmatrix: <http://abdmatrix.com/site/openrepository/files/Laminate%20Analysis.pdf>
- Actueel Hoogbestand Nederland. (2016, 05 30). *Viewer*. Retrieved from Actueel Hoogbestand Nederland: <http://www.ahn.nl/pagina/apps-en-tools/viewer.html>
- Autodesk. (2014, December 01). *[ABD] Matrices and [ABD] Inverse Matrices*. Retrieved February 24, 2016, from Autodesk: <https://knowledge.autodesk.com/support/helius-composite/learn-explore/caas/CloudHelp/cloudhelp/2015/ENU/ACMPDS/files/GUID-FC91F385-B1FF-4836-B52C-3150F01ABC9A-htm.html>
- Autodesk. (2015). *Finite element analysis*. Retrieved December 21, 2015, from Autodesk: <http://www.autodesk.com/solutions/finite-element-analysis>
- Civieltechnisch Centrum Uitvoering Research en Regelgeving. (2003). *CUR - Aanbeveling 96 - Fibre reinforced plastics in civil engineering supporting frameworks*. Gouda: CUR Net.
- CROW. (2016, 05 30). *Crow kennisplatform*. Retrieved from CROW: <http://www.crow.nl/>
- DINOloket. (2016). *Ondrgrondmodellen*. Retrieved from DINOloket.
- European Committee for Standardisation. (2006). *Eurocode 3 - Design of steel structures - Part 1-5: Plated structural elements*. Brussels: European Union.
- European Committee for standardization. (2002). *Eurocode 0 - Basics of structural design*. Brussels: European Union.
- European Committee for standardization. (2003). *Eurocode 1: Actions on structures - Part 1-5: General actions - Thermal actions*. Brussels: European Union.
- Feldmann, M. P.-I., & Heinemeyer, C. D.-I. (2008, December). *Human induced Vibrations of Steel Structures - Design of Footbridges*. Retrieved from Institut und Lehrstuhl für Stahlbau Leichtmetallbau: http://www.stb.rwth-aachen.de/projekte/2007/HIVOSS/docs/Footbridge_Background_EN02.pdf
- FiberCore Europe. (2016). *"Innovative material solutions for economical composite bridges with large spans and constrained slenderness"*. Rotterdam, the Netherlands: FiberCore Europe. Retrieved February 2016
- Gokhale, N. S., Deshpande, S. S., Bedekar, S. V., & Thite, A. N. (2008). *Practical Finite Element Analysis*. Maharashtra, India: Finite to Infinite.
- Gurit. (2016). *Guide to Composites*. Retrieved February 18, 2016, from Gurit: <http://www.gurit.com/files/documents/guide-to-compositesv5webpdf.pdf>
- Hauffe, A. (2016, 04 13). *eLamX 2.3*. Retrieved from Technische Universität Dresden: https://tu-dresden.de/die_tu_dresden/fakultaeten/fakultaet_maschinenwesen/ilr/aero/download/laminatetheory/index_html
- Hibbeler, R. (2011). *Mechanics of Materials, Eight edition*. London: Prentice Hall.



- Infosteel. (2007). *Design of Footbridges - Background Document*. Retrieved December 21, 2015, from Infosteel: http://www.infosteel.be/hivoss/HIVOSS_FR/Footbridge_Background.pdf
- MSC Software. (2016). *About Us*. Retrieved from MSC Software: <http://www.mscsoftware.com/page/msc-software>
- MSC Software. (2016). *About Us*. Retrieved February 17, 2016, from MSC Software: <http://www.mscsoftware.com/page/msc-software>
- Parker, J. (2007, December 4). *Normal Stress, Bending Stress, & Shear Stress*. Retrieved from StruCalc: <http://www.strucalc.com/engineering-resources/normal-stress-bending-stress-shear-stress/>
- Philpot, P. T. (2011). Retrieved from Missouri University of Science and Technology: http://web.mst.edu/~mecmovie/chap08/m08_16_steel_alum.swf
- Razdolsky, L. P. (2014). *Probability based fire load*. Chicago: Cambridge University Press.
- Rijkswaterstaat. (2016, 05 30). *Waterstand t.o.v. NAP*. Retrieved from Rijkswaterstaat: <https://www.rijkswaterstaat.nl/kaarten/waterstand-tov-nap.aspx>
- TNO Geologische Dienst. (2016, 05 30). *Ondergrondmodellen*. Retrieved from DINOloket: <https://www.dinoloket.nl/ondergrondmodellen>
- Warnet, L., & Akkerman, R. (2008-2009). *Classical Lamination Theory*. In L. Warnet, & R. Akkerman, *Composites Course* (p. 4.5). Twente: University of Twente.
- Wikipedia. (2016, January 23). *Limit state design*. Retrieved from Wikipedia, the free Encyclopedia: https://en.wikipedia.org/w/index.php?title=Limit_state_design&oldid=701304540
- Wilken, A. (2015). *Innovative material solutions for economical composite bridges with large spans and constrained slenderness*. Rotterdam: FiberCore Europe. Retrieved December 20, 2015



Appendix 1 – validation of Excel spreadsheet

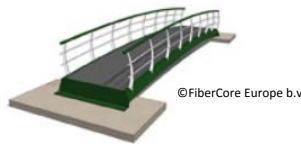
The purpose of the current appendix is to certify the validity of the excel spreadsheet and ensure that all results obtained with it can be relied upon.

The validation was performed as follows. A hand calculation for the deflection is provided and, in parallel, the same calculation with the parameters, calculated by Excel is given.

$$\begin{aligned}
 f_n &= \frac{K_n}{2\pi} * \sqrt{\frac{\frac{EI}{\gamma_{m,SLS} * \gamma_{cl,v}} * g}{(q_M + d_{TC} * b_{eff}) * L^4}} = \frac{11,647}{2\pi} * \sqrt{\frac{\frac{1575300737,03 \text{ Nm}^2}{1 * 1,21} * 9,81 \frac{\text{m}}{\text{s}^2}}{\left(7677,602 \frac{\text{N}}{\text{m}} + 0,5 \text{ m} * 4,1 \text{ m}\right) * (30 \text{ m})^4}} \\
 &= 1,8537 * \sqrt{\frac{1301904135,562 \text{ Nm}^2 * 9,81 \frac{\text{m}}{\text{s}^2}}{\left(7677,602 \frac{\text{N}}{\text{m}} + 2,05 \text{ m}^2\right) * (30 \text{ m})^4}} = \\
 &= 1,8537 * \sqrt{\frac{12771653082,863}{(7679,652) * (30 \text{ m})^4}} = 1,8537 * \sqrt{\frac{12771653082,863}{6220518120}} \\
 &= 1,8537 * \sqrt{2.05315} = 1,8537 * 1,4329 = 2,656
 \end{aligned}$$

Natural frequency check		
Original Kn	-	9,87
Correction factor	-	1,18
Kn corrected	-	11,6466
EI	Nm ²	1575300737,03
g	m/s ²	9,81
q(M) - self weight of deck	N/m	7677,602332
d(TC)	P/m ²	0,5
b(eff)	m	4,1
L span	m	30
f (K, dTC)	Hz	2,656
fn min	Hz	2,3
fn check	-	0,87

It can be observed that the result from the hand calculation is 2,656 and the result from the Excel spreadsheet is 2,656. The two results are equal up to the 3rd decimal which is sufficiently accurate for the current project. Therefore, it can be concluded that the Excel spreadsheet can be relied upon.



Appendix 2 – thermal expansion and thermal stresses algorithm

The current appendix presents the algorithm used for determining the thermal expansion and stresses of the steel and GFRP. Furthermore, the CTEs are given and their origin explained.

As stated in the theoretical framework, there are no regulatory guidelines for thermal loads acting on composite bridges. In practice the temperatures are derived from the NEN.EN.1991.1.5 standard with national annexes [NEN 1] and [NEN 2].

The CTE of steel, as provided in Annex C of EN.1991.1.5.2003 is: $\alpha_T = 12 * 10^{-6} \frac{m}{m * K}$ or $\left(\frac{m}{m * C}\right)$

However, according to Note 6 of Annex C of EN.1991.1.5.2003, (European Committee for standardization, 2003), the coefficient of thermal expansion of the steel component may be smaller in order to neglect restraining effects from different CTE values. Therefore, the lowered value is:

$$\alpha_T = 10 * 10^{-6} \frac{m}{m * K} \text{ or } \left(\frac{m}{m * C}\right)$$

The CTE of GFRP, can be determined through Classical Laminate Theory, since the individual components vary depending on the fibre volume content and the fibre orientation. During the current research, the CTE of the laminate was used, not the ones of the individual materials. Consequently, The CTEs of the composite laminate that comprise the top and bottom skin in the x and y directions, as used by FiberCore Europe, (2016) are:

$$\alpha_x = 8.22 * 10^{-6} \frac{m}{m * K} \text{ or } \left(\frac{m}{m * C}\right) \quad \text{and} \quad \alpha_y = 3.71 * 10^{-5} \frac{m}{m * K} \text{ or } \left(\frac{m}{m * C}\right)$$

With the CTE of the two materials, the individual expansions can be calculated for each one with the formula for linear expansion and the thermal stresses with Hooke's law.

$$\Delta l = L * \alpha * \Delta T \quad \text{and} \quad \sigma = E * \varepsilon \rightarrow \sigma = E * \alpha * \Delta T$$

Because of the temperature variation, the two materials expand (or contract). Due to the difference in CTEs between them, they expand differently when not constrained, with the steel expanding more than the GFRP skins in case of elevated temperatures. However, because they are bonded together along the entire length, in the end, both materials are constrained to reach the same length. This means that the steel is in compression and the skin in tension. These two axial forces have equal magnitude and opposite directions:

$$F_{steel} - F_{skin} = 0 \rightarrow F_{steel} = F_{skin}$$

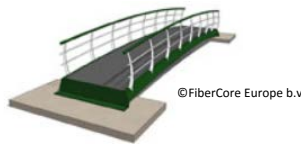
Furthermore, according to (Hibbeler, 2011), the axial thermal stresses between the two materials are determined by combining the thermal and displacement relationships.

$$\begin{aligned} \delta &= (\delta_{steel})_T + (\delta_{steel})_F = (\delta_{skin})_T + (\delta_{skin})_F \rightarrow \\ \rightarrow (\alpha_{steel} * \Delta T * L) + \frac{F_{steel} * L_{steel}}{A_{steel} * E_{steel}} &= (\alpha_{skin} * \Delta T * L) + \frac{F_{skin} * L_{skin}}{A_{skin} * E_{skin}} \end{aligned}$$

Rearranging the equation, F was determined:

$$F = \frac{\Delta T * L * (\alpha_{skin} - \alpha_{steel})}{\frac{L_{steel}}{A_{steel} * E_{steel}} - \frac{L_{skin}}{A_{skin} * E_{skin}}}$$

Subsequently, the corresponding axial stresses were determined with the formula: $\sigma = \frac{F}{A}$



Appendix 3 – deflection due to creep algorithm

The current appendix presents the steps of the algorithm defined in the CUR-aanbevelingen 96. (Civieltechnisch Centrum Uitvoering Research en Regelgeving, 2003) for calculation of deflection resulted from creep for a composite material.

The first step of the algorithm is to define the proportions of fibres in the three directions as follows.

Laminate: (x%/y%/z%) [0/90/+45]

The notation above describes the fibre orientation in one ply of the laminate. Therefore, x% of the fibres are spanning in the 0 degrees direction (i.e. x direction), y% of the fibres are spanning in the 90 degrees direction (i.e. y direction) and the remaining z% of the fibres are equally spanning in the +45 and -45 degrees direction.

Furthermore, the stiffnesses of one ply in the x and y directions according to FiberCore Europe, (2016) were:

- in fibre direction: $E_1 = 39.7 \text{ GPa}$
- perpendicular to fibre direction: $E_2 = 9.5 \text{ GPa}$

Afterwards, the stiffnesses of the laminate in the x and y directions were required. These properties were calculated in the eLamX software using the Classical lamination Theory, after inputting the desired layup. The values were written as: $E_{lam} = \begin{pmatrix} E_{lam,x} \\ E_{lam,y} \end{pmatrix} \text{ GPa}$

The CUR-96 states that the following parameters are required:

$t_{life} = 100 \text{ years}$ and $n = 0.01$ for GFRP laminate with all fibres in one direction.

With these parameters, the ply reduction factor could be determined with the following formula:

$$\gamma_{ck,UD} = \left(\frac{t_{life}}{hr} \right)^n$$

Afterwards, the reduced stiffness value for the UD ply could be calculated: $E_{lam,red} = \begin{pmatrix} 64\% \\ 21\% \end{pmatrix} * E_1$

Furthermore, the reduction factor for the laminate could be determined: $\gamma_{ck,lam} = \frac{E_{lam}}{E_{lam,red}} * \gamma_{ck,UD}$

And finally, the stiffness of the laminate including the creep factor could be calculated:

$$E_{lam,\gamma,ck} = \frac{E_{lam}}{\gamma_{ck,lam}}$$

Subsequently, the deflection due to creep can be calculated using this stiffness value. An additional modification also specified in the CUR-96 is that the load used for creep caused deflection consists of the permanent load together with 15% of the live load.

Appendix 4 – plate buckling algorithm

The current appendix presents the algorithm contained in the CUR-aanbevelingen 96 (Civieltechnisch Centrum Uitvoering Research en Regelgeving, 2003) for determining the stability of an orthotropic plate under compression. This method is only valid for uniformly distributed loads, consequently the buckling effect could only be checked analytically for the SLS UDL.

This algorithm is used to determine the critical buckling factor. This factor can be multiplied with the applied load to determine the critical buckling load. In order to have a stable member, the factor has to be larger than 1, thereby proving that the applied load was smaller than the critical one and consequently, the web did not buckle.

The formula for determining the critical buckling factor is:

$$\lambda_{cr\ ij} = \frac{\left[D_{11} * \left(\frac{\alpha_1}{L_x} \right)^4 + 2 * (D_{12} + 2 * D_{66}) * \frac{\alpha_4 * \alpha_5}{L_x^2 * L_y^2} + D_{22} * \left(\frac{\alpha_3}{L_y} \right)^4 \right]}{N_{x0} * \frac{\alpha_4}{L_x^2} + N_{y0} * \frac{\alpha_5}{L_y^2}}$$

In order to be able to implement it, several D values from the ABD matrix are required. In order to obtain them, the layup of the web was inputted in the eLamX program. The corresponding ABD matrix is shown in Figure 19.

140320,4	44581,0	0,0	0,0	0,0	-0,0
44581,0	140320,4	0,0	0,0	0,0	0,0
0,0	0,0	47869,7	-0,0	0,0	0,0
0,0	0,0	-0,0	486233,9	245975,1	54581,9
0,0	0,0	0,0	245975,1	413458,0	54581,9
-0,0	0,0	0,0	54581,9	54581,9	258351,1

Figure 19 - ABD matrix of web

Therefore, the required D values were:

$$D_{11} = 486233,9 \text{ Nmm}; \quad D_{12} = 245975,1 \text{ Nmm}; \quad D_{22} = 413458 \text{ Nmm}; \quad D_{66} = 258351,1 \text{ Nmm}.$$

Furthermore, the α_1 , α_3 , α_4 and α_5 had to be determined. For these, the CUR provided several guidelines, as shown in Figure 20:

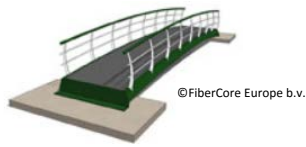
Table 4-1: Approximate expressions for the coefficients α_i on α_4			Table 4-2: Approximate expressions for the coefficients α_i on α_4		
α_i	α_i	i	α_i	α_i	j
$i\pi$	$(i\pi)^2$	1,2,3,...	$j\pi$	$(j\pi)^2$	1,2,3,...
$(j+0,25)\pi$	$\alpha_i(\alpha_i - 1)$	1,2,3,...	$(j+0,25)\pi$	$\alpha_j(\alpha_j - 1)$	1,2,3,...
$4,730$ $(j+0,5)\pi$	$\alpha_i(\alpha_i - 2)$ $\alpha_i(\alpha_i - 2)$	1,2,3,4,...	$4,730$ $(j+0,5)\pi$	$\alpha_j(\alpha_j - 2)$ $\alpha_j(\alpha_j - 2)$	1,2,3,4,...

(i represents the number of half waves in X-direction) (j represents the number of half waves in Y-direction)

Figure 20 – α coefficients

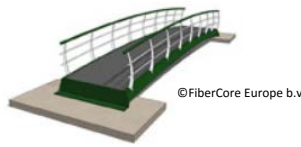
In the current project, the webs are clamped along all four sides because of the way the bridge is built (i.e. with the top and bottom skin being connected through continuous fibres that run along the web) Moreover, since the smallest value for the critical factor was of interest, number of waves in x and y direction (i.e. i and j) were assumed to be 1. Therefore:

$$\alpha_1 = 4,73; \quad \alpha_3 = 4,73; \quad \alpha_4 = (4,73 * (4,73 - 2)) = 12,91; \quad \alpha_5 = 4,73 * (4,73 - 2) = 12,91$$



Furthermore, since the webs run along the length of the bridge, the L_x was 30000 mm and the L_y was 974,8 mm. The latter value corresponds to the height of the web.

Lastly, the forces acting along the x and y directions were required. Since in the current situation, there was only a vertical load acting on the web, N_x was considered 0. Subsequently, N_y was the uniformly distributed live load (since this algorithm is only valid for UDLs), namely 18 kN/m. Due to the fact that the spacing between two webs is 200 mm, there are a minimum of 4 webs in 5 meter width. Therefore, the decisive UDL for 1 web was: $18/5 = 3,6$ kN/m



Appendix 5 – Interface shear stresses algorithm

The current appendix describes the algorithm for calculating the shear stresses between two materials with different elasticity moduli.

Therefore, in order to determine whether the adhesive bond between the steel plates and the GFRP skin is suitable and to prove that the shear stresses in this connection are not higher than the design shear strength of the glue, the following check has to be performed.

The following algorithm is used for determining shear stresses at the interface between two bodies made of different materials.

The main formula used for determining the shear stresses is: $\tau = \frac{V * Q}{b * I}$

Where

- Q – calculated static moment: $Q = A_1 * a_1 + A_2 * a_2 + \dots + A_n * a_n$
- V – Maximum shear near end supports
- I – Moment of inertia around neutral axis
- b – width of the member

The first step involved creating a connection between the two materials by calculating a ratio from their elasticity moduli as follows. Material 1 with area A1 and E modulus E1 and Material 2 with area A2 and E modulus E2.

$$if E_2 > E_1 \rightarrow n = \frac{E_2}{E_1} = \frac{210000 \frac{N}{mm^2}}{30190 \frac{N}{mm^2}} = 6,95 \text{ and } \sigma_2 = n * \sigma_1$$

These shear stresses occurred at the adhesive bond between the steel and the top skin. The same stresses occurred at the bottom part of the cross section. Therefore, the static moment was calculated:

$$Q = n * A_{skin} * a_{skin}$$

Furthermore, using the moment of inertia of the cross section and the maximum shear force, the shear stress in the adhesive bond were determined:

Appendix 6 – Transformed area method

The current appendix presents the transformed area method for transforming a 2 material heterogeneous cross section, to an equivalent 1 material homogenous one.

According to (Philpot, 2011), the first step is to determine the characteristics of the transformed cross section that are required so that it is equivalent to the actual steel and GFRP cross section. In order to be able to transform the hybrid section, a reference point is required, such as the bending strains equation. Consequently, the transformed cross section should yield the same bending strains as the actual cross section. Bending strains are defined by: $\varepsilon_x = -\frac{y}{\rho}$

Where y = the coordinate measured from the neutral surface and ρ = radius of the curvature.

(Philpot, 2011) continues to explain that from this relationship, it results that the y coordinates of the transformed cross section must be kept identical to those of the actual cross section if the strains are to be the same in both, therefore, the height cannot be modified. Moreover, ρ must be the same in the transformed cross section. The radius of curvature is defined by: $\frac{1}{\rho} = \frac{M}{EI}$

Due to the fact that M must be the same in both cases, EI remains the only variable that can be modified.

Due to the fact that the fibre glass will be transformed into an equivalent steel bar, the new steel bar must have the same value of EI as the actual steel bar. Consequently, the width of the former will be modified to satisfy the requirement: $(EI)_{GFRP} = (EI)_{steel}$

Therefore, the moments of inertia of the new steel bar is: $I_{steel} = \frac{E_{steel;GFRP}}{E_{steel}} * I_{steel;GFRP}$

This ratio can be defined as follows: $n_{GFRP} = \frac{E_{GFRP}}{E_{steel}}$

Therefore: $I_{steel} = n * I_{GFRP}$

Where n is termed the modular ratio.

The moment of inertia for the GFRP bar is then calculated using the parallel axis theorem:

$$I_{GFRP} = \frac{b * h^3}{12} + a^2 * A = \frac{b * h^3}{12} + a^2 * (b * h)$$

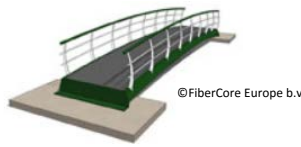
Where: b = width, h = height and a = the distance between the element's and the composite's centroid.

In order to satisfy $I_{steel} = n * I_{GFRP}$, the moment of inertia of the equivalent steel bar becomes:

$$I_{steel; GFRP} = n * \left(\frac{b * h^3}{12} + a^2 * (b * h) \right)$$

To analyse the GFRP and steel composite beam using the transformed area method, the width of the GFRP has to be multiplied with the ratio n . (Philpot, 2011) states that the transformed beam cross section has the same curvature and the same strains as the actual GFRP and steel composite beam.

Having established the algorithm, it can now be implemented for the actual values. Therefore, in order to use the transformed-section method to analyse the composite member, the following steps are taken:



First of all, the modular ratio n will be computed for GFRP: $n_{GFRP} = \frac{29.45 \text{ GPa}}{210 \text{ GPa}} = 0.14$

Subsequently, the equivalent width of the GFRP skin is: $w_{GFRP \text{ steel eq}} = 0.2 * 0.14 \text{ m} = 28 \text{ mm}$

Furthermore, considering that the section is symmetrical (i.e. the location of the centroid does not change), the section properties, namely the moment of inertia (I) have been determined with the help of the Excel spreadsheet:

$$I_{z, total} = I_{steel; GFRP} + I_{steel} = 5.216.099.890,45 \text{ mm}^4 = 5,21 * 10^9 \text{ mm}^4$$

Consequently, the area of the new, all steel section per core cell is:

$$A_{1 \text{ core}} = 2 * b_{steel} * h_{steel} + 2 * b_{GFRP} * h_{GFRP} = 2 * 0,1 * 0,01 + 2 * 0,028 * 0,0126 = 0,0027056 \text{ m}^2 = 2.705,6 \text{ mm}^2$$

Therefore, considering that the cross section has 20 cells, the total area of the cross section is:

$$A_t = 20 * 2.705,6 = 54.136 \text{ mm}^2$$

These values were used for the analytical ULS checks.

Below, in Figure 21 the cross section of one of the cross section's core cells with the layer names and thicknesses is presented. Additionally, on the right, the transformed cross section is presented where the GFRP has been converted to steel. Again, the PU foam is not considered. Moreover, the equivalent width is given.

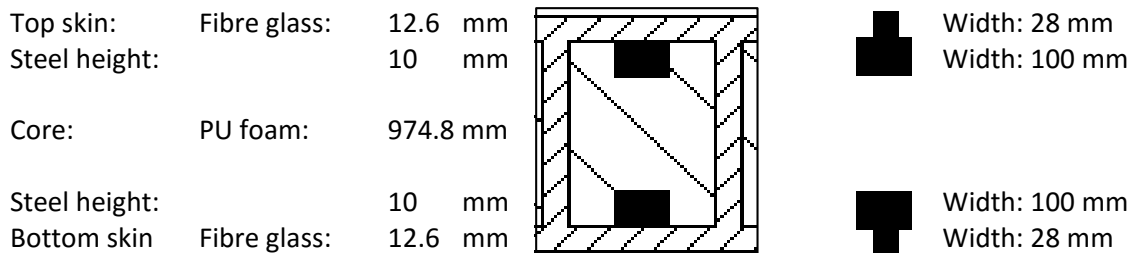


Figure 21 - Cross section of one normal core cell with thicknesses and one converted to steel with the transformed area method with equivalent widths

Appendix 7 – Concept designs – advantages and disadvantages

A7.1. Concept design 1 – Steel bars

The first concept proposes the introduction of steel members as steel bars, fully enclosed in the GFRP deck, attached to the bottom of the top skin and the top of the bottom skin in every core cell (see Figure 22). Below, the advantages and disadvantages posed by this design are described

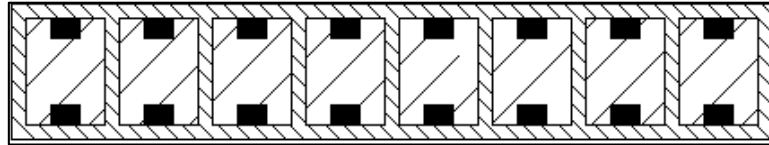


Figure 22 – GFRP deck with steel bars; drawing not on scale

- Advantages
 - The steel bars will be flexible (due to their small thickness), therefore, they will bend in the mould and follow the curvature of the bridge deck;
 - The shape of the steel members will be standard (i.e. no additional grooves or holes) because the resin will be able to flow around it through the GFRP skins;
 - The contribution of the steel members to the bending stiffness of the deck is maximum due to the fact that the bars are placed far from the neutral axis;
 - Stress concentrations are relatively low due to the fact that steel members are evenly spread all over the cross section.
- Disadvantages
 - Design challenges
 - The steel members need to be fully connected to the GFRP skin in order to contribute to the section's stiffness. This needs to be achieved with either an adhesive bond or with mechanical means.
 - Procurement challenges
 - Steel members need to be procured. The size of the members will be standard in order to keep the costs and delivery times low;
 - Foam blocks with a different runner pattern will be required in order to ensure proper spreading of the resin.
 - Lead time will increase due to the waiting time until steel member delivery.
 - Production of custom made steel members and foam blocks will cause an increase in costs;
 - Manufacturing challenges
 - At least two cranes will be required to place the steel members into position due to their weight and size;
 - The production time will increase (with approximately 30 minutes for every steel member) due to the need to place additional elements;
 - The steel members will need to be placed on one side of the core cell in order to allow the central grooves to transport the resin along its normal course;
 - The design of the webs will be different in order to accommodate the steel bars. Wrapping each foam block will no longer be possible as it is presently being done because the steel member will be continuous in the longitudinal direction. Therefore, a new technique will have to be developed and tested.
 - Any changes in the manufacturing process pose risks and need to be tested and therefore cannot be implemented immediately.

A7.2. Concept design 2 – Steel sheets

The second concept design is similar to the first one. The difference is that the steel bars are wider so that they fill the entire width of the core cell. As before, the steel sheets will be present both at the top and bottom of the cross section (see Figure 23).

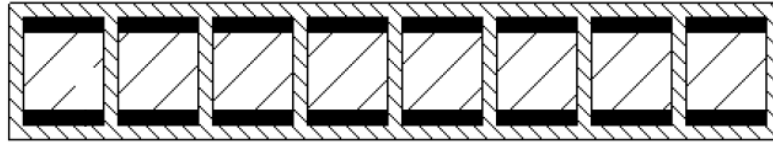
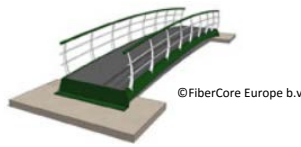


Figure 23 – GFRP deck with steel strips; drawing not on scale

- Advantages
 - The steel bars will be flexible (due to their small thickness), therefore, they will bend in the mould and follow the curvature of the bridge deck;
 - The contribution of the steel members to the bending stiffness of the deck is maximum due to the fact that the bars are placed far from the neutral axis;
 - Stress concentrations are relatively low due to the fact that steel members are evenly spread all over the cross section;
- Disadvantages
 - Design challenges
 - The steel members need to be fully connected to the GFRP skin in order to contribute to the section's stiffness. This needs to be achieved with either an adhesive bond or with mechanical means
 - Procurement challenges
 - Steel members need to be procured. The size of the members will be standard in order to keep the costs and delivery times low;
 - The shape of the steel members will need to be custom made. Holes and grooves will be required in order to allow the transport of resin to the skin;
 - The edges of the steel members will need to be chamfered in order to protect the fibres that will be wrapped around them;
 - Production of custom made steel members will determine longer lead time;
 - Foam cores with a different pattern will be required in order to ensure the resin is spread uniformly;
 - Production of custom made steel members and foam blocks will cause an increase in costs;
 - Manufacturing challenges
 - At least two cranes will be required to place the steel members into position due to their weight and size.
 - The production time will increase (with approximately 30 minutes for every steel member) due to the need to place additional elements,
 - The fabrication of the webs will be different because the foam cores will need to be wrapped in glass fibres separately while the steel will be a continuous member along the full length of the bridge
 - Any changes in the manufacturing process pose risks and need to be tested and therefore cannot be implemented immediately



A7.3. Concept design 3 – Rectangular hollow profiles

The last concept proposes the introduction of steel rectangular hollow sections only in the outermost core cells (see Figure 24), thus acting as the beams supporting the concrete slab on a traditional bridge.

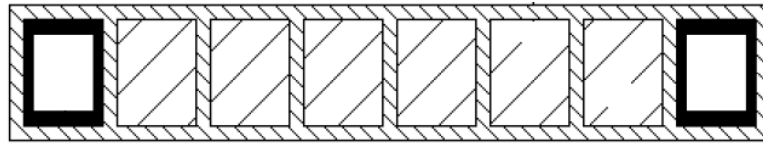


Figure 24 – GFRP deck with rectangular hollow steel profiles; drawing not on scale

- Advantages
 - Only two steel profiles are required;
 - The steel members can easily be placed after all the foam cores are positioned in the mould and the GFRP plies can simply be wrapped around them;
 - There will be no changes to the central part of the section since the steel is only present at the sides;
 - No adhesive bond is required since the neutral axis of the steel members is the same as that of the deck section. Therefore, when the bond fails, the steel provides the same amount of bending stiffness;
 - The steel members can remain empty, therefore, less foam blocks are required;
 - The rectangular sections can increase the torsional rigidity of the section.
- Disadvantages
 - Design challenges
 - The steel is concentrated at the sides which will focus the stresses around them.
 - Procurement challenges (will cause an increase in costs and delivery / production time)
 - Steel members need to be procured. The size of the steel profiles will not be standard since it needs to match the depth of the deck.
 - In case the necessary size cannot be manufactured, separate sheets need to be bought and welded together
 - The outer faces of the steel beams will need to feature holes and grooves in order to allow the transport of resin to the skin.
 - The edges of the steel members will need to be chamfered in order to protect the fibres that will be wrapped around them
 - The beams will need to be pre-cambered since they are rigid and they will not bend under their own weight on the mould.
 - Lead time will increase due to the need of customized steel profiles
 - Procurement costs will increase due to the need of customized steel profiles
 - Manufacturing challenges
 - At least two cranes will be required to place the steel members into position due to their weight and size.
 - The production time will increase (with approximately 1 hour for every steel member) due to the need to place additional elements
 - The steel members will need to be airtight during the vacuum process in order to prevent resin from entering them. Additionally, a pressure difference may cause deformations of the steel beam.
 - Any changes in the manufacturing process pose risks and need to be tested and therefore cannot be implemented immediately

Appendix 8 – Initial dimensions and cross section design

The current appendix lists the deck dimensions used in the preliminary design and the cross sectional design associated with it.

For the preliminary design, the dimensions from Table 9 will be considered. The values will be adjusted during the calculations described in Chapter 3.4.6 in order to obtain advantageous results and the final dimensions will be presented in another table in Chapter 4.1.

Table 9 – Bridge dimensions in meters and millimetres

Dimension	Unit	Initial value
bridge length (L)	mm	30000
bridge width (b)	mm	4500
Bridge effective width (b_eff)	mm	4448,64
bridge height (h)	mm	1000
thickness top skin (t _u)	mm	12,6
thickness bottom skin (t _l)	mm	12,6
thickness webs (t _{1p})	mm	6,72
height webs (h _c)	mm	974,8
number of core profiles	mm	21
height core (h _c)	mm	974,8
width per core profile (w _c)	mm	204,8
width of flange	mm	25,68
number of steel bar pairs	mm	21
width of steel bars (w _s)	mm	100
Height of steel bars (h _s)	mm	10

The cross section to which these dimensions apply is the most feasible one, as resulted from the trade-off analysis and is presented in Figure 25. It features GFRP skins and webs, steel members connected both to the top and bottom skins along the full length of the deck and PU foam core that connects the top and bottom layers.

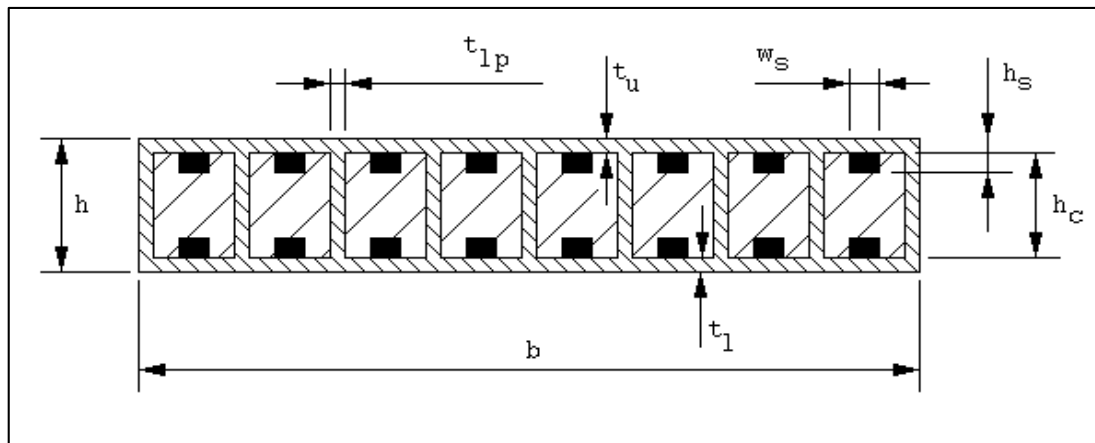


Figure 25 – Cross section of bridge deck; drawing not on scale

Appendix 9 – Material properties – Young moduli, strength values, densities

The current appendix lists the material stiffnesses (see Table 10), strengths and Poisson ratios (see Table 11).

Table 10 – Material stiffnesses

Material stiffnesses (E.)				
E_steel	Gpa = kN/mm ²	210,00	Mpa = N/mm ²	210.000,00
E_glass/epoxy skin 0°-dir.	Gpa	39,70	Mpa	39.700,00
E_glass/epoxy skin average	Gpa	29,70	Mpa	29.700,00
E_glass/epoxy webs 0°-dir.	Gpa	11,50	Mpa	11.500,00
E_glass/epoxy web average	Gpa	21.5	Mpa	21.500,00
E_core	Gpa	0,0030	Mpa	3,00
E GFRP adjusted for creep	Gpa	17,26	Mpa	17.260,00

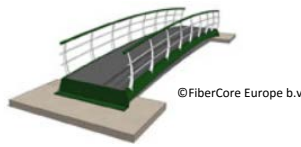
Table 11 – Material strengths and Poisson's ratios

Material strengths			Poisson's ratios	
top skin ($\sigma_{(ts,x,c)}$)	N/mm ²	365	Steel	0.29-0.33
bottom skin ($\sigma_{(bs,x,t)}$)	N/mm ²	375	GFRP	0.25-0.28
bottom skin ($\sigma_{(bs,x,c)}$)	N/mm ²	365	Laminate Ply	0.26
web strength ($\sigma_{(web.z,c)}$)	N/mm ²	132		
web strength ($\tau_{(web,xz)}$)	N/mm ²	72		
steel	N/mm ²	235		
PU foam	N/mm ²	1		

Furthermore, the densities and weights of the materials are given in Table 12. Additionally, the percentage of fibres for the skins and webs are given. This value indicates how many fibres and how much resin there will be in the laminates.

Table 12 – Densities and weights

Densities and weights				
density steel	kg/m ³	7850	kN/m ³	76,9822025
density glass	kg/m ³	2550	kN/m ³	25,0069575
density polyester	kg/m ³	1193	kN/m ³	11,69933345
Fiber volume fraction top and bottom skin	-	53%		
Fiber volume fraction webs	-	28%		
density upper and lower skin	kg/m ³	1912,21	kN/m ³	18,7523742
density webs	kg/m ³	1572,96	kN/m ³	15,42546818
density core	kg/m ³	35	kN/m ³	0,34323275
Density resin	Kg/ m ³	1080	kN/m ³	10,8
railings	kg/m	50	kN/m	0,4903325



Appendix 10 – Calculated properties – moment of inertia, bending stiffness, weights

The current Appendix presents the calculated properties of the bridge deck. In order to determine them, the values presented above were used.

Using the material stiffnesses and the dimensions, the total moment of inertia (Table 13) and the flexural rigidity (Table 14) can be calculated as follows. The total values represent the summation of the individual values.

Table 14 – Moment of inertia

Second moments of areas ($I = \frac{1}{12} b * h^3 + A * a^2$)				
top skin	m ⁴	0,0138	mm ⁴	13820790564,0000
bottom skin	m ⁴	0,0138	mm ⁴	13820790564,0000
webs	m ⁴	0,0114	mm ⁴	11411881921,3414
core	m ⁴	0,3359	mm ⁴	335946536950,6590
top steel bars	m ⁴	0,0049	mm ⁴	4887079960,0000
bottom steel bars	m ⁴	0,0049	mm ⁴	4887079960,0000
Total second moment of area	m ⁴	0,3848	mm ⁴	384774159920,0000

Table 13 – Flexural rigidity

Bending stiffness / Flexural rigidities ($E * I$)				
top skin	Nm ²	4,07E+08	Nmm ²	407.022.282.109.800,00
bottom skin	Nm ²	4,07E+08	Nmm ²	407.022.282.109.800,00
webs	Nm ²	2,40E+08	Nmm ²	240.231.526.326.159,00
core	Nm ²	1,01E+06	Nmm ²	1.006.644.697.891,06
top steel bars	Nm ²	1,03E+09	Nmm ²	1.026.286.791.600.000,00
bottom steel bars	Nm ²	1,03E+09	Nmm ²	1.026.286.791.600.000,00
Total EI	Nm ²	3,11E+09	Nmm ²	3,11E+15

From the total values of Tables 13 and 14, the total modulus of elasticity of the cross section can be determined by dividing the total flexural rigidity to the total moment of inertia.

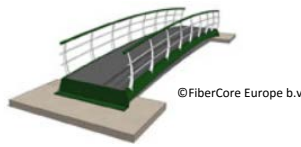
Total E	GPa	8,085	N/mm ²	8085,461855
----------------	-----	-------	-------------------	-------------

Furthermore, the densities and weights of the materials are given in Table 8. Additionally, the percentage of fibres for the skins and webs are given. This value indicates how many fibres and how much resin there will be in the finished product.

Using the dimensions and the densities, the mass of the individual elements and the total mass can be determined (see Table 15).

Table 15 – Masses

top skin	kg	3230
bottom skin	kg	3230
webs	kg	6801
core	kg	4455
steel bars	kg	4946
wearing surface	kg	1620
Railings	kg	1500
Total mass bridge	kg	25780



Appendix 11 – Loads

The loads described in the current appendix are characteristic to a cycling and pedestrian bridge and are taken from the NEN-EN.1990+A1+A1/C2/NB:2011 (European Committee for standardization, 2003).

A11.1. Permanent loads

The permanent load is represented by the self-weight of the bridge and it includes the coatings and railings. The weight of each element as well as the total load is:

$$q_{top,skin} = q_{bottom,skin} = \frac{4,5 \text{ m} * 30 \text{ m} * 0,0126 \text{ m} * 1898,64 \frac{\text{kg}}{\text{m}^3} * 9,81 \frac{\text{m}}{\text{s}^2}}{1000} = 31,67 \text{ kN}$$

$$q_{webs} = 22 * \frac{0,00672 \text{ m} * 30 \text{ m} * 0,9748 \text{ m} * 1572,96 \frac{\text{kg}}{\text{m}^3} * 9,81 \frac{\text{m}}{\text{s}^2}}{1000} = 66,69 \text{ kN}$$

$$q_{core} = 21 * \frac{0,207 \text{ m} * 30 \text{ m} * 0,9748 \text{ m} * 35 \frac{\text{kg}}{\text{m}^3} * 9,81 \frac{\text{m}}{\text{s}^2}}{1000} = 43,63 \text{ kN}$$

$$q_{steel,bars} = 21 * 2 * \frac{0,1 \text{ m} * 30 \text{ m} * 0,01 \text{ m} * 7850 \frac{\text{kg}}{\text{m}^3} * 9,81 \frac{\text{m}}{\text{s}^2}}{1000} = 97 \text{ kN}$$

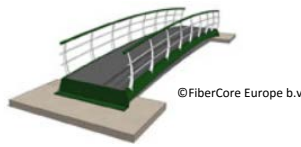
$$q_{handrails} = 2 * \frac{30 \text{ m} * 50 \frac{\text{kg}}{\text{m}} * 9,81 \frac{\text{m}}{\text{s}^2}}{1000} = 29,43 \text{ kN}$$

$$q_{wearing \ surface} = \frac{4,5 \text{ m} * 30 \text{ m} * 12 \frac{\text{kg}}{\text{m}^2} * 9,81 \frac{\text{m}}{\text{s}^2}}{1000} = 15,89 \text{ kN}$$

$$q_{total} = q_{top,skin} + q_{bottom,skin} + q_{webs} + q_{core} + q_{steel,bars} + q_{handrails} + q_{wearing \ surface}$$

$$q_{total} = 31,676 + 31,67 + 66,69 + 43,63 + 97 + 29,43 + 15,89 = 315,97 \text{ kN}$$

$$q_M = \frac{315,97 \text{ kN}}{30 \text{ m}} = \frac{10,53 \frac{\text{kN}}{\text{m}}}{4,5 \text{ m}} = 2,34 \frac{\text{kN}}{\text{m}^2}$$



A11.2. Live loads

There are several live loads required to determine the dimensions and structure of the bridge:

- Uniformly distributed load
- Concentrated load
- Maintenance vehicle load
- Unauthorized vehicle load
- Load on handrail
- Load of pedestrian traffic

A11.2.1. Uniformly distributed load

It usually determines the dimensions of the bridge's main structure and it is commonly set at 5kN/m². When the bridge spans more than 10 m ($L > 10$ m), the uniform load can be decreased as follows:

$$q_{fk} = 2 + \frac{120}{L + 30}$$

For the current project, the required span of the bridge is $L = 30$ meters. Therefore,

$$q_{fk} = 2 + \frac{120}{30 \text{ m} + 30} = 2 + \frac{120}{60} = 2 + 2 \rightarrow q_{fk} = 4 \frac{\text{kN}}{\text{m}^2} * 4,5 \text{ m} = 18 \frac{\text{kN}}{\text{m}}$$

The horizontal load should be 10% of the total load, in compliance with the uniformly distributed load

$$Q_{h,q} = 0.1 * 4 * L_{\text{bridge}} * B_{\text{eff}} = 0.1 * 4 * 30 * 4.5 \rightarrow Q_{h,q} = 54 \text{ kN}$$

A11.2.2. Concentrated load

It is a force acting on a single point, such as one caused by the wheels of a vehicle. It mainly determines detailing such as the deck's thickness. The bicycle and pedestrian bridge should be designed for a concentrated load of 7 kN over a surface of 0.1 x 0.1 meters. Therefore,

$$Q_{fvd} = 7 \text{ kN acting on } B_{fvd} = 0.1 \text{ m} * 0.1 \text{ m}$$

A11.3.3. Maintenance vehicle load

The bridge has to be accessible to maintenance vehicles as well, and semi-permanent vehicle access restriction such as a removable bollard is in place, the load caused by a maintenance vehicle must be taken into account as well. The specifications for a such a vehicle are:

- 2 axles with 3 m wheelbase;
- Axle load of 25 kN;
- 2 wheels per axle with a 1.75 m track width;
- 0.25 m x 0.25 m contact surface per wheel.

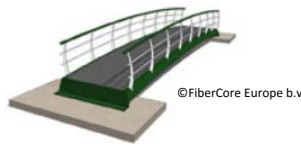
Therefore, the vertical load of the maintenance vehicle is

$$Q_{serv} = 12.5 \text{ kN acting on } B_{w,serv} = 0.25 \text{ m} * 0.25 \text{ m}$$

And the horizontal load of the maintenance vehicle due to braking is 60% of the vertical load,

$$Q_{h,serv} = 60\% * (12.5 + 12.5) \text{ kN} \rightarrow Q_{h,serv} = 15 \text{ kN}$$

The main issue associated with maintenance vehicles is represented by the wheel loads which will induce higher local loading.



A11.3.4. Unauthorized vehicle load

In case no physical barriers are provided, it is necessary to take into account the loading caused by any type of vehicle. The specifications for this category are:

- 2 axles with 3 m wheelbase - B_{eff} ;
- Characteristic axle load of 40 kN and 80 kN;
- 2 wheels per axle with a 1.3 m track width;
- 0.2 m x 0.2 m contact surface per wheel.

Due to the fact that these loads are much larger than those caused by a standard maintenance vehicle, normally by taking them into account a much larger and more expensive structure would be required. However, in the present situation, due to the span of the bridge being large enough, this will not be the decisive loading, therefore it can be considered. Therefore, the maximum vertical load of an unauthorized vehicle is:

$$Q_{acc} = 40 \text{ kN acting on } B_{w,acc} = 0.2 \text{ m} * 0.2 \text{ m}$$

The horizontal load of the unauthorized vehicle due to braking can be calculated as for the maintenance vehicle, as 60% of the vertical load,

$$Q_{h,acc} = 60\% * (40 + 40) \text{ kN} \rightarrow Q_{h,acc} = 48 \text{ kN}$$

A11.3.5. Load on handrail

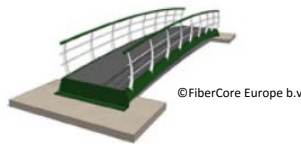
Horizontal line load on handrail is considered:

$$q_{lk} = 3 \text{ kN/m}$$

According to NEN-EN.1990+A1+A1/C2/NB:2011, (2011).

A11.3.6. Load of pedestrian traffic

To check whether pedestrians can excite the bridge in its own frequency a flow of pedestrians is taken into account. According to EUR23984 "Design of lightweight footbridges for human induced vibrations" the weight of each pedestrian is $P_1 = 800 \text{ N}$ and the flow has a density of $d_{TC3} = 0.5 \frac{P}{m^2}$.



Appendix 12 – Partial factors

The current appendix lists the partial factors (i.e. load, material, conversion and combination factors) that correspond to consequence class 1 (i.e. CC1).

Therefore, the partial factors according to the Eurocode (EN1991-2+C1) for the ultimate limit state and the serviceability limit state are:

Load factor ULS: $\gamma_G = 1.1$ $\gamma_Q = 1.2$ $\gamma_{pos} = 0.9$

Load factor SLS: $\gamma_f = 1.0$

Material factors differ for ULS and SLS checks. For a post cured composite material, the Dutch guideline CUR-aanbevelingen 96 gives:

Material factor ULS: $\gamma_{m1} = 1.35$ $\gamma_{m2} = 1.2$ $\gamma_{m,ULS} = \gamma_{m1} * \gamma_{m2} = 1.62$

Material factor SLS: $\gamma_{m,SLS} = 1.0$

In addition to material factors, for uncertainties in material properties, the CUR-aanbevelingen 96 mentions “conversion factors” to account for environmental influences and ageing:

ULS permanent loads: $\gamma_{cp,s} = 1.52$ $\gamma_{cp,b} = 1.68$ $\gamma_{cp,f} = 1.21$

ULS live loads: $\gamma_{cl,s} = 1.21$ $\gamma_{cl,b} = 1.33$ $\gamma_{cl,f} = 1.21$

SLS permanent loads: $\gamma_{cp,d} = 1.68$ $\gamma_{cp,v} = 1.33$ $\gamma_{cp,1} = 1.68$

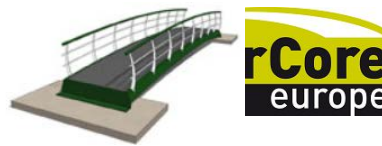
SLS live loads: $\gamma_{cl,d} = 1.21$ $\gamma_{cl,v} = 1.21$ $\gamma_{cl,1} = 1.33$

Where subscript c stands for conversions, l for live loads, p for permanent loads, d for deflection, v for vibration, 1 for first crack occurrence, s for strength, b for buckling and f for fatigue.

For determining the design value for the loads acting on the bridge, the characteristic values determined above must be combined with the partial factors in order to form Load Cases. All load cases and loads according to EN.1990+A1+A1/C2:2011 can be seen in Table 16.

Table 16 - Load Cases according to EN.1990+A1+A1/C2:2011

	Load	Subscript	Reduction factors (ψ)											
			Load combinations											
			1	2	3	4	5	6	7	8	9	10	11	12
Permanent loads	permanent	G	1	1	1	1	1	1	1	1	1	1	1	1
	pre tension	G	1	1	1	1	1	1	1	1	1	1	1	1
	settlements	G		1										
Live load (traffic)	uniformly distributed load	q			1	0,8			0,4	0,32	0,4	0,32		0,4
	horizontal load	h			1	1			0,4	0,4	0,4	0,4		0,4
	service vehicle	serv				1				0,4		0,4	0,8	
	concentrated force	fwk					1							
	accidental vehicle	sv						1						
Live load (other)	wind	w			0,3	0,3			1	1	0,3	0,3	0,3	
	temperature	t			0,3	0,3					1	1	0,3	
	snow	s											1	
Accidental loads	collision on or under the bridge	A												1
	earthquake load	A												



Appendix 13 – Load combinations

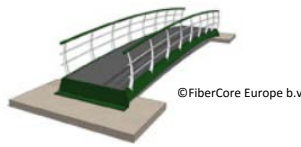
The current Appendix presents an overview of the characteristic loads in Table 17 and the final UDL and point load values in Table 18.

Table 17 - Characteristic loads according to Chapter 3.4.3

		Vertical loads			Area		Horizontal loads
		kN/m ²	kN/m	kN	side (mm)	m ²	kN
Permanent load	Uniformly distributed (qM)	1,8282	8,2270	246,8097	N/A	N/A	0
Variable load	Uniformly distributed (H=10%) (qfk)	4	18	540	N/A	N/A	54
	Concentrated load			7	0,1	0,01	
	Maintenance vehicle load (H=60%) (Qserv)			12,5	0,25	0,0625	15
	Unauthorized vehicle load (H=60%) (Qacc)			40	0,2	0,04	48

Table 18 - Load combinations according to Chapter 3.4.5

Load Combinations																									
	partial factor for perm. action		Perm. load		partial factor for variable action		Var. load		Total UDL (kN/m)	Mmax (kNm) = 1/8*UDL*L ²		part. factor for maint. vehicle		maint. vehicle load		part. factor for concentr. load		concentr. load		part. factor for acc. load		accid. load		Total UDL+PL (kN)	M max incl point loads (kNm)
Load case 3	1,1	*	8,227	+	1,2	*	18	=	30,65	3448,09	+	0	*	25	+	0	*	7	+	0	*	40	=	919,49	3448,09
Load case 4	1,1	*	8,227	+	=0.80,96	*	18	=	26,33	2962,09	+	1	*	25	+	0	*	7	+	0	*	40	=	814,89	3149,59
Load case 5	1,1	*	8,227	+	0	*	18	=	9,05	1018,09	+	0	*	25	+	1	*	7	+	0	*	40	=	278,49	1070,59
Load case 6	1,1	*	8,227	+	0	*	18	=	9,05	1018,09	+	0	*	25	+	0	*	7	+	1	*	40	=	311,49	1318,09



Appendix 14 –Material properties

The current Appendix contains the material properties that need to be introduced in Patran in order to perform the analysis. The values presented in Table 19 have been provided by FiberCore Europe, (2016).

Table 19 - Material properties

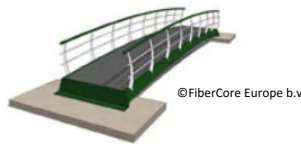
Structural properties					
Property	Unit	GFRP Ply	Steel	Foam	Polyester resin
E11	MPa = N/mm ²	39700	210000	1	3800
E22	MPa	9500	210000	1	3800
E33	MPa	6050	210000	1	3800
G12 = Shear modulus	MPa	3000	79300	1	1350
G23	MPa	1370	79300	1	1350
G31	MPa	1370	79300	1	1350
Poisson's ratio 12	-	0,26	0,3	0.3	0.38
Poisson's ratio 23	-	0,31	0,3	0.3	0.38
Poisson's ratio 31 = E33/E11*	-	0,05	0,3	0.3	0.38
Poisson 13					
Density	ton/mm ³	1,90E-09	7,85E-09	3,5E-11	10E-06
Thermal properties					
CTE 11	m/m/K	8,22E-06	1,00E-05		50-120E-06
CTE 22	m/m/K	3,71E-05	1,00E-05		50-120E-06
thermal conductivity 11	W/m/K	0,66	25		
thermal conductivity 22	W/m/K	0,18	25		
specific heat	mm ² /s ² /K	1,17E+09	4,60E+08		
reference temperature	K	283,15	283,15		

Furthermore, the design interlinear tensile and shear strengths of the resin is given by the CUR aanbevelingen 96 and shown in Table 20

Table 20 - Nominal value for shear strength

Type of resin of GRP laminate	Interlaminar tensile strength ILTS (MPa)	Interlaminar shear strength ILSS (MPa)
Polyester resin	10,0	20

In addition, as determined by Wilken, (2015), the resin's shear strength between steel and GFRP is 5,9 MPa.



Appendix 15 – Patran input – Laminates layup

The current appendix lists the properties that have to be inputted in Patran for all the laminates used in the bridge design. Table 21 presents the layup of the web.

Table 21 - Plies layup in the webs

Orientation	Percentage	Thickness (mm)	Web Thickness
+45/-45	50%	3,36	6,72
0/90	50%	3,36	

The bulkheads are built from half the Z layers (0/90 plies) of the top and bottom skin together with the ones from one web resulting in the thickness shown in Table 22.

Table 22 - properties of bulkhead laminate

Orientation	Percentage	Thickness (mm)	Bulkhead Thickness
0/90	100%	8,8	8,8

Below, Table 23 presents the composition of the top skin, Table 24 shows the structure of the core in the areas with and without steel and Table 25 shows the composition of the bottom skin.

Table 23 - properties of top skin laminate

Orientation	Percentage	Thickness (mm)	Top skin Thickness
0	64,3%	8,1	12,6
90	21,4%	2,7	
+45	7,15	0,9	
-45	7,15	0,9	

Table 24 – structure of the core with and without steel members

Grouping Laminate 1	Layer thickness			Grouping Laminate 2
Steel rod	mm	10	974.8	PU core
PU core	mm	954,8		
Steel rod	mm	10		

Table 25 – properties of bottom skin laminate

Orientation	Percentage	Thickness (mm)	Top skin Thickness
0	69,2%	8,1	11,7
90	23,1%	2,7	
+45	3,85	0,45	
-45	3,85	0,45	

According to FiberCore Europe, (2016), the thickness of the flange has to be approximately 30 mm this is achieved by combining the Z layers (0-90 plies) of the top and bottom skin and adding an additional amount of 0/90 plies. Therefore, the composition of the flange is presented in Table 26:

Table 26 – properties of flange laminate

Orientation	Percentage	Thickness (mm)	Top skin Thickness
0	50%	15,3	30,6
90	50%	15,3	

From the flange, the Z layers of the bottom skin together with the additional ones go down the side of the deck to form the side laminate whose composition is shown in Table 27.

Table 27 – properties of side laminate

Orientation	Percentage	Thickness (mm)	Top skin Thickness
0	50%	12,6	25,2
90	50%	12,6	

Appendix 16 – soil information

The current appendix presents the soil layers at the project location (see Figure 27) together with a map showing the exact position of the CPT tests (see Figure 26), obtained from (DINOloket, 2016). Additionally, the position of the bridge is indicated by the green line.

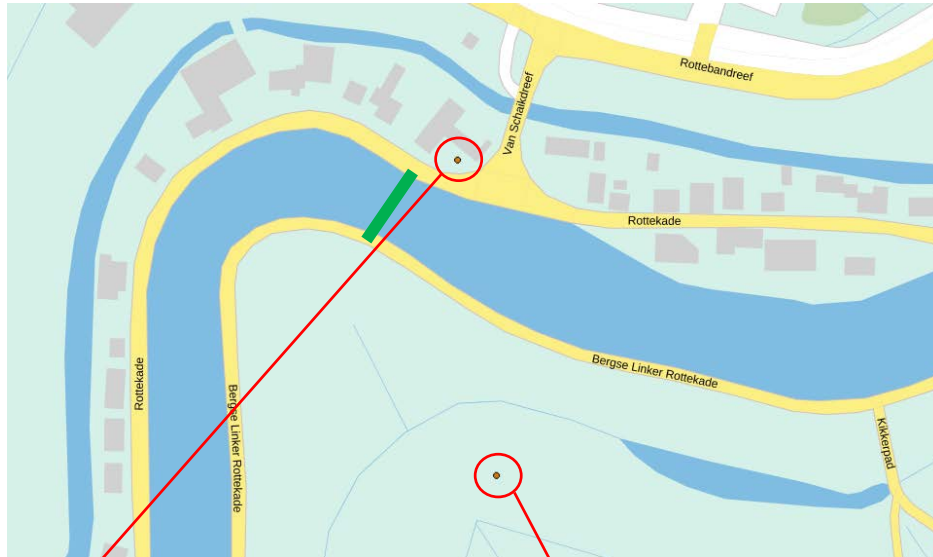


Figure 26 - Map showing the positions of the two CPT test in relation to the project location

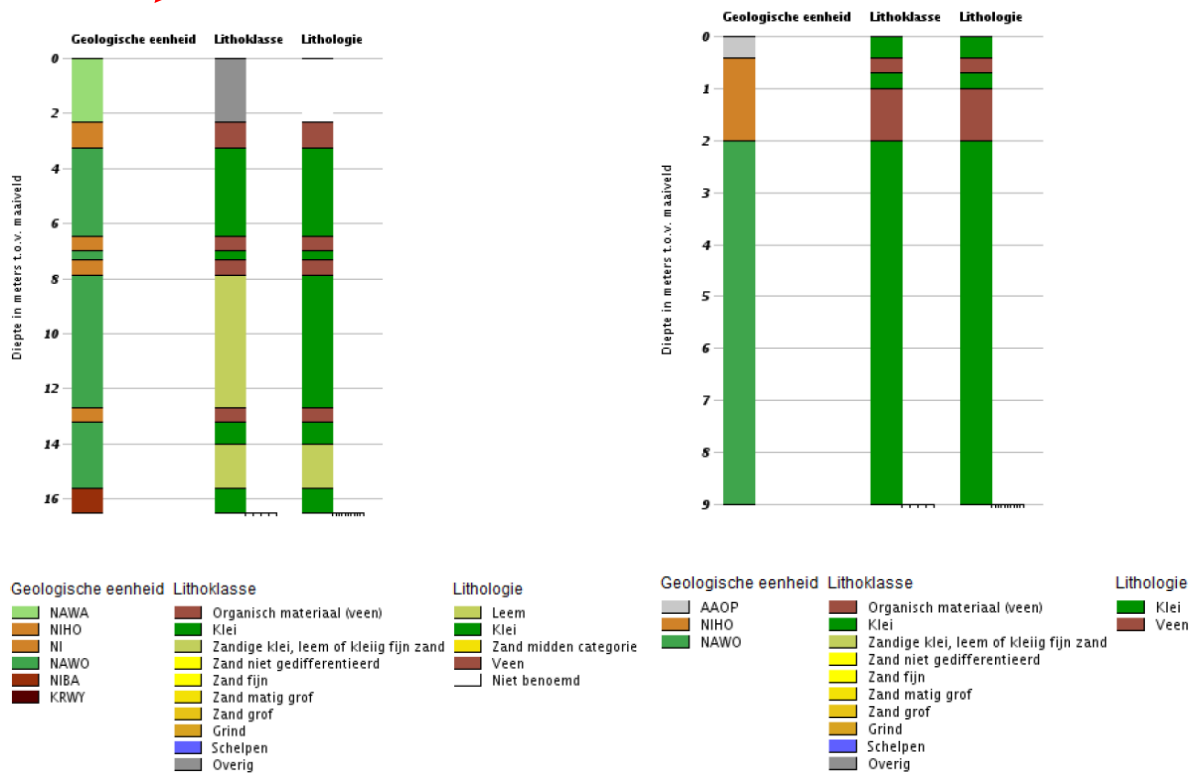


Figure 27 - Soil profiles for the north (left) and south (right) bank of the Rotte

Therefore, considering their proximity to the project site and the fact that more accurate data is difficult to obtain, it is assumed that the same soil is present in the area next to the bridge's abutments.

Appendix 17 – surface and water levels

The current appendix shows the levels of the river banks together with the location on the map.

Therefore, Figure 28 shows the levels of the road surfaces in relation to NAP at the locations where the bridge connects to the existing road network.

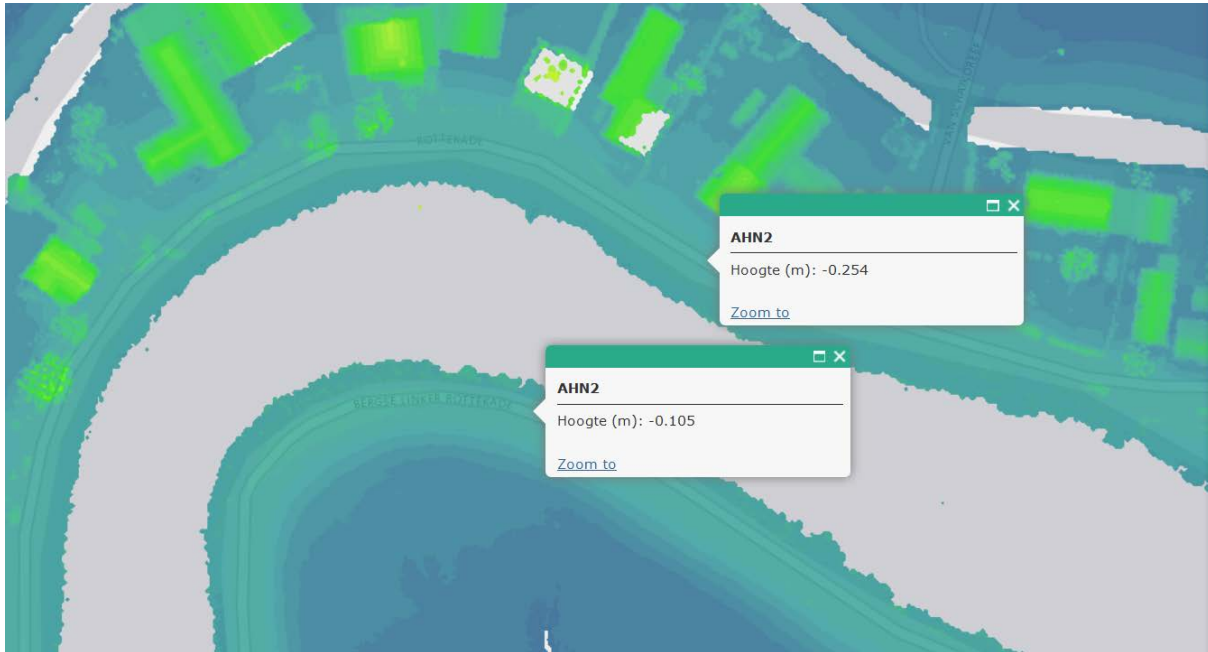
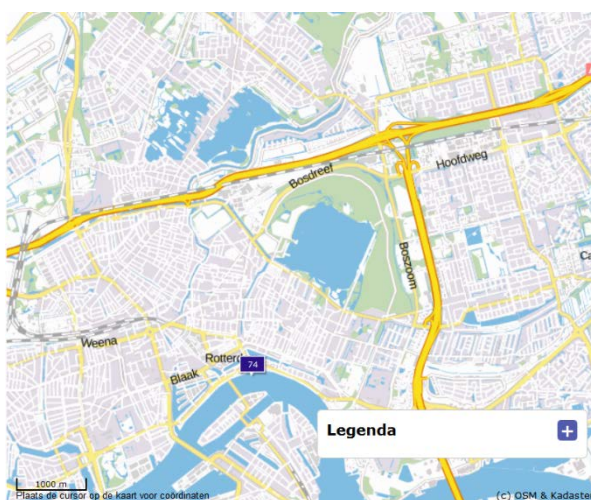


Figure 28 - road level for the north and south bank of the Rotte at the location of the proposed bridge

Furthermore, Figure 29 shows the location where the tidal information is monitored in relation to the project area. It can be observed that the monitoring station is near the location where the Rotte enters the Rhine. Additionally, in the right hand side, a table showing the lowest water level that occurred on the 14th of May is provided. Consequently, the value of -0.6 m tow NAP was considered the water level in the Rotte.

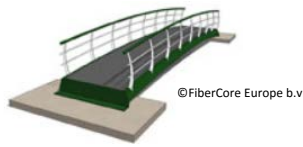


18-5-2016 - 13:30 uur - Rotterdam

		Waterhoogte	Astronomisch	Verwachte
dag	tijd	cm NAP	getij	waterstand
		cm NAP	cm NAP	
14/05	05:40	-31	-52	
14/05	05:30	-33	-53	
14/05	05:20	-36	-53	
14/05	05:10	-38	-54	
14/05	05:00	-43	-55	
14/05	04:50	-45	-56	
14/05	04:40	-47	-57	
14/05	04:30	-48	-58	
14/05	04:20	-48	-59	
14/05	04:10	-49	-59	
14/05	04:00	-48	-59	
14/05	03:50	-47	-59	
14/05	03:40	-47	-58	
14/05	03:30	-44	-57	
14/05	03:20	-40	-55	
14/05	03:10	-37	-52	
14/05	03:00	-32	-49	

Grafiek 

Figure 29 - Location of the water level information and table showing the minimum water level towards NAP



Appendix 18 – list of requirements

The current appendix shows the requirements of the current project and categorises them for a clear understanding.

The main purpose of prerequisites is to ensure that the function of the bridge is fulfilled. Furthermore, the limits and checks given below were used during calculations. In order to categorise them based on their origin, the requirements have been divided into standards and requirements from the client. These had been translated into technical requirements representing a checklist of criteria the proposed design had to achieve.

A18.1. Standards

For the current project, the following standards and regulations had to be used:

- Bouwbesluit – general regulations for construction in the Netherlands;
- Eurocode 0, EN 1990.2002 – limit states, design limits, combinations and load factors; (European Committee for standardization, 2002)
- Eurocode 1, EN 1991.2.2003 – actions on bridges, permanent and live loads; (European Committee for standardization, 2003)
- CUR-aanbevelingen 96 – material factors for GFRP. (Civieltechnisch Centrum Uitvoering Research en Regelgeving, 2003)

A18.2. Functional requirements imposed by the city of Rotterdam:

The following section contains requirements given by the client

Primary requirements:

- The bridge will be placed over the river “De Rotte” between Prins Alexander district and the city of Bergschenhoek;
- The bridge will be used by cyclists and pedestrians
- The design should be cost effective
- The material should be a GFRP hybrid;
- The lifespan should be 100 years;
- The bridge should have one span;
- The length of the bridge is 30 meters;
- The width of the bridge is 4.5 meters;
- The bridge should provide a clearance of 1,2 * 4 meters;

Secondary requirements:

- The bridge has to be easy to access;
- Rainwater should drain efficiently;
- The bridge should not become slippery due to snow or ice,
- The bridge should be comfortable to use with respect to vibrations.
- The bridge should require little or no maintenance;
- The bridge should be installed over the course of one day in order to avoid disruptions;
- The bridge design should be innovative.



A18.3. Technical design requirements:

The technical requirements are derived below from the two abovementioned categories. They are divided into primary and secondary ones. The former are required in order to ensure the safety of the deck and the latter ensure comfortable use of the bridge.

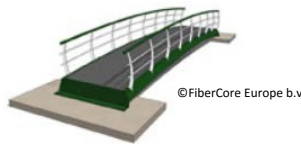
Primary requirements:

- Cost effective design;
- Cycling and pedestrian bridge loading condition, according to EN.1991.2.2003;
- Unauthorised vehicle wheel load support according to NEN-EN.1990+A1+A1/C2/NB:2011;
- Durable bonding layer between steel and GFRP for the lifespan of the structure;
- Free expansion and contraction of the deck under temperature variations prescribed in NEN-EN-1991-1-5 standard with national annexes NEN 1 and NEN 2;
- 30-meter-long deck;
- 4,5-meter-wide deck.

Secondary requirements:

- Deflection under SLS udl of largest between LC 3 and LC4 (acc. to NEN-EN.1990+A1+A1/C2/NB:2011) lower than $\max \delta = L/100^1$
- Natural frequency under SLS udl of largest between LC 3 and LC4 (acc. to NEN-EN.1990+A1+A1/C2/NB:2011) higher than 2.3 Hz;
- Anti-slip coating;
- Fully encapsulated steel members to prevent corrosion;
- Long term deflection due to creep should not cause the bridge to lose the arch function;
- Slope between 1 and 4%;
- 1,2 meters high * 4 meters wide clearance;

¹ Value chosen by FiberCore in order to ensure comfortable use of the bridge, due to the fact that currently, neither the Eurocodes, nor the Dutch law does not prescribe limits for maximum deflection for composite bridges.



Appendix 20 – Detailed calculation algorithms

The current appendix describes the calculation algorithms used for determining the values from the preliminary design.

A20.1. Preliminary design

Below the results of the analytical calculations are described, in the same order as they were introduced in chapter 3.4.6.

A20.1.1. SLS checks

In this subchapter, the SLS calculations and the results as described in chapter 3.5.7.1. are given.

A20.1.1.1. Natural frequency

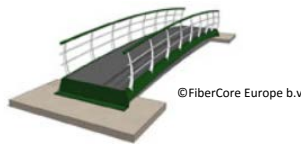
The natural frequency of the bridge is calculated with the formula:

$$f_n = \frac{K_n}{2\pi} * \sqrt{\frac{\frac{EI}{\gamma_{m,SLS} * \gamma_{cl,v}} * g}{(q_M + d_{TC} * b_{eff}) * L^4}} = \frac{11,65}{2\pi} * \sqrt{\frac{\frac{3,09 * 10^9 Nm^2}{1 * 1,21} * 9,81 \frac{m}{s^2}}{\left(9,81 \frac{kN}{m} + 0,5 m * 4,5 m\right) * (30 m)^4}} = 3,29$$

Subsequently, the result can be compared with the design value of 2.3

$$f_{n,check} = \frac{f_{n,min}}{f_n} = \frac{2,3}{3,29} = 0,7$$

The result is given in the shape of a unity check where the calculated value (i.e. f_n) must be higher than the required one. Since this is the case, it can be concluded that the bridge fulfils the SLS criterion regarding natural frequency.



A20.1.1.2. Deflection check

The deflection due to the self-weight is calculated with the formula:

$$\delta_{sw} = \frac{5}{384} * \frac{q_M * L^4}{EI} = \frac{5 * 9,81 \frac{kN}{m} * 30^4 m}{384 * 3.094.319,77 kNm^2} = 0,0334 m = 33,4 mm$$

Furthermore, the creep influence is calculated with the algorithm provided in the CUR-aanbevelingen 96 together. (Civieltechnisch Centrum Uitvoering Research en Regelgeving, 2003)

Laminate 1: (64%/21%/14%) [0/90/+45]

The stiffnesses of the ply are:

- in fibre direction: $E_1 = 39.7 GPa$
- perpendicular to fibre direction: $E_2 = 9.5 GPa$

Therefore, the stiffness of the laminate in the x and y direction obtained from eLamX software following the input of the desired layup, is: $E_{lam} = \begin{pmatrix} 30.191 \\ 17.297 \end{pmatrix} GPa$

The economic life span of the bridge is: $t_{life} = 100 years$ and $n = 0.01$ for GFRP laminates with all fibres in one direction. Therefore, the reduction factor of the ply is:

$$\gamma_{ck,UD} = \left(\frac{t_{life}}{hr} \right)^n = \left(\frac{100yrs}{hr} \right)^{0.01} = (100 * 365 * 24)^{0.01} (876000)^{0.01} = 1.15$$

Subsequently, the reduced stiffness value for the UD ply is:

$$E_{lam,red} = \begin{pmatrix} 64\% \\ 21\% \end{pmatrix} * E_1 = \begin{pmatrix} 39.7 * 0.64 \\ 39.7 * 0.21 \end{pmatrix} = \begin{pmatrix} 25.52 \\ 8.51 \end{pmatrix} GPa$$

Furthermore, the reduction factor for the laminate can be determined:

$$\gamma_{ck,lam} = \frac{E_{lam}}{E_{lam,red}} * \gamma_{ck,UD} = \frac{\begin{pmatrix} 30.191 \\ 17.297 \end{pmatrix}}{\begin{pmatrix} 25.52 \\ 8.51 \end{pmatrix}} * 1.15 = \begin{pmatrix} 1.18 \\ 2.03 \end{pmatrix} * 1.15 = \begin{pmatrix} 1.356 \\ 2.331 \end{pmatrix}$$

And finally, the stiffness of the laminate including the creep factor can be calculated:

$$E_{lam,\gamma,ck} = \frac{E_{lam}}{\gamma_{ck,lam}} = \frac{\begin{pmatrix} 30.191 \\ 17.297 \end{pmatrix}}{\begin{pmatrix} 1.356 \\ 2.331 \end{pmatrix}} = \begin{pmatrix} 22.26 \\ 7.42 \end{pmatrix} GPa$$

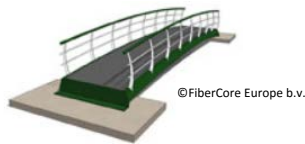
Subsequently, the deflection can be calculated using this stiffness value. The load used in this formula is the dead load plus 15% of the live load.

$$\delta_{ck} = \frac{5}{384} * \frac{q_{ck} * L^4}{E_{lam,\gamma,ck} * I} = \frac{5 * (9,81 + 0,15 * 18) \frac{kN}{m} * 30^4 m}{384 * 22,26 * 10^6 \frac{kN}{m^2} * 0,3844 m^4} = 0,01556 m = 15,56 mm$$

Therefore, the total deflection due to the self-weight and creep is:

$$\delta = \delta_{sw} + \delta_{ck} = 33,4 mm + 15,56 mm \rightarrow \delta = 49 mm$$

The next step is to determine the deflection caused by the live load. The same formula will be used.

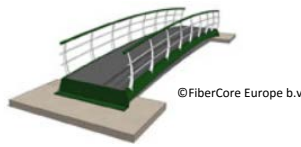


$$\delta_{fk} = \frac{5}{384} * \frac{q_{fk} * L^4}{EI} = \frac{5 * 18 \frac{kN}{m} * 30^4 m}{384 * 3.094.319,77 kNm^2} = 0,06764 m \rightarrow \delta_{fk} = 67,64 mm$$

The largest value between the two will be compared with the maximum allowed deflection which has been set by FiberCore Europe, (2016) at $1/100 * L = 300$ mm.

$$\delta_{check} = \frac{\delta_{fk}}{\delta_{max}} = \frac{67,64}{300} = 0.225$$

It can be observed from the table above that the deflection caused by the live load is 87 mm which is considerably lower than the maximum value for a span of 30 meters, therefore, the deflection is acceptable.



A20.1.2. ULS checks

In this subchapter, the results from the ULS checks described in chapter 3.5.7.2. are presented.

A20.1.2.1. Normal stress

Considering the cross sectional area obtained from the transformed area method and the largest horizontal load caused by the rear axle of the accidental vehicle during breaking, the normal stresses are:

$$\sigma_N = \frac{96 * 10^3}{57.362} = 2.4 \text{ N/mm}^2$$

The design strengths of the transformed cross section is:

$$\sigma_{N,x,c,all} = \frac{f_{yd}}{\gamma_{m,ULS} * \gamma_{cl,s}} = \frac{235}{1.62 * 1.21} = 120 \text{ N/mm}^2$$

The last step is to perform the unity check:

$$uc_{\sigma,ts} = \frac{\sigma_N}{\sigma_{N,x,c,all}} = \frac{2.4}{120} = 0.02 < 1$$

The value of the unity check is smaller than 1 which means the cross section satisfies the ultimate limit state regarding strength against normal stresses.

The N-line corresponding to the loading described above is shown in Figure 30.

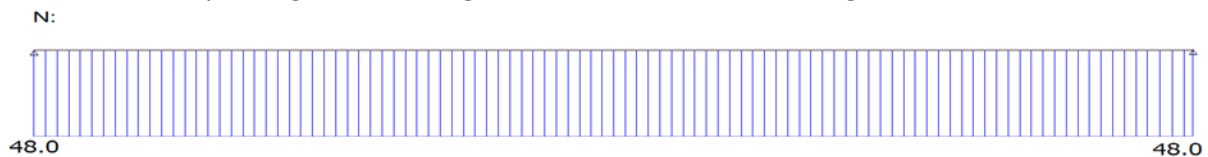


Figure 30 – N line of largest horizontal load

A20.1.2.2. Bending stress – Skin bending strength

Skin strength is checked for the largest combination between LC3 and LC4. The moment line is shown in Figure 31.

Md:

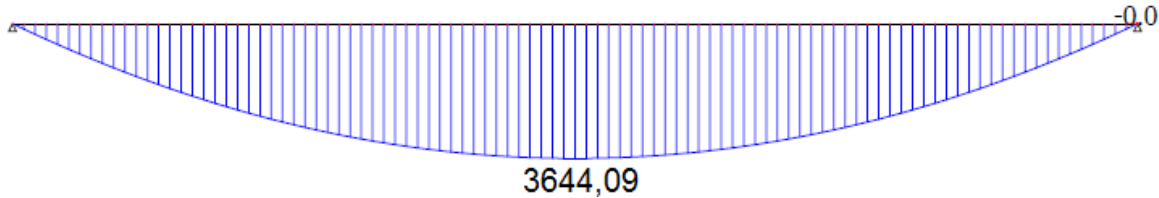


Figure 31 – M-line of Load case 3 – decisive

The bending moments in the bridge are causing tensile and compressive stresses in the skins. The maximum bending moments in the bridge for the different load cases are:

$$M_{LC3,max} = 3644,09 \text{ kNm}$$

$$M_{LC4,max} = 3158,09 \text{ kNm}$$

Therefore, the normative bending moment is the maximum value between the two:

$$M_{LC3,max} = 3644,09 \text{ kNm}$$

The bending stresses depend on the area, moment of inertia and distance of the outer fibre to the neutral axis.

Moment of inertia the cross section is

$$I_{xx} = 2 * \left(\frac{b * h^3}{12} + a^2 * A \right)_{skin} + 2 * \left(\frac{b * h^3}{12} + a^2 * A \right)_{steel} = 13,596 * 10^9 \text{ mm}^4$$

Distance between the top/bottom of the deck and the centre line: $a_{top} = a_{bottom} = 500 \text{ mm}$

Maximum bending stresses in the steel members and GFRP skins are:

$$\sigma_{x; steel,top,bottom} = \left(\pm \frac{M * y}{I_{xx}} \right) = \pm \frac{3644,09 * 10^6 \text{ Nmm} * 500 \text{ mm}}{13,596 * 10^9 \text{ mm}^4} = 134,01 \frac{\text{N}}{\text{mm}^2}$$

$$\sigma_{x; 1,steel,bar} = \left(\pm \frac{M * y}{I_{xx}} \right) / \text{number of core profiles} = \pm \frac{134,01}{21} = 6,38 \text{ N/mm}^2$$

$$\sigma_{x; GFRP,ts,bs,x,c} = \pm n_{GFRP} * \frac{M * y}{I_{xx}} = \pm 0,14 * 134,01 = \pm 19,07 \text{ N/mm}^2$$

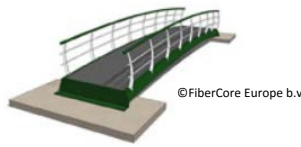
Furthermore, the unity checks have to be done with the respective design values for each material.

The design strengths of the steel, GFRP skin in longitudinal direction are:

$$\sigma_{steel,x,c,all} = \frac{\sigma_{steel,x,c}}{\gamma_{m,ULS} * \gamma_{cl,s}} = \frac{235}{1,62 * 1,21} = 119,88 \text{ N/mm}^2$$

$$\sigma_{ts,x,c,all} = \frac{\sigma_{ts,x,c}}{\gamma_{m,ULS} * \gamma_{cl,s}} = \frac{\sigma_{bs,x,c}}{\gamma_{m,ULS} * \gamma_{cl,s}} = \frac{365}{1,62 * 1,21} = 186,21 \text{ N/mm}^2$$

Therefore, the unity checks are:



$$uc_{\sigma,tsteel} = uc_{\sigma,bsteel} = \frac{\sigma_{tsteel,max,c}}{\sigma_{tsteel,x,c,all}} = \frac{\sigma_{bsteel,max,c}}{\sigma_{bsteel,x,c,all}} = \frac{6,38}{119,88} = 0.053 < 1$$

$$uc_{\sigma,ts} = uc_{\sigma,bs} = \frac{\sigma_{ts,max,c}}{\sigma_{ts,x,c,all}} = \frac{\sigma_{bs,max,c}}{\sigma_{bs,x,c,all}} = \frac{19,07}{186,21} = 0.102 < 1$$

The values of the unity checks are lower than 1, which means the cross section satisfies the ultimate limit state regarding strength of the skins against bending stresses.

A20.1.2.3. Shear stress – Web shear strength

The shear webs are checked for load combinations 3 and 4. The shear force line is given in Figure 32.

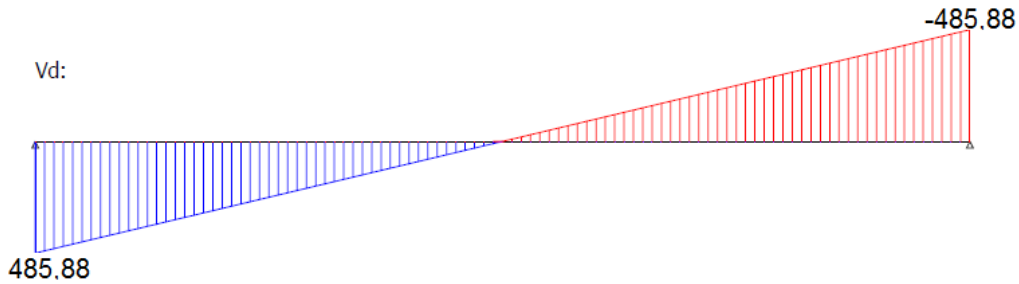


Figure 32 – V-line of Load case 3 – decisive

$$V_{LC3,max} = 485,88 \text{ kN} \qquad V_{LC4,max} = 40 \text{ kN}$$

$$n_{web} = 22 \qquad n_{web} = 1$$

With these values, the normative shear force acting on one web can be determined:

$$V_{web,max} = \max\left(\frac{485,88}{22}; \frac{40}{1}\right) = 40 \text{ kN}$$

The maximum shear stress in one web is:

$$\tau_{web,max} = \frac{3}{2} * \frac{V_{web,max}}{h_{web} * t_{web}} = \frac{3 * 40 * 10^3}{2 * 0,97 * 0,0067 * 10^6} = 9,16 \text{ N/mm}^2$$

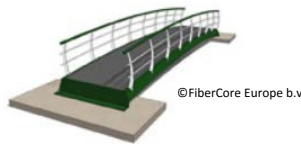
And the allowable shear stress in one web is:

$$\tau_{web,xz,all} = \frac{\tau_{web,xz}}{\gamma_{m,ULS} * \gamma_{cl,s}} = \frac{72}{1,62 * 1,21} = 36,73 \text{ N/mm}^2$$

Therefore, the unity check shows that:

$$uc_{\tau,web} = \frac{\tau_{web,max}}{\tau_{web,xz,all}} = \frac{9,16}{36,73} = 0,25 < 1$$

The value of the unity check is lower than 1, which means the cross section satisfies the ultimate limit state regarding strength of the webs against shear stresses.



A20.1.2.4. Compression stress – Webs compression strength

The strength of the webs in compression is checked for load case 5. For this check it is assumed that the concentrated load is located directly above a web.

Therefore, maximum compressive stress in one web is calculated with the following formula:

$$\sigma_{web,c} = \frac{\gamma_G * q_M * \frac{B_{w,acc}^2}{B_{eff}} + \gamma_Q * Q_{acc}}{B_{w,acc} * t_{web}} = \frac{1,1 * 9,81 \frac{kN}{m} * \frac{(0,2 m)^2}{3 m} + 1,2 * 40 kN}{0,2 m * 0,00672 m} = 35,8 \frac{N}{mm^2}$$

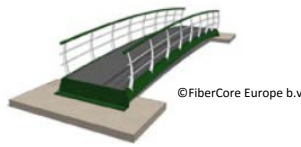
The maximum allowable compressive stress in one web is calculated according to the following formula:

$$\sigma_{web,z,c,all} = \frac{\sigma_{web,z,c}}{\gamma_{m,ULS} * \gamma_{cl,s}} = \frac{132 \frac{N}{mm^2}}{1,62 * 1,21} = 67,34 \frac{N}{mm^2}$$

Subsequently, the unity check shows that:

$$uc_{\sigma,web} = \frac{\sigma_{web,c}}{\sigma_{web,z,c,all}} = \frac{35,8}{67,34} = 0,53 < 1$$

Due to the fact that the above value is smaller than 1, the web is strong enough in compression against the largest point load, namely against the unauthorised vehicle.



A20.1.2.5. Maximum shear stress

Shear stress results when a load is applied parallel to an area and will vary across the cross sectional area. The general formula for calculating shear stress is: (Parker, 2007)

$$\tau = \frac{V * Q}{b * I}$$

Where

- Q – calculated static moment

$$Q = A_1 * a_1 + A_2 * a_2 + \dots + A_n * a_n$$

- V – Maximum shear near end supports
- I – Moment of inertia around neutral axis
- b – width of the member

The maximum shear stresses will occur at the middle of the cross section, therefore, the static moment becomes:

$$Q = A_{skin} * a_{skin} + A_{steel} * a_{steel} + A_{foam} * a_{foam}$$

$$Q_{skin} = 4500 \text{ mm} * 12,6 \text{ mm} * \left(\frac{1000 \text{ mm}}{2} - \frac{12,6 \text{ mm}}{2} \right) = 27,99 * 10^6 \text{ mm}^3$$

$$Q_{steel} = 21 * 100 \text{ mm} * 10 \text{ mm} * \left(\frac{1000 \text{ mm}}{2} - 12,6 \text{ mm} - \frac{10 \text{ mm}}{2} \right) = 10,13 * 10^6 \text{ mm}^3$$

$$Q = Q_{skin} + Q_{steel} = (27,99 + 10,13) * 10^6 \text{ mm}^3 = 38,12 * 10^6 \text{ mm}^3$$

Furthermore, the maximum shear force next to the end supports for Load Case 3 is:

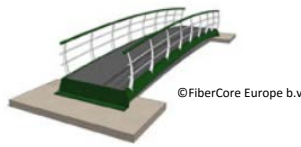
$$V_{LC3,max} = 485,88 \text{ kN} = 485.880 \text{ N}$$

The moment of inertia of the cross section is:

$$I = 3,84 * 10^{11} \text{ mm}^4$$

Therefore, the maximum shear stress in the cross section is:

$$\tau_{max} = \frac{4,85 * 10^5 \text{ N} * 38,12 * 10^6 \text{ mm}^3}{4.500 \text{ mm} * 3,094 * 10^{11} \text{ mm}^4} = 0,013 \frac{\text{N}}{\text{mm}^2}$$



A20.1.2.6. Shear stress – Web buckling

Using all the parameters from Appendix 3, the formula can be filled in and the critical buckling parameter can be determined:

$$\lambda_{cr_{ij}} = \frac{\left[D_{11} * \left(\frac{\alpha_1}{L_x} \right)^4 + 2 * (D_{12} + 2 * D_{66}) * \frac{\alpha_4}{L_x^2} * \frac{\alpha_5}{L_y^2} + D_{22} * \left(\frac{\alpha_3}{L_y} \right)^4 \right]}{N_{x0} * \frac{\alpha_4}{L_x^2} + N_{y0} * \frac{\alpha_5}{L_y^2}}$$

$$= \frac{\left[486.233,9 * \left(\frac{4,73}{30000} \right)^4 + 2 * (245.975,1 + 2 * 258.351,1) * \frac{12,91 * 12,91}{30.000^2 * 974,8^2} + 413.458 * \left(\frac{4,73}{974,8} \right)^4 \right]}{0 * \frac{12,91}{30.000^2} + 3,6 * \frac{12,91}{974,8^2}}$$

→ $\lambda_{cr_{ij}} = 4,69$

Therefore, according to this method, the critical buckling factor is 4,69.

This factor can also be obtained from the eLamX software for a specified laminate. It can be observed from Figure 33 that by introducing a laminate with the same dimensions, clamped along all four edges to mimic its connections with the skins and ends and with the same load acting on it, the program calculates the critical buckling factor (i.e. called eigenvalue here) to be 4,78.

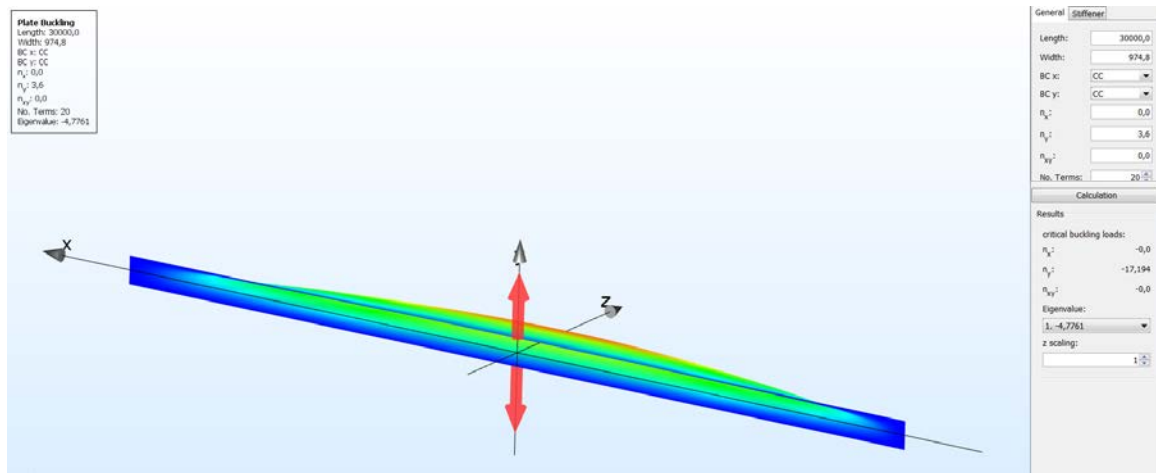
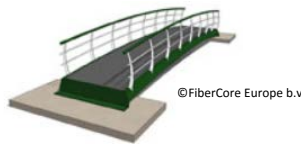


Figure 33 – buckling of the web under SLS load in eLamX

Considering that from two different sources, similar values for the buckling factor were obtained, it can be concluded that the values are comparable and therefore sufficiently accurate at this stage.



A20.1.3. Thermal expansion analysis

According to the formula for linear expansion, the elongation of the two materials is:

$$\Delta l_{steel,contraction} = 30 \text{ m} * 10 * 10^{-6} \frac{\text{m}}{\text{m} * \text{C}} * 27^{\circ}\text{C} = 0,0081 \text{ m} = 8,1 \text{ mm}$$

$$\Delta l_{steel,expansion} = 30 \text{ m} * 10 * 10^{-6} \frac{\text{m}}{\text{m} * \text{C}} * 22^{\circ}\text{C} = 0,0066 \text{ m} = 6,6 \text{ mm}$$

$$\Delta l_{steel,range} = \Delta l_{steel,contraction} + \Delta l_{steel,expansion} = 8,1 + 6,6 = 14,7 \text{ mm}$$

$$\Delta l_{GFRP,x,contraction} = 30 \text{ m} * 8,22 * 10^{-6} \frac{\text{m}}{\text{m} * \text{C}} * 27^{\circ}\text{C} = 0,006658 \text{ m} = 6,658 \text{ mm}$$

$$\Delta l_{GFRP,x,expansion} = 30 \text{ m} * 8,22 * 10^{-6} \frac{\text{m}}{\text{m} * \text{C}} * 22^{\circ}\text{C} = 0,005425 \text{ m} = 5,425 \text{ mm}$$

$$\Delta l_{GFRP,x,range} = \Delta l_{GFRP,x,contraction} + \Delta l_{GFRP,x,expansion} = 6,658 + 5,425 = 12,08 \text{ mm}$$

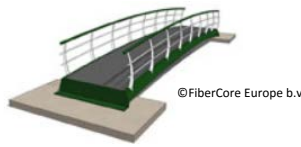
Furthermore, axial force in the two materials can be determined:

$$F = \frac{\Delta T_{contraction} * L * (\alpha_{ts,x} - \alpha_{steel})}{\frac{L}{A_{steel} * E_{steel}} - \frac{L}{A_{ts} * E_{ts}}} =$$

$$= \frac{27 * 30 \text{ m} * (8,22 * 10^{-6} - 1 * 10^{-5})}{\frac{30 \text{ m}}{0,1 \text{ m} * 0,01 \text{ m} * 2,1 * 10^{11} \frac{\text{N}}{\text{m}^2}} - \frac{30 \text{ m}}{0,1 \text{ m} * 0,0126 \text{ m} * 2,99 * 10^{10} \frac{\text{N}}{\text{m}^2}}} = 2,2 \text{ N}$$

Subsequently, axial stresses in each material can be determined:

$$\sigma_{steel} = \frac{F}{A_{steel}} = \frac{2,2 \text{ N}}{0,001 \text{ m}^2} = 2,2 \frac{\text{N}}{\text{mm}^2} \quad \text{and} \quad \sigma_{skin} = \frac{F}{A_{steel}} = \frac{2,2 \text{ N}}{0,00126 \text{ m}^2} = 1,75 \frac{\text{N}}{\text{mm}^2}$$



A20.1.4. Shear stresses in the adhesive bond between steel plate and GFRP skin

The first step involves creating a connection between the two materials by calculating a ratio from their elasticity moduli:

Material 1 with area A_1 and E modulus E_1 and Material 2 with area A_2 and E modulus E_2 .

$$\text{if } E_2 > E_1 \rightarrow n = \frac{E_2}{E_1} = \frac{210000 \frac{N}{mm^2}}{30190 \frac{N}{mm^2}} = 6,95 \text{ and } \sigma_2 = n * \sigma_1$$

Furthermore, the maximum shear force next to the end supports for Load Case 3 is:

$$V_{LC3,max} = 497,78 \text{ kN} = 497780 \text{ N}$$

The moment of inertia of the cross section is:

$$I = 3,84 * 10^{11} \text{ mm}^4$$

The shear stresses calculated in this chapter occur at the adhesive bond between the steel and the top skin. The same stresses occur at the bottom part of the cross section. Therefore, the static moment is calculated:

$$Q = n * A_{skin} * a_{skin}$$

$$Q = 6,95 * 4500 \text{ mm} * 12,6 \text{ mm} * \left(\frac{1000 \text{ mm}}{2} - \frac{12,6 \text{ mm}}{2} \right) = 194,55 * 10^6 \text{ mm}^3$$

Therefore, the maximum shear stress in the cross section is:

$$\tau_{adhesive,bond} = \frac{4,98 * 10^5 \text{ N} * 194,55 * 10^6 \text{ mm}^3}{4500 \text{ mm} * 3,84 * 10^{11} \text{ mm}^4} = 0,056 \frac{N}{mm^2}$$

A20.1.5. Foundation calculations

The current section presents the calculation procedure for determining the foundation's rotational stiffness.

$$k_{pile} = \frac{E * A}{1,5 * L} = \frac{35.000 * 31.415,92}{1,5 * 5000} = 146.607,66 \frac{N}{mm} = 146.607,66 \frac{kN}{m}$$

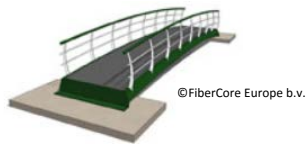
$$F_1 = 3 * 979 \text{ mm} * F_{foundation}[N] = 2.937 * F_{foundation}[N]$$

$$M = (2 * 529 \text{ mm} * 1.587 \text{ mm} * F_{foundation}) = 5.750.646 * F_{foundation} \text{ Nmm}$$

$$u_{max} = \frac{2.937 * F_{foundation}}{3 * 146.607,66} = 0,0067 * F_{foundation} \text{ mm}$$

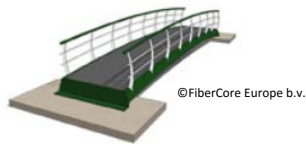
$$\varphi = \frac{0,0067 * F_{foundation} \text{ mm}}{979 \text{ mm}} * F_{foundation} = 6,28 * 10^{-6} * F_{foundation} \text{ rad}$$

$$C = \frac{5.750.646 * F_{foundation} \text{ Nmm}}{6,28 * 10^{-6} * F_{foundation} \text{ rad}} = 8,43 * 10^{11} \frac{Nmm}{rad} = 843.088,74 \frac{kNm}{rad}$$



Appendix 21 – Drawings of 30 meter bridge

The current appendix contains the drawings for the 30 meter bridge, as described in chapter 4.9.



Appendix 22 – drawings of 60 meter bridge

The current appendix contains the drawings for the 30 meter bridge, as described in chapter 4.9.

Appendix 23 – CROW section related to cycling and pedestrian bridge design

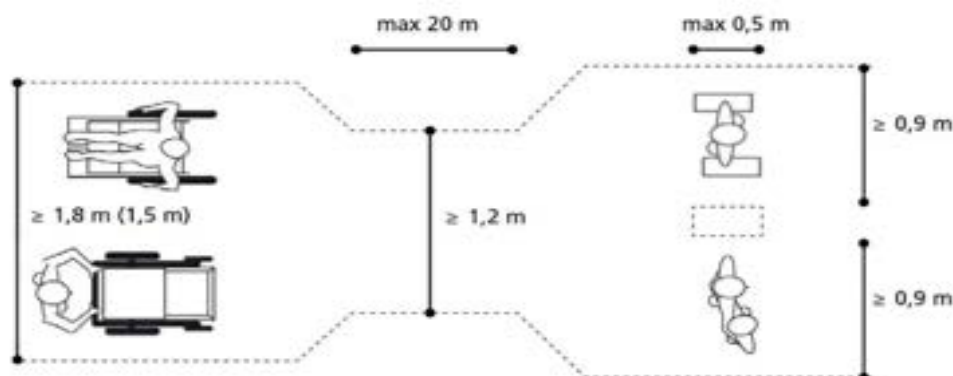
The following information is as given in “CROW_Fiets_Ontwerpwijzer bruggen voor langzaam verkeer_3.1.1 Voetgangers” and “CROW_Fiets_Ontwerpwijzer bruggen voor langzaam verkeer_3.1.2 Fietsers”

Hoeveel ruimte hebben voetgangers nodig?

CROW-publicatie 723 ‘ASVV 2012’ [2] en CROW-publicatie 337 ‘Richtlijn toegankelijkheid’ [8] beschrijven de ruimte die voetgangers nodig hebben.

Vanuit toegankelijkheidsperspectief verdient het de voorkeur de laatste publicatie als uitgangspunt te gebruiken. Deze publicatie beschrijft de volgende richtlijnen voor vrije breedte:

- voorkeursmaat $\geq 1,8$ m;
- minimum maat $\geq 1,5$ m;
- bij plaatselijke versmalling en over een lengte van maximaal 20 m geldt een minimale vrije breedte van 1,2 m;
- bij plaatselijke versmallingen (puntvernauwing) over een lengte van maximaal 0,5 m geldt een minimale vrije breedte van 0,9 m [8].



Figuur 3.5. Vrije doorgangsbreedte bij puntvernauwing

Hoogteverschil

Voor hoogteverschillen groter dan 0,21 m is overbrugging door een vaste trap of hellingbaan verplicht [6] [7]. Is een hellingbaan of trap onvermijdelijk, pas dan de hiervoor geldende richtlijnen toe (zie hoofdstuk 9). De belangrijkste uitgangspunten voor hellingbaan en trap lichten we hieronder alvast kort toe.

CROW-publicatie 337 ‘Richtlijn toegankelijkheid’ [8] beschrijft richtlijnen voor het loopoppervlak. Vanuit toegankelijkheidsperspectief is het aan te raden deze publicatie als uitgangspunt te gebruiken en voor een vlak loopoppervlak te zorgen, waarbij onregelmatigheden maximaal 5 mm bedragen.

Hellingbaan

Conform het Bouwbesluit [7] heeft een hellingbaan een breedte van ten minste 1,1 m en een hoogte van niet meer dan 1 m. Is het hoogteverschil groter dan 1 m, dan is opsplitsing nodig in stukken die ieder maximaal 1 m hoogteverschil overbruggen. De stukken hellingbaan

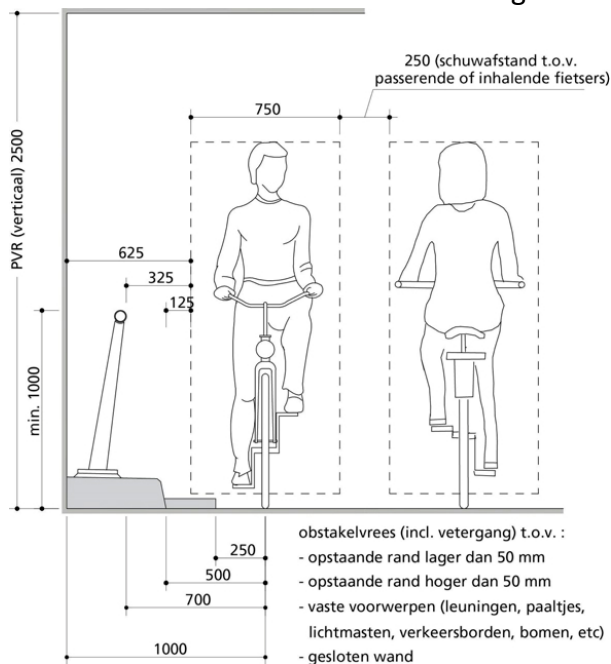
moeten dan aan elkaar verbonden zijn door vlakke stukken (rustvlakken). Deze uitgangspunten gelden specifiek voor voetgangers.

Uitsluiting

Uitgangspunt is dat het wegprofiel van het fietspad dat op de brug aansluit, doorloopt op de brug. Uitgebreidere informatie over het ontwerpen van fietspaden is te vinden in CROW-publicatie 230 'Ontwerpwijzer fietsverkeer' [4].

Hoeveel ruimte hebben fietsers nodig?

Een fietser met standaardfiets bestrijkt in de breedte 0,75 m [4]. Een fietspad (op een brug) is echter altijd breder, ook een eenrichtingspad. De breedte hangt af van het gebruik (een- of tweerichtingsverkeer; het kunnen inhalen of passeren van een andere fietser), de te verwachten verkeersintensiteit, de vetergang van een fietser en de benodigde afstand tot obstakels als troittoirbanden en leuningen. Dat leidt tot figuur 3.11.



Figuur 3.11. Objectafstanden fiets (op basis van [4])

Vaak dient het aansluitende fietspad als uitgangspunt. Houd er echter rekening mee dat op de brug andere objectafstanden gelden (bijvoorbeeld ten opzichte van de leuning) dan buiten de brug (veelal geen leuning aanwezig).

De basismaat van één fietser is zoals gemeld 0,75 m (exclusief vetergang of objectafstanden). Per extra fietser komt er 1 m bij; 0,75 m + 0,25 m schuwafstand ten opzichte van een andere fietser.

In de publicaties van CROW waarin breedtes van fietspaden besproken worden, wordt onderscheid gemaakt tussen fietspaden en (brom)fietspaden. Op fietspaden waar ook bromfietzers verwacht/toegestaan worden, wordt de totale breedte veelal met 0,5 m vergroot.

Na bespreking van de enkele aandachtspunten, wordt in een aantal voorbeelden de benodigde breedte voor fietsers op een brug verder geïllustreerd.